HELIOTEK
A Division of textron Inc
12500 GLADSTONE AVE, SYLMAR CALIFORNIA 91342 TWX 910-496-1488 Area Code (213) 365-4611

Development of an Integrated Lightweight Flexible Silicon Solar Cell Array

FINAL REPORT

SEP 12 1970

Prepared for

Jet Propulsion Laboratory
California Institute of Technology
4800 Oak Grove Drive
Pasadena, California

Prepared under
Contract No. 952560

by

Heliotek, Division of Textron, Inc
12500 Gladstone Avenue
Sylmar, California 91342

N70-39507

DEVELOPMENT OF AN INTEGRATED LIGHTWEIGHT FLEXIBLE SILICON SOLAR CELL ARRAY

Heliotek, Division Textron, Incorporated
Sylmar, California

12 September 1970

7%

562

5320

Development of an Integrated
Lightweight Flexible Silicon Solar Cell Array

F I N A L   R E P O R T

JPL Contract No. 952560

This work was performed for the Jet Propulsion Laboratory, California Institute of Technology, as sponsored by the National Aeronautics and Space Administration under Contract NAS7-100.

Prepared by

E. L. Ralph
E. F. Zimmerman
P. M. Stella

Heliotek, Division of Textron, Inc.
12500 Gladstone Avenue
Sylmar, California 91342

This report contains information prepared by the Heliotek Division of Textron Incorporated, under JPL Subcontract. Its content is not necessarily endorsed by the Jet Propulsion Laboratory, California Institute of Technology, or the National Aeronautics and Space Administration.

TABLE OF CONTENTS

List of Figures

List of Figures (cont)

LIST OF TABLE

1.0 SUMMARY

It is the intent of this summary to provide a comprehensive and complete description of the pertinent portions of this program in a self-contained format. For this reason some information and a number of figures will be repetitious with material within the report's main body.

The objective of this program was to develop methods and analytical techniques which could be used to fabricate an integrated lightweight flexible silicon solar cell array blanket with the following goals that the array be capable of (1) providing 120 watts per pound of array weight, (2) being manufactured at a cost of $100 per watt of raw power, and (3) being produced in modular prefabricated sections.

The study effort was divided into seven major tasks in order to examine individual components comprising the total array concept. These areas were

1. Solar cell and contacts
2. Coverslide assembly study
3. Solar cell interconnects
4. Substrate and cell bonding
5. Integrated power distribution
6. Demonstration module fabrication
7. Documentation

The last two tasks were specifically concerned with demonstrating and exhibiting the manufacturability of the systems and concepts evolved from the 5 major component studies. The development efforts concluded under these programs were as follows

1. Solar Cell and Contacts With the solar cell being the active element and also the major cost component, efforts were directed towards optimizing the ratio of power to weight per cost of the solar cell by considering effects of cell thickness, size, and contact configuration. Although the original intent was to base the data on quotes from various cell manufacturers, incomplete replies redirected efforts to examination of cell prices obtained over the past decade and then examining for cost trends and relationships. Basic cost trends indicated that

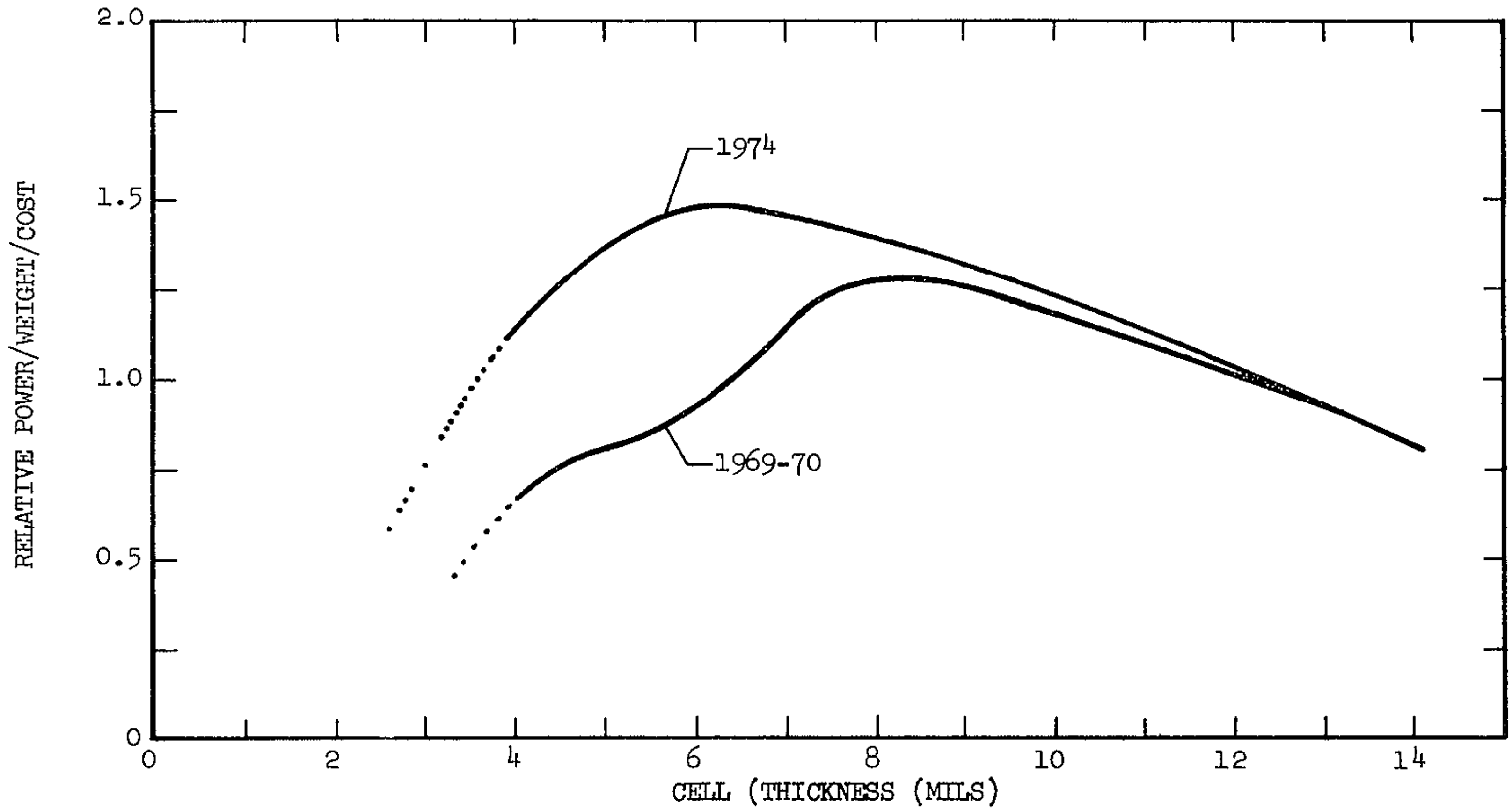

Figure 1 1-1 POWER/WEIGHT/COST
NORMALIZED TO 12 MIL CELL = 1.0

TABLE 1.2-1

PRICE COMPARISON OF COVERED SOLAR CELLS								
COVER MATERIAL	.006" 7940 FUSED SILICA 50,000 PCS.				006" 0211 MICROSHEET 50,000 PCS.			
COVER AND INSTALLATION SPECIFICATIONS	TIGHT		RELAXED		TIGHT		RELAXED	
COATING ON COVER	A.R.ONLY	A.R.& BLUE	A.R.ONLY	A.R. & BLUE	A.R.ONLY	A.R. &BLUE	A.R.ONLY	A.R. &BLUE
COATING COST CHANGE	-.42	0	-.42	0	-.17	0	- 17	0
COVER COST	2.50	2.40	1.73	1.83	1.32	1.25	67	1.85
INSTALLATION COST	1.60	1.60	1.00	1.00	1.60	1.60	1.00	1.00
TOTAL COST	3.68	4.00	2.31	2.83	2.75	2.85	1.50	1.85

(1) The cost for a particular cell (size, thickness, contact configuration) decreases as time passes--reflecting the manufacturing learning curve and customer use.

(2) The cost for a particular thickness decreases as time passes.

(3) Each new parameter of a cell such as reduced thickness, larger size, or contact configuration initially commands a very high price and as demand and manufacturing experience increase, the cost becomes reduced. The time interval required to reduce th cell cost is dependent on the "encouragement" given to the manufacturer by purchasers.

Based on these trends and relative prices for the cell as a function of thickness, size, and contact configuration, trade-offs were performed to provide an optimized cell. The contact analysis indicated that only the bar contact cell was presently economical and that only for relatively thick cells, i.e., 12 mils thick, the large area cells would provide a cost savings. Consequently the primary trade-offs involved varying thicknesses in bar contacted 2 x 2 cm cells. These results are summarized in Figure 1.1-1. Clearly the 8 mil cell provides the greatest power/weight value per dollar at present. Yet, present thickness versus cost versus time rates indicates this optimum cell will be at 6 mils by 1974.

2. Coverslide Assembly Study The coverslide study was directed towards reducing the cost of the coverslide system, including assembly. In addition to examining various types of covers such as platelet, integral, and ribbon, the cost impacts of AR coatings and filters was examined. A summary for platelet systems of fused silica and microsheet is shown in Table 1.2-1.

Sizeable cost savings thru the use of integral and ribbon glass systems were realizable over the conventional platelet. The considerable cost reduction for the ribbon glass AR coating reflects the economy of coating a continuous ribbon. These savings

TABLE 1.2-2

COMPARATIVE COVER COSTS

	Integral	CONVENTIONAL Fused Silica	Microsheet	Ribbon
Material	$0.02	$2.04	$0.78	$0.16
AR Coating	0.30	0.30	0.27	0.03
Installation Labor (Burdened)	0.54	1.15	1.39	0.46
Total Cost	0.86	3.49	2.44	0.65

are clearly exhibited in Table 1.2-2. A continuous process ribbon glass cover assembly was investigated during this program. This was evaluated in an effort to reduce coverslide costs by reducing the cost of both material and labor. This automated continuous process consists of two major steps (1) Bonding the continuous glass ribbon to the solar cells, and (2) Trimming the coverglass to the correct size.

Adhesive selection and application, explained in detail in the text, was performed and Dow Corning XR-6-3489 was selected. Rolling produced a thin bond line about 0.001 inch in thickness and cure times could be accelerated to about five minutes.

Three methods of trimming were evaluated (1) Scribing with a diamond, (2) Melting with a hot wire, and (3) Abrasive trimming with a high velocity jet of aluminum oxide. The abrasive method proved to be most satisfactory and was selected for use in fabricating the demonstration module.

3. Interconnector Study Major emphasis in the interconnector study was aimed at improving interconnection reliability. The program defined 4 prime failure modes for interconnectors

(1) Interconnectors stressing silicon beyond ultimate strength.
(2) Interconnector being stressed beyond ultimate strength.
(3) Interconnector fracture due to fatigue.
(4) Solder joint fracture due to fatigue.

Efforts to prevent failures under 1 and 2 have been straightforward and successful in the past so that study efforts were directed at preventing fatigue failures per items 3 and 4. The accomplishments under item 3 included the derivation of an equation which gives the minimum height for a stress loop required to provide no fatiguing. This is for small changes in the interconnector loop bend radius

$$h' = R + \left[\frac{Y' - R_f}{R_f - R} \left(\frac{2R_f}{\pi} \right) \right], \text{ where } R_f = \frac{R}{1 - \frac{S_f R}{Ed}}$$

where h' = minimum height of stress loop

Y' = half the maximum cell spacing due to array motions

E = modulus of elasticity for interconnector

d = thickness of interconnector

S_f = fatigue strength of interconnector material

R = radius of curvature of stress loop

Additionally, a number of different interconnector configurations were found which provided significantly greater fatigue resistance than standard Z tab low stress loop interconnectors. The various interconnector configurations examined and tested are shown in Figures 1.3-1 and 1.3-2. Flexure/tensile tests of sample modules utilizing the various interconnector types shown in Figures 1.3-1 and 1.3-2 resulted in the data exhibited in Figure 1.3-3. An improvement in fatigue resistance by the wraparound concepts is clearly demonstrated in these tests.

The examination of the thermal stress problem at the solder joint resulted in the equation,

$$S_i = E_i \left(\alpha \, \Delta T - \frac{R}{L} \right)$$

where the index, i, refers to the members of the trimetallic bond--interconnector, solder, or silicon. Hence

S_i = average stress in the ith member

E_i = elastic modulus

α_i = thermal coefficient of expansion

ΔT = temperature change

L = length of the members,

and R = resultant length change given by

$$R = \frac{L \sum_{i=1}^{3} t_i E_i \alpha_i \Delta T}{\sum_{i=1}^{3} t_i E_i}$$

where t_i is the material thickness.

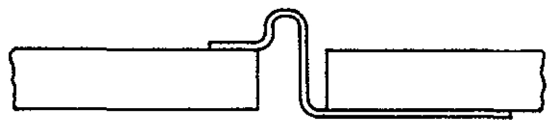

Z TAB CONFIGURATION

(a)

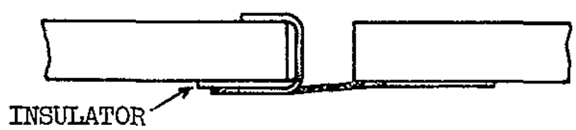

WRAPAROUND

(b)

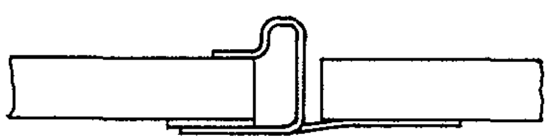

STRESS-RELIEVED WRAPAROUND

(c)

FIGURE 1.3-1 INTERCONNECTOR CONFIGURATIONS A

TOTAL SPAN WRAPAROUND

(a)

TOP VIEW

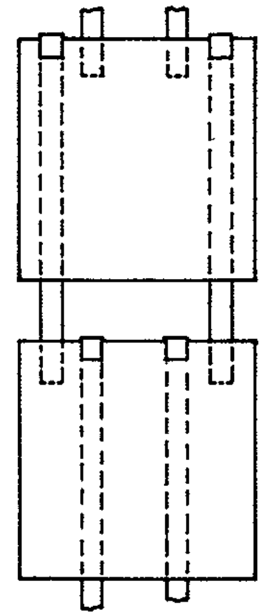

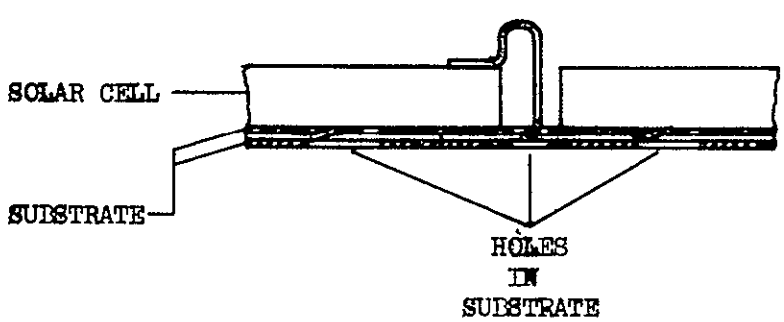

LAMINATED INTERCONNECTOR

(b)

FIGURE 1.3-2 INTERCONNECTOR CONFIGURATIONS B

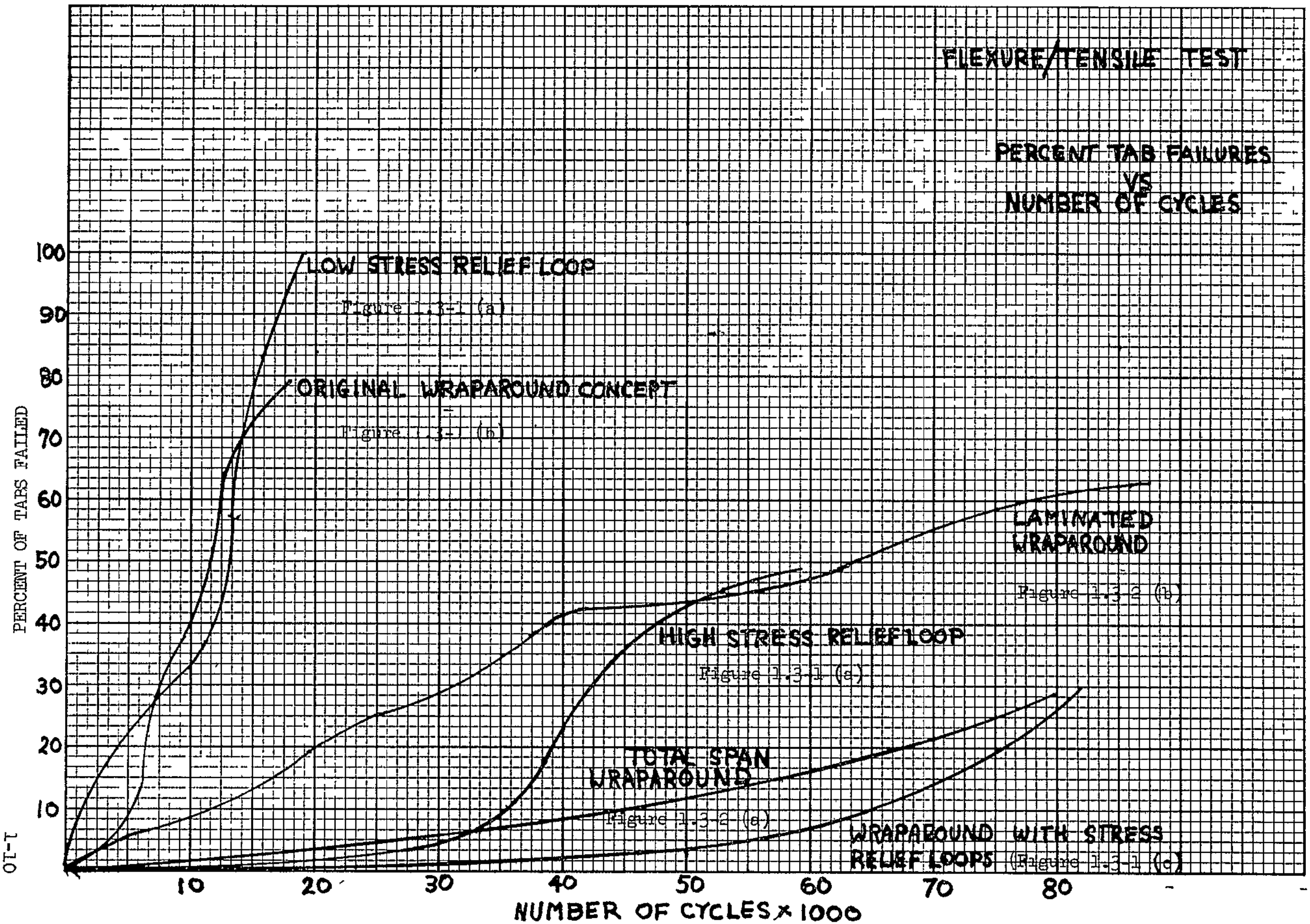
FLEXURE/TENSILE TEST
PERCENT TAB FAILURES
VS
NUMBER OF CYCLES
LOW STRESS RELIEF LOOP
Figure 1.3-1 (a)
ORIGINAL WRAPAROUND CONCEPT
Figure 1.3-1 (b)
LAMINATED
WRAPAROUND
Figure 1.3-2 (b)
HIGH STRESS RELIEF LOOP
Figure 1.3-1 (c)
TOTAL SPAN
WRAPAROUND
Figure 1.3-2 (a)
WRAPAROUND WITH STRESS
RELIEF LOOPS (Figure 1.3-1 (c)
PERCENT OF TABS FAILED
10
20
30
40
50
60
70
80
90
100
10
20
30
40
50
60
70
80
NUMBER OF CYCLES x 1000

FIGURE 1.3-3

Based on this model, a family of stress curves exhibiting the silicon stress dependence on material type and thickness is exhibited in Figure 1.3-4. Furthermore, calculated solder stresses at temperatures higher than 150°C and lower than -100°C approached quite close to the solder yield strength and indicated that the solder would be a weak link in the bond.

4 Cell Support Substrate Lightweight polyimide in flat sheets and in narrow ribbon configurations was examined as a possible cell substrate. The effects of ribbon width and adhesive coverage were examined as shown in Table 1.4-1. The ribbon concept provided sufficient strength for mechanical integrity when compared to a flat sheet substrate. Subsequent module wrap tests indicated that complete edge coverage of the solar cell was required to prevent cell lifting under array bending. Furthermore, the interconnector flexure/fatigue tests showed a slightly greater fatigue rate for wraparound interconnectors when a ribbon substrate was used when compared to a sheet substrate. This appeared to be due to a poorer distribution of stress loads by the substrate resulting in higher stresses along some ribbons and consequently greater cell spacing changes and higher interconnector failure rates. It is felt that further development of fabrication techniques can prevent the uneven distribution of stresses by the ribbon substrate, hence allowing the use of the approximately 50% weight savings offered by the ribbon concept

5 Integrated Power Distribution System The mechanical-electrical integrity of metallic-polyimide laminates was examined under tensile and bending tests. A vacuum deposited copper-etched polyimide system was found to provide both mechanical and electrical integrity suitable for array utilization throughout the testing. The evaporation process consisted of resistance heating fine copper wire held in a tungsten basket Evaporation pressures were on the order of 5×10^{-4} torr, although the evaporation pressure was not a sensitive parameter in terms of good copper adherence to the polyimide

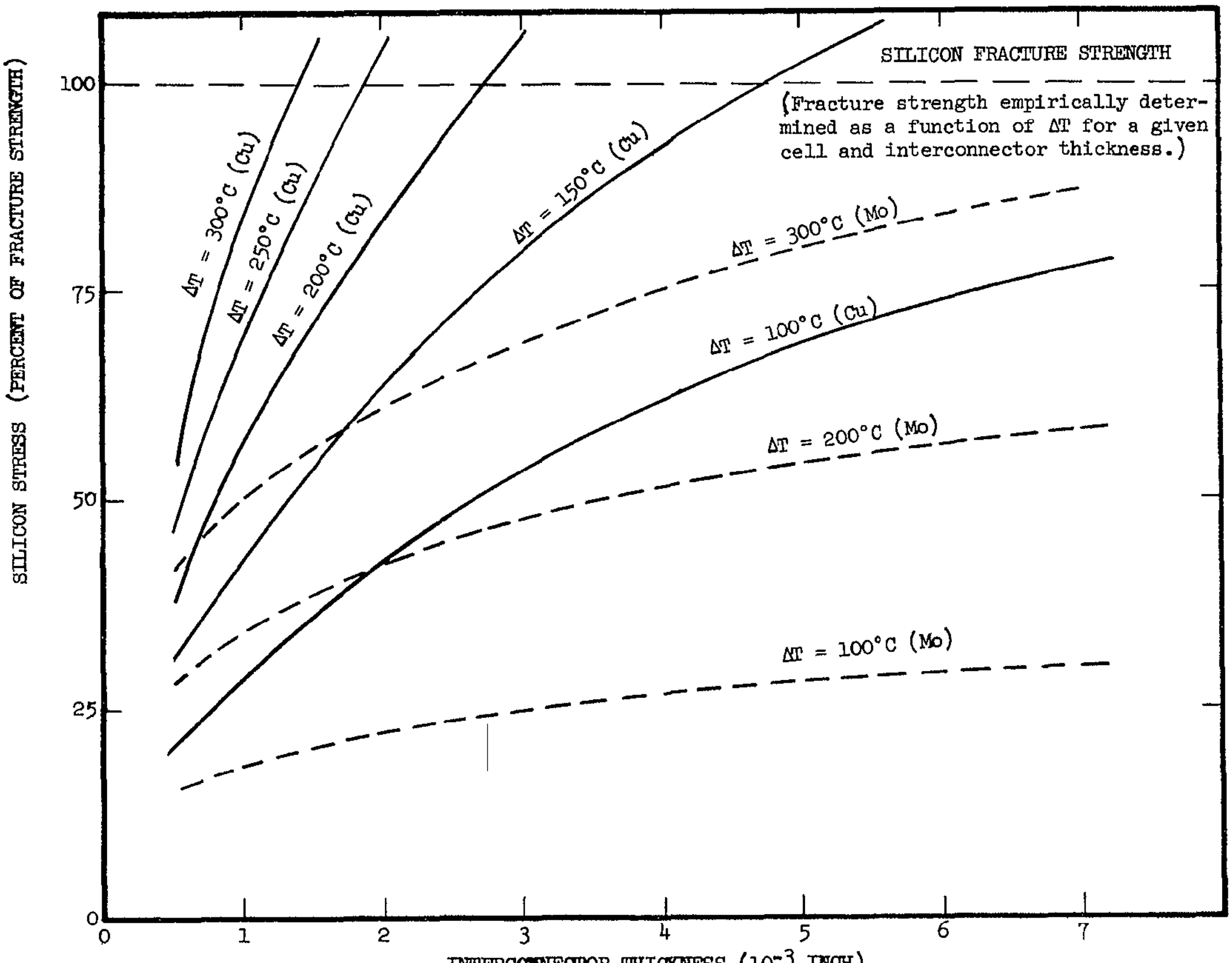

Figure 1.3-4. Thermal stresses in silicon under a metal tab of various thicknesses.

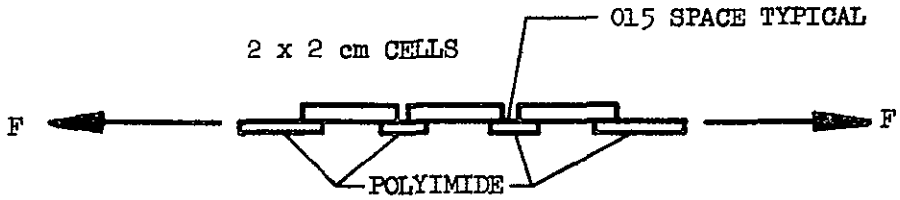

Adhesive	DC 90-024
Thickness	0.0015 inches
Primer	DC 90-198
Substrate	0.001 inch polyimide

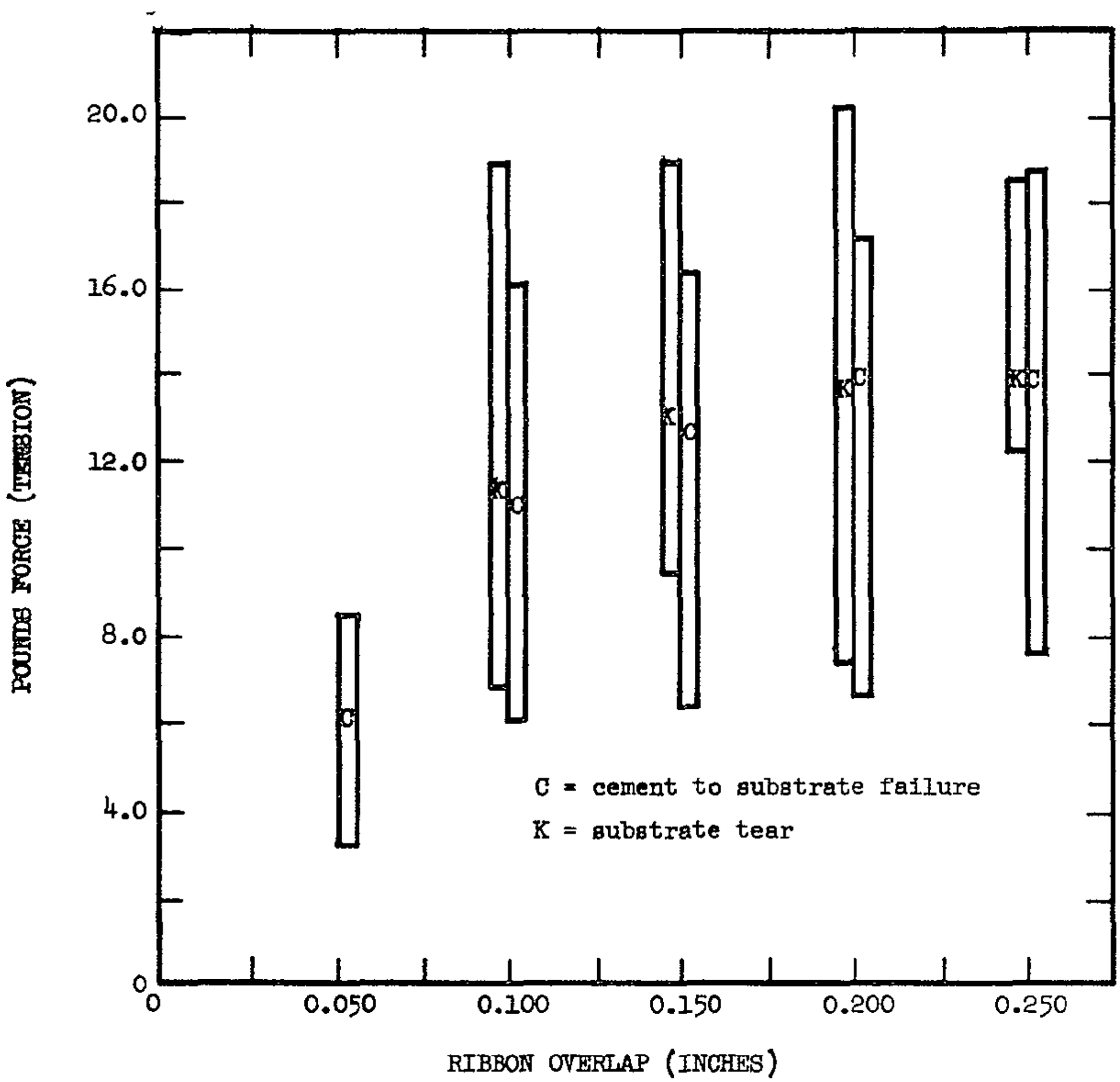

TABLE 1.4-1 TENSILE TEST OF RIBBON SUBSTRATE

6. Demonstration Modules and Documentation Demonstration modules were fabricated exhibiting the manufacturability and compatibility of the optimized components determined in Phases 1 thru 5 above. These included 7 and 8 mil thick bar contacted silicon solar cells, 1.3 mil thick ribbon glass covers, wraparound (high fatigue resistant) interconnectors, and the polyimide sheet substrate. Photographs and fabrication documentation were prepared for the manufacturing process.

7. The pertinent findings of this study include

   - 8 mil thick 2 x 2 cm bar contact cells provide optimum power/weight/cost at the present time.
   - 6 mil thick 2 x 2 cm bar contact cells will provide optimum power/weight/cost by 1974.
   - Integral and ribbon glass cover systems can reduce the cover cost per cell from $2.50 minimum for a platelet system to less than $0.86.
   - A generalized equation relating interconnector stress loop height and fatigue resistance was derived.
   - Deposited metal - polyimide laminates used as interconnectors can provide substrate mechanical strength and electrical integrity.
   - Minimum adhesive coverage between solar cell and ribbon substrate was determined.
   - Silicon stress versus interconnector thickness for various temperature cycling ranges were calculated for copper and molybdenum material.

2.0 TECHNICAL DISCUSSION

Efforts to provide a basic silicon solar cell array providing 120 watts per pound at a cost of $100 per watt were broken down into seven major tasks. The primary emphasis in each task was guided by the program's basic power to weight and cost goals and additionally by specific goals peculiar to each task. These guidelines provide an outline of the specific efforts described in the main body of the technical discussion and reflect the task efforts conducted during the previous year. Additionally, brief discussions are included so as to indicate why each task was treated in its particular manner.

2.1 SOLAR CELL EVALUATION AND SELECTION

The intent of the cell evaluation part of the lightweight array study was to determine the cell configuration which would provide the best power to weight ratio at the least cost and be readily adaptable to use on a modular array concept. Ideally, a trade-off study such as this should be easily obtained by comparing costs of various size and thickness solar cells and relating this to the power output values. Actually this is not simple since there are many cell types available and the number of variables becomes very large. Also the cell costs are highly dependent upon the degree of development or the availability of tooling and experience of a particular cell type. In spite of these problems, an attempt was made to develop a matrix of cell types, and current costs were requested. The following variables were considered important for this program and were included in the matrix.

1. Standard bar contact cells 2 x 2 cm
2. Wraparound contact cells 2 x 2 cm
3. Large area cells 2 x 4 cm, 2 x 6 cm
4. Various cell thicknesses 12, 8, 6, and 4 mils
5. Cell quantities from 10K to 2M.

This request for power output and general cost information resulted in either no information submitted or at best only partial answers to selected portions of the variable matrix. Analyzing the few data points thus available, it became apparent that it would be impossible to gain any relevant trade-off information this way.

It was therefore decided that if current cost and performance data was not readily available, then possibly the trade-off design study could still be performed if some of the principles of cell economics could be defined. In order to define these principles, a study was made of solar cell prices over the past years so as to determine what kinds of trends might be noticeable. If definite trends were found, then it was felt that extrapolations could be made to the present and future regarding such variables as new cell design acceptance, cell costs, performance and time factors.

In regard to solar cell costs it was concluded that at any particular time in history, the thinner the cell the higher the cost. Actually there normally was a range of cell thicknesses which were available at essentially the same price and then as the thickness was decreased below this minimum (or conventional) thickness, the price increased at a very rapid rate due to the uncertainty of production yields. Figure 2.1-1 shows this relationship over a fairly long period of time. Although these are basically schematic curves, there are usually several historical points on each curve that generally fixed the shape and magnitude of the curve. The curves were normalized to 1.0 for the thickest (least expensive) cell for the given period of time so that only thickness effects were analyzed and general cost variations due to cell design, production efficiency, time period, size, etc., were put on an equal basis. Characteristically the base line cost price has decreased with time from $6.00 for an 18 mil 1 x 2 cm cell in 1958 to $4.60 for a 2 x 2 cm cell in 1969.

The value "one" represents basically the state-of-the-art large volume production cell for each period of time. The first obvious fact that is evident is that the trend is to provide thinner solar cells as time goes on. Also, the critical point where the cell price increases rapidly with decreasing cell thickness changes to thinner cells with time. Since these curves are continually changing, information today will not be satisfactory for projecting cost effective designs for future array designs. Therefore, for example, a curve is shown for a 1974 projected estimate that can be used in this study for making a cost effective array design. This 1974 curve is expected to be similar to the general patterns seen in the past, but will be shifted so that the critical break occurs between 6 and 8 mils cell thickness. The curve for 1974 was established by constructing the set of curves presented in Figure 2.1-2. This set of curves was constructed by determining the intersection points of a line corresponding to constant relative price values of 1.25, 1.5, 2.0 and 3.0, and the year curves from Figure 2.1-1. These data points were plotted and a smooth curve drawn and extrapolated to generate the 1974 estimated curve in Figure 2.1-1.

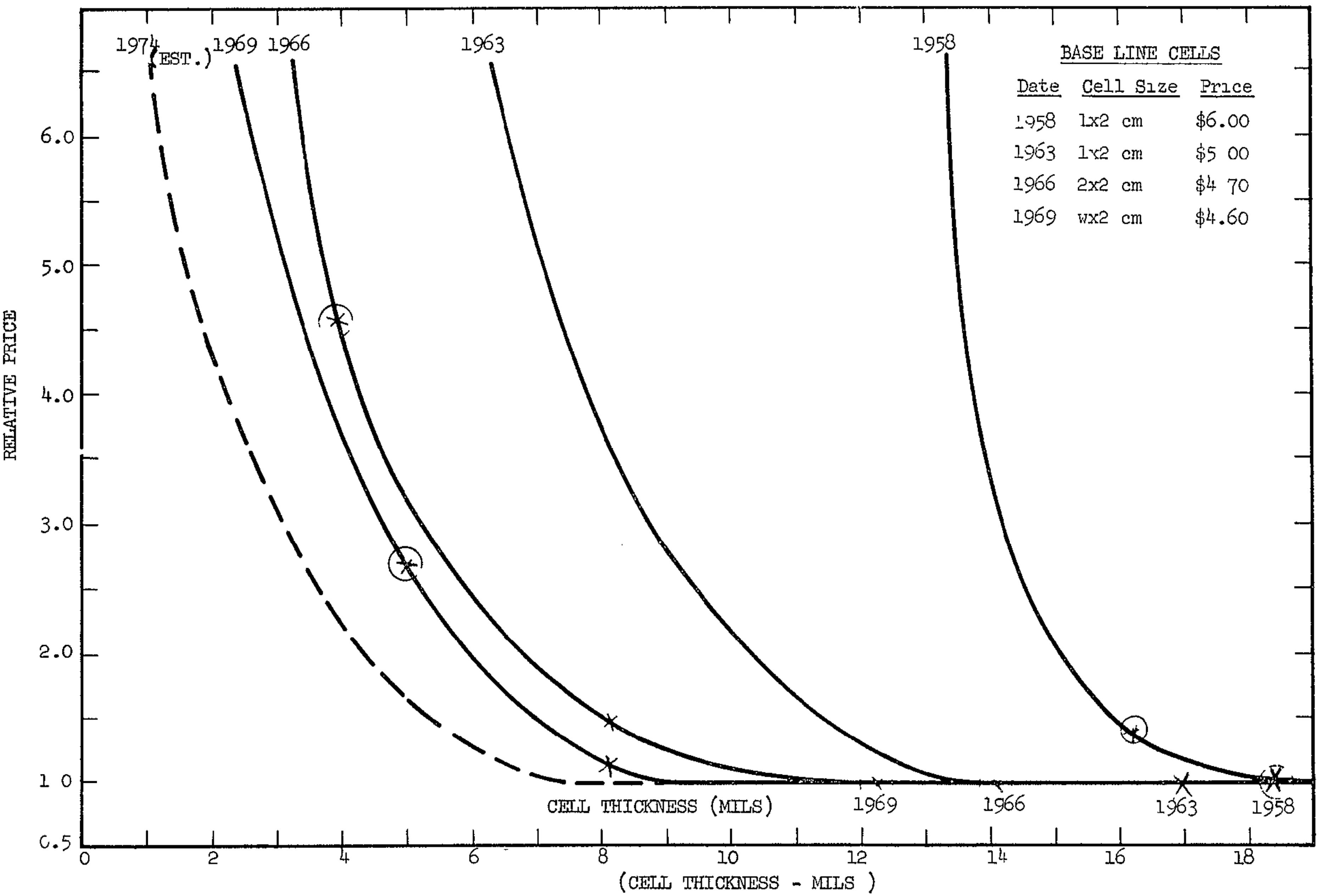

FIGURE 2 1-1. CELL PRICE VS THICKNESS FOR PARTICULAR PRICING YEAR.

Several significant historical design changes have taken place and can be used as examples. For instance, the change from P/N to N/P cells, the change from nickel contacts to titanium-silver contacts, the use of thinner cells, and the use of larger area cells. All of these examples had learning curve characteristics associated with the change that reflected in the cell costs. In all cases the initial change resulted in higher costs with a subsequent drop to a base level that was usually close to the initial base level. Some types of cell design changes make a quick recovery, while other changes are more severe and require much time (years) to reach the base level. Figure 2.1-3 shows schematically how these cell design changes typically appear in a cost analysis. For instance, N/P cells had a significant cost impact at first, but soon reached P/N cost levels.

The 8 mil thick cells also had a significant cost impact, but were much slower to approach the thicker cell base line. The large area cells are an example where only a small cost impact was initially seen, then the learning curve was rapid and the costs dropped below the original base line level which was set at the low price value for the 12-14 mil 2 x 2 cm cell. The wraparound cells are presently following a very slow learning curve, however, it is unknown whether this may be due to lack of interest or due to basic cost factors. In any case, it is apparent that future cell design changes will follow these basic cost patterns and they must be characterized and predicted for any new cell design utilized in a cost analysis of new arrays.

If new cell design cost considerations (such as large area and wraparound contact cells) are combined with the thickness effects, we get a schematic curve such as that shown in Figure 2.1-4. Both large area cells and wraparound cells are of interest for this lightweight array study and are shown in this figure. In this plot the 1974 projected values show that the thin large area cells are more expensive

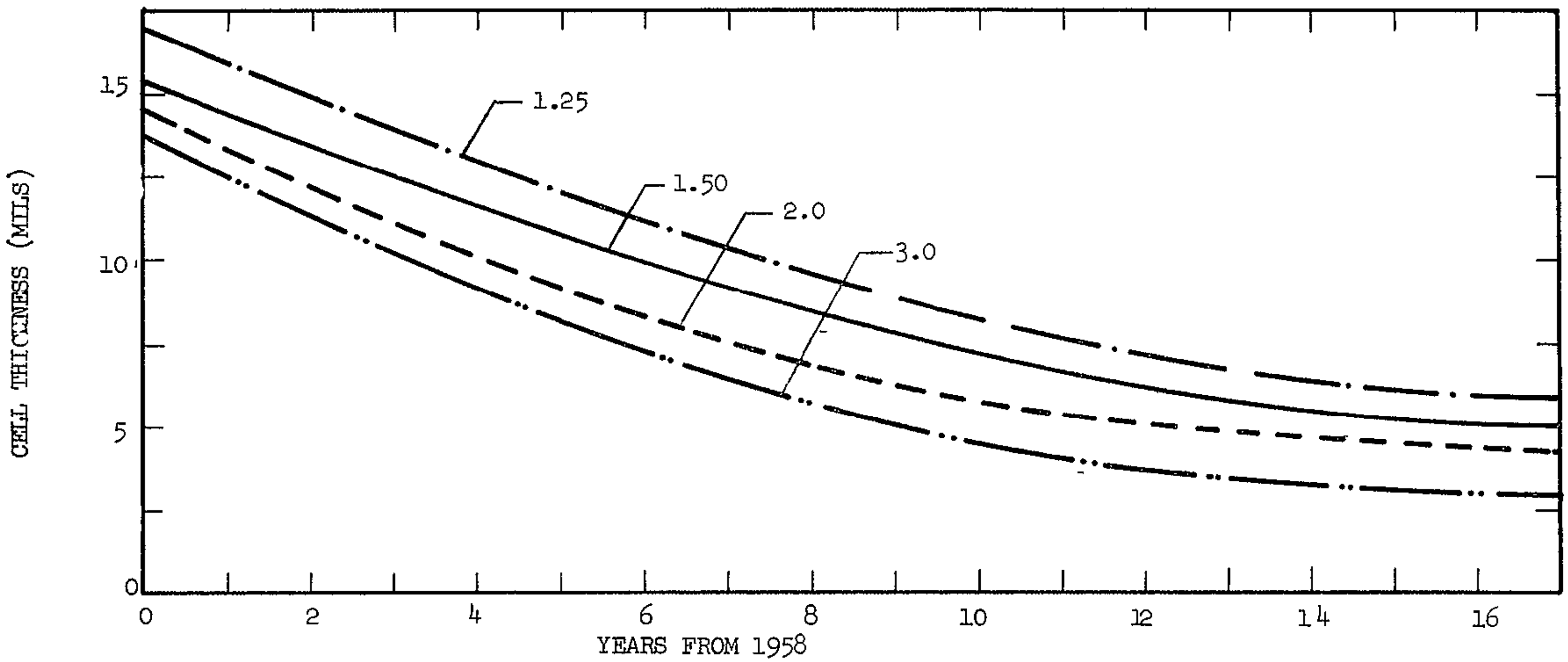

FIGURE 2.1-2 THICKNESS VS TIME FOR A FIXED RELATIVE CELL COST DATA USED TO GENERATE 1974 COST ON FIGURE 2.1-1.

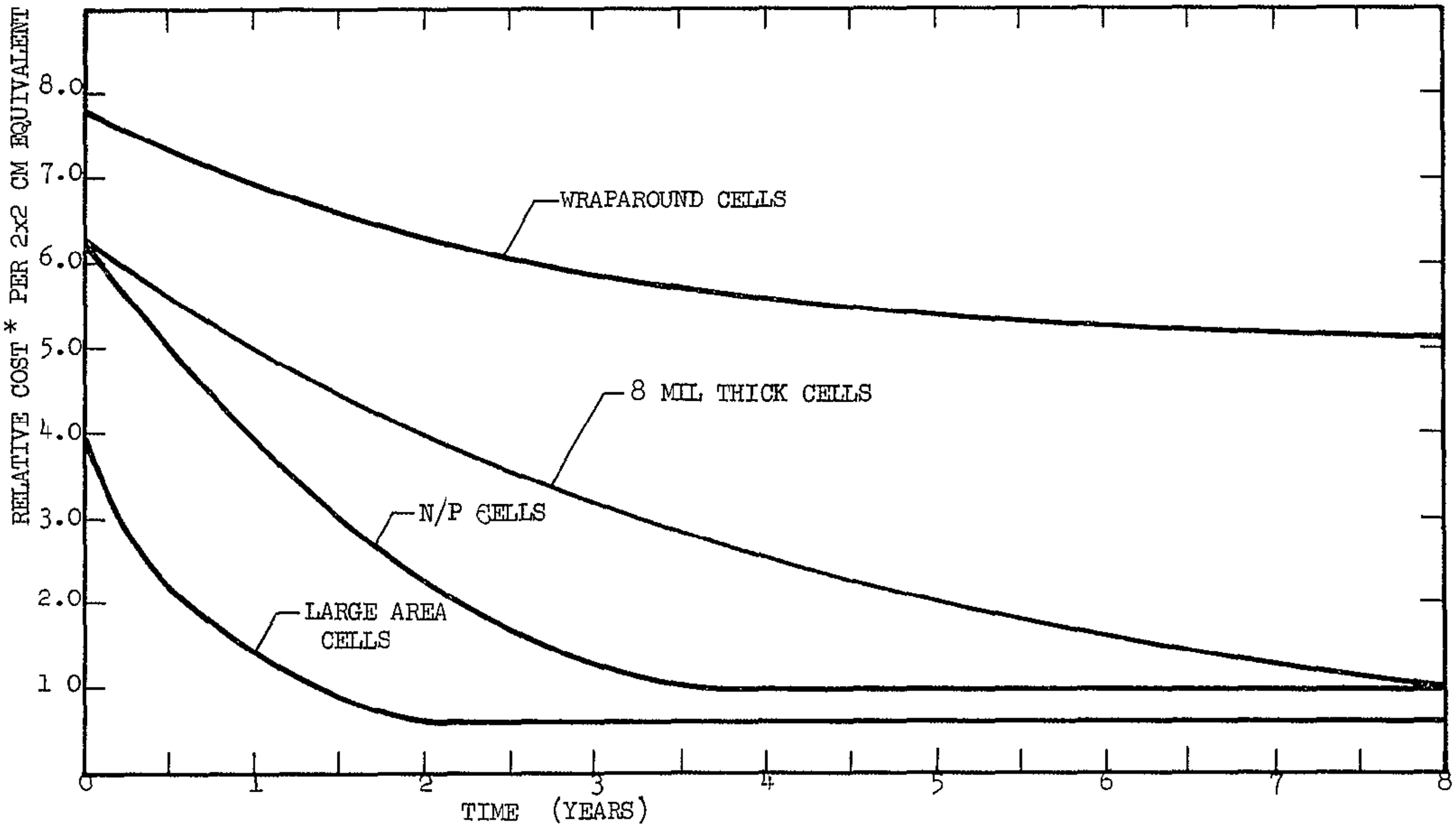

* Relative to base line cell price
for that time.

FIGURE 2.1-3. RELATIVE CELL COST VS TIME

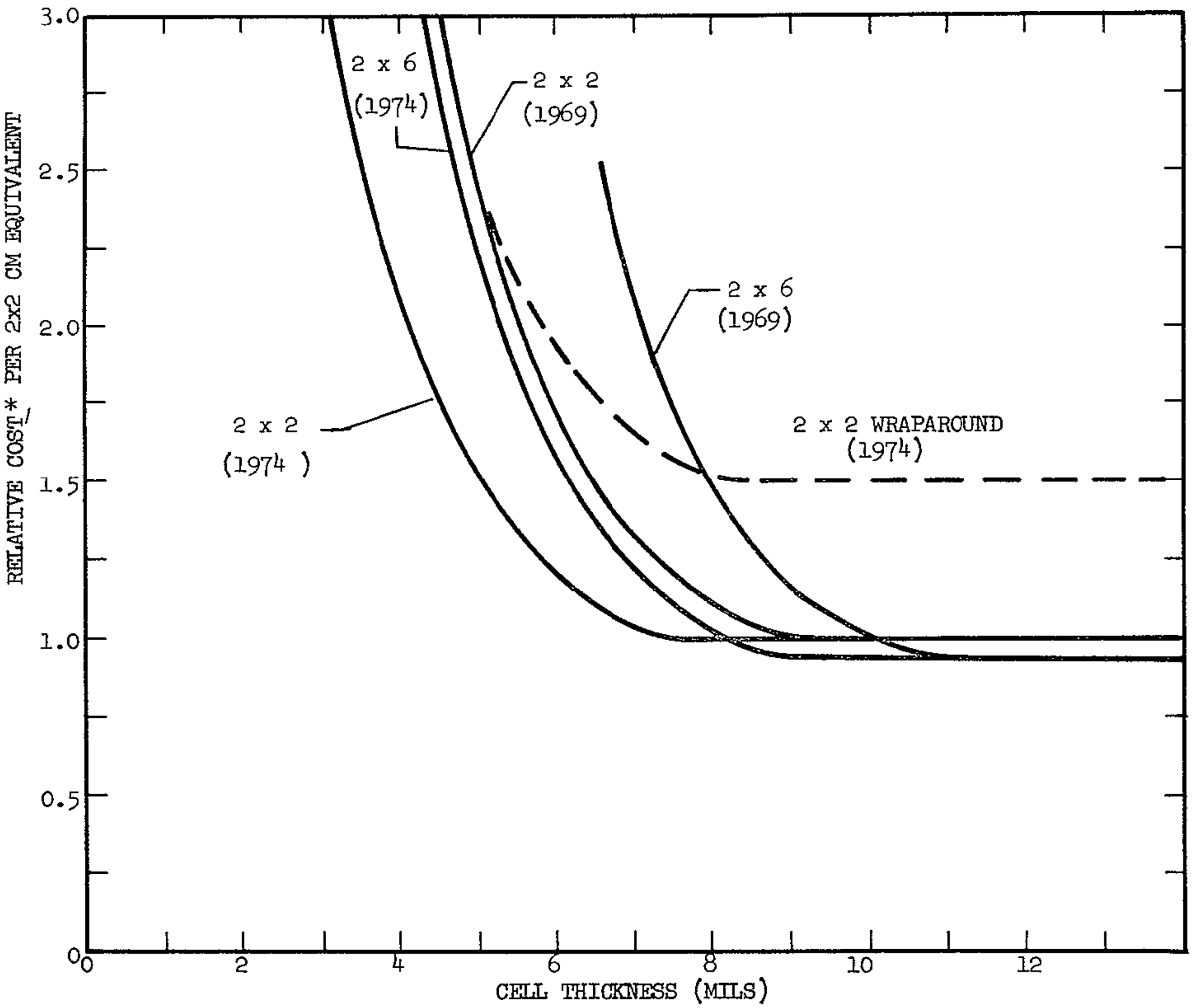

FIGURE 2.1-4. POWER/WEIGHT/COST VS CELL THICKNESS

*RELATIVE TO BASE LINE
CELL (2x2) PRICE FOR
THAT TIME

than the thin 2 x 2 cm cells while the thicker large area cells are less expensive. The wraparound cells are shown to be more expensive than both other cell types in 1974, although this picture is likely to change if an extensive effort were placed on developing this type of cell.

If the results of the data in Figure 2.1-4 are incorporated with the cell performance data[1] for each type of cell, the outcome of this analysis is exhibited in Figure 2.1-5. This figure shows the relative power/weight/cost data for various types of cells as a function of cell thickness. A curve representing present-day conditions and one for estimated conditions in 1974 are shown. These are again normalized to the present-day 12 mil cell. The present-day curve indicates that the 8 mil cell is optimum, with a shift to the 6 mil cell in approximately 4 to 5 years. Again, since the newer type cell prices reflect the requirement of a learning period, any increase or decrease in emphasis of effort in these areas will greatly effect the period of time required before they reach the base line conditions and become straightforward production items. Table 2.1-1 is a summary of data presented in previous illustrations to emphasize progress in cost reduction.

---

[1] Performance of Very Thin Silicon Solar Cells, E. L. Ralph, Sixth Photovoltaic Specialists Conference, Cocoa Beach, Florida, March 1967

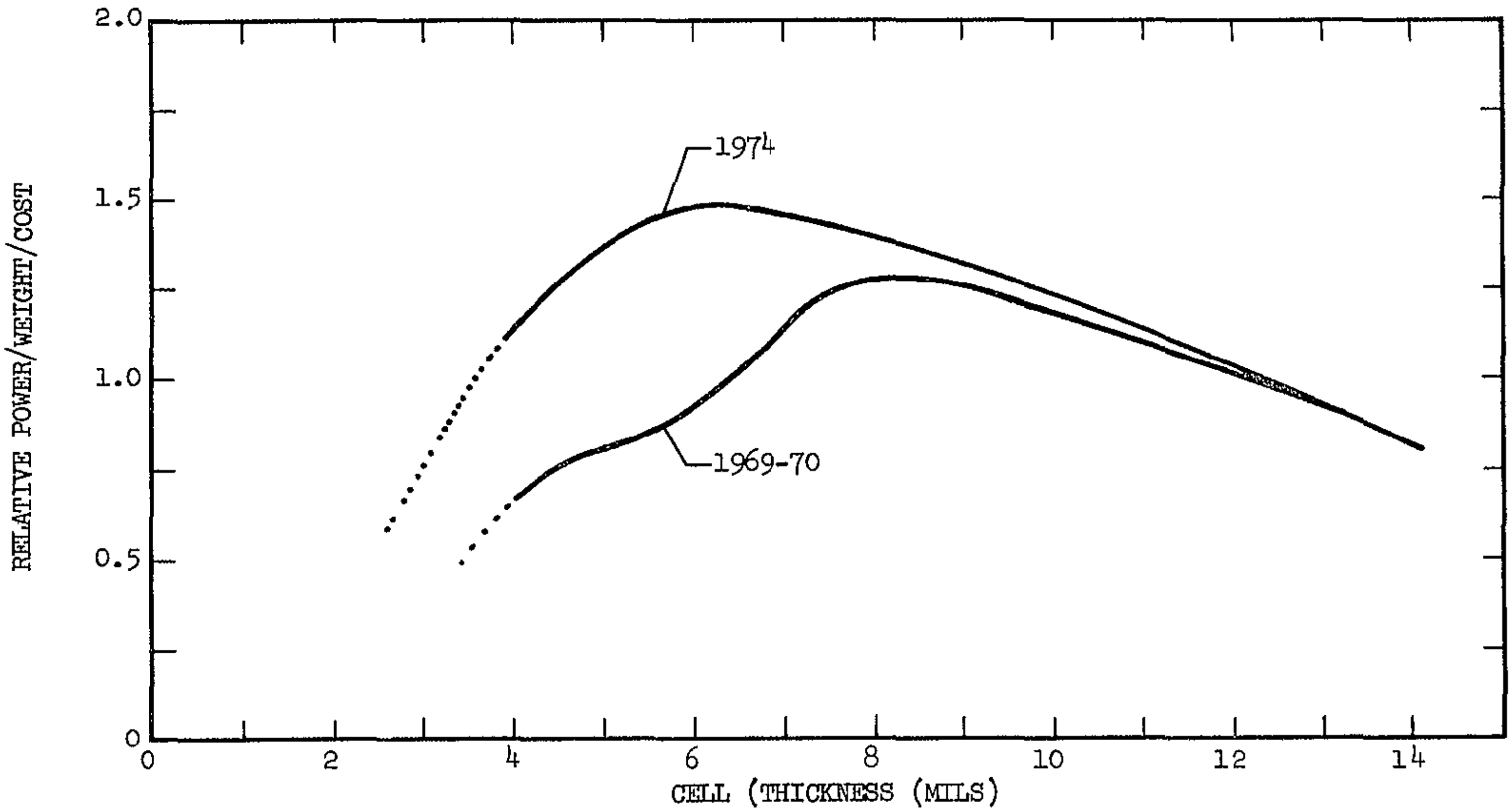

FIGURE 2.1-5. POWER/WEIGHT/COST
NORMALIZED TO 12 MIL CELL = 1.0

TABLE 2.1-1

POWER TO WEIGHT VS THICKNESS

BARE CELLS 2 OHM-CM

CELL THICKNESS (MILS)	POWER/WEIGHT	1969		1974 (ESTIMATE)	
		RELATIVE COST	RELATIVE POWER/WEIGHT/COST	RELATIVE COST	RELATIVE POWER/WEIGHT/COST
12	95.3	1.0	1.0	1.0	1.0
8	135.3	1.1	1.29	1.0	1.42
6	170.2	1.9	.94	1.2	1.49
4	242.2	3.55	.72	2.2	1.15

2.2 COVERSLIDE ASSEMBLY STUDY

The object of this segment of the integrated array study was to develop an inexpensive lightweight solar cell cover system.

A comprehensive cost analysis of various types of solar cell cover systems was performed to determine the variables that affect cover costs. The purpose of the study was to supply information for a cost effectiveness analysis and did not include an analysis of the design parameters such as light transmission characteristics of quartz and 0211 microsheet, the properties of various filters, or the shielding properties of various material thicknesses.

2.2.1 Coverglass Material Costs

The cost of the cover is essentially determined by the cover substrate material used, the type of optical coating and filter applied to the cover, and the tolerances on the dimensions of the cover, i.e., length, width, and thickness.

Currently there are two materials that are typically used, these are Corning Glass Works #7940 fused silica, and Corning Glass Type 0211 microsheet. For applications requiring a cover with an AR coating and a blue cuton filter there is 100 percent price penalty for similar cover thicknesses if fused silica is employed instead of the 0211 microsheet. This price differential is primarily due to the fact that the fused silica must be sliced from a block of solid material, then lapped and polished. The microsheet, which is available in the desired thickness in 13 x 14 inch panels, is merely rough-cut, bonded together in stacks and cut to size. The principle price increase is due to the additional labor involved in preparing the silica covers which is accompanied by a modest difference in basic material cost. The basic material costs are quite small. The manufacturer's 1965 price of 0211 microsheet was $1.35 for a sheet 13 x 14 inches 0.006 inch thick, and $1.20 for a sheet 13 x 14 inches 0.003 inch thick. If 100 percent utilization of a sheet could be achieved, material costs for a 2 cm x 2 cm 0211 cover would be only about one penny.

Three different and distinct solar cell thin film interference-type optical coatings are available. They are the antireflective coating, the ultraviolet reflecting filter, and the blue-red filter. The blue-red filter is essentially a heat reflecting filter which transmits maximum energy in a bandwidth corresponding to the spectral response curve of the solar cell. Since current pricing data was not made available for the various coatings as separate items, coverglass pricing information was developed from historical data. The filter cost data presented in Figure 2.2-1 was obtained from quotations during the period 1967-1969 and is assumed to be representative of current trends. This figure shows price variations as a function of the type of coating applied to the cover substrate. To facilitate cost effectiveness studies, the base line of zero in Figure 2.2-1 was selected to correspond to the most commonly used coverglass filter design (i.e., AR plus blue cuton). Figure 2.2-2 shows the coverglass price with an AR coating and a blue filter on the platelet. Therefore, this corresponds to the base line (or zero line) on Figure 2.2-1. If the filter is changed to either AR only or AR plus blue-red the values in Figure 2.2-1 must be added to the values in Figure 2.2-2. For example, if a 2 x 2 cm 0.006 inch thick microsheet cover with an AR coating and a blue filter costs $1.00, a similar cover with an AR coating but with a blue-red filter would cost the $1.00 base price plus an additional $0.30 to $0.40 depending upon the quantity and the quality specifications. The coating prices in Figure 2.2-1 also must be increased in relation to the number of 2 cm x 2 cm size equivalents for larger area covers.

The third set of parameters which influences solar cell cover prices is the tolerance on the cover dimensions, principally length, width, thickness, and edge/corner chip specifications. Typical dimensional tolerances are ±0.003 inch on length and width and ±0.001 inch on thickness. Tightening of a tolerance slightly, will increase the cover base price by 5 to 10 percent. Nominal edge and corner chip

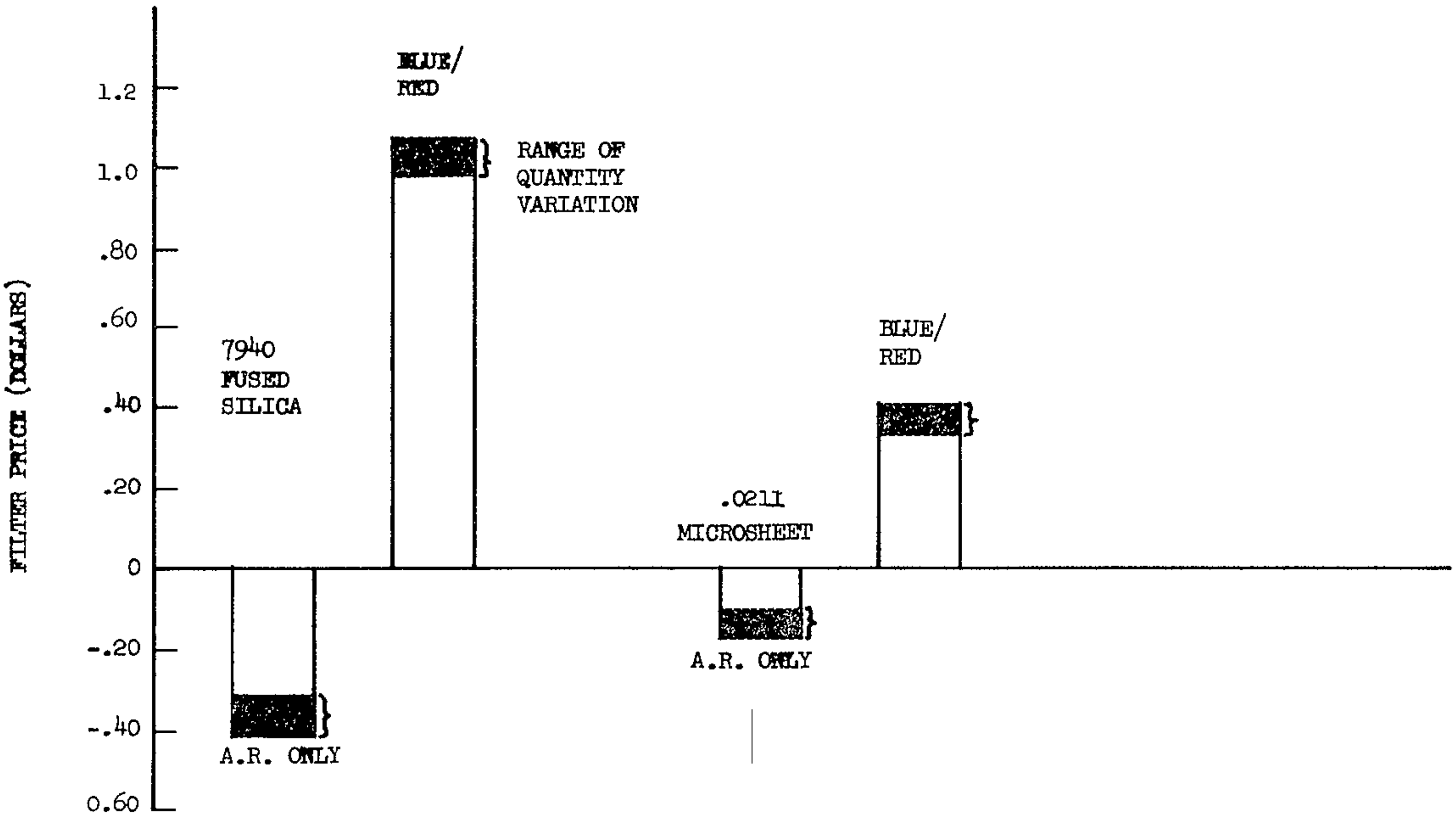

FIGURE 2.2-1 PRICE OF VARIOUS FILTER TYPES ON SOLAR CELL COVERS. BASELINE IS A BLUE FILTER PLUS AN A.R. COATING. ALL FOR 2 CM x 2 CM EQUIVALENT AREA.

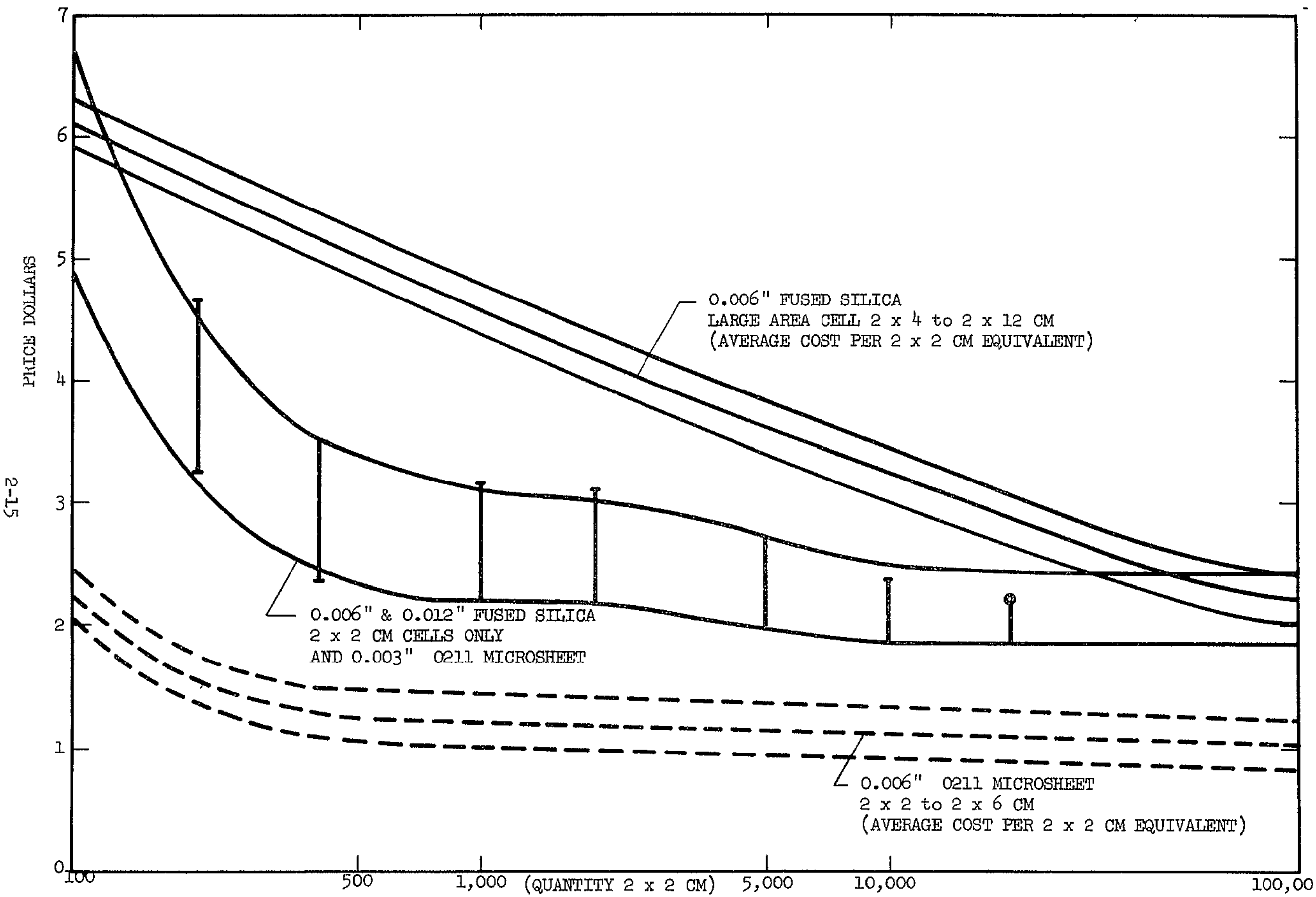

FIGURE 2.2-2 SOLAR CELL COVER PRICE. ALL COVERS HAVE A.R. COATING AND BLUE REFLECTING FILTER FOR THE PERIOD 1967-69

specifications are 0.010 inch maximum projection into the face of the cover. Tightening of this nominal tolerance will cause another 5 percent in the price of a cover. Relaxation of the tolerances and physical characteristics similarly will result in a corresponding cost reduction.

The price of various solar cell covers from the 1967-1969 data is presented in Figure 2.2-2 which illustrates the effect of size, thickness and material type on the price of a cover. Furthermore, each category is represented by a broad curve which indicates the price range resulting from loose and tight specifications governing size and chip tolerances. The cover prices are also based on an equivalent 2 x 2 cm area, therefore the price of a large area cover must be determined using the area factor and the proper curve. The area enclosed by the center curves represent the price range of three types of substrate. The 0.006 inch and 0.012 inch thick fused silica costs are similar because of material cost and yield trade off. The 0.003 inch thick 0211 microsheet price is due primarily to handling difficulties and lack of large quantity yield data. Once sufficient experience is accumulated, the cost of the 0.003 inch 0211 microsheet can be expected to be between the cost value of fused silica and the 0.006 inch thick 0211 microsheet.

2.2.2 Coverglass Installation Costs

The major portion of the solar cell installation cost is generated by direct labor and is a function of specification requirements. The most important considerations in determining installation prices are thickness of the cover (because of breakage), cover-to-cell location tolerances, and the type of cover bonding adhesive used. It is therefore difficult to establish an exact price relationship for the numerous combinations which could be evolved. The cover thickness influences the price primarily due to the more sophisticated handling equipment and techniques required for thinner covers, particularly with the 0.003 inch thick covers. Extreme care must be exercised especially during the cleaning and cementing steps. Handling of the thin covers usually necessitates the use of vacuum probes. This is an inherently slower procedure with a high resistance to automation.

Positioning or indexing a solar cell coverglass during the bonding process has become a very precise operation because of the requirements of the "zero gap" configuration. This concept requires 100 percent coverage of the solar cell active area. The increased cost of the "zero gap" cover is due to the higher cost of the necessary precision tooling needed for indexing. Additional costs are also incurred by the higher reject and rework rate and more stringent in-process inspection.

The final consideration is the type of adhesive used to bond the cover to the solar cell. The most commonly used adhesives are Epocast 15E, RTV602, Sylgard 182, and Dow Corning XR63-489. The RTV602 is the most economical because of the ease of handling, cleaning, and replacing coverglasses. When 15E is used, repair is not practical because of the high bond strength. The Sylgard 182 and XR63-489 are almost identical in properties, but excess adhesive is difficult to remove due to their hardness and high tensile strength. Since it would be impossible to establish prices for all of the possible cell cover lay-down parameters, the cost data generated in this study is based upon diametrically opposed requirements covering the two extreme conditions (or degree of difficulty) experienced in applying solar cell covers.

The least expensive approach utilized loose cell and cover dimension tolerances, an inexpensive 0211 microsheet substrate, and the easily applied RTV602 coverglass adhesive. In the more difficult and costly approach, tight cell and coverglass tolerances, a #7940 fused silica substrate, extremely rigid ("zero-gap") cover placement tolerances, and the most costly adhesive (XR6-3489) were assumed.

Figure 2.2-3 indicates the approximate range of installation prices for various cover thicknesses as a function of the quantity installed. The price includes typical burdened labor and a nominal breakage allowance. The curves were based on prevailing prices in effect during the period 1967 to 1969. The upper and lower limits for each type c cover correspond to the two expenditure limits described above.

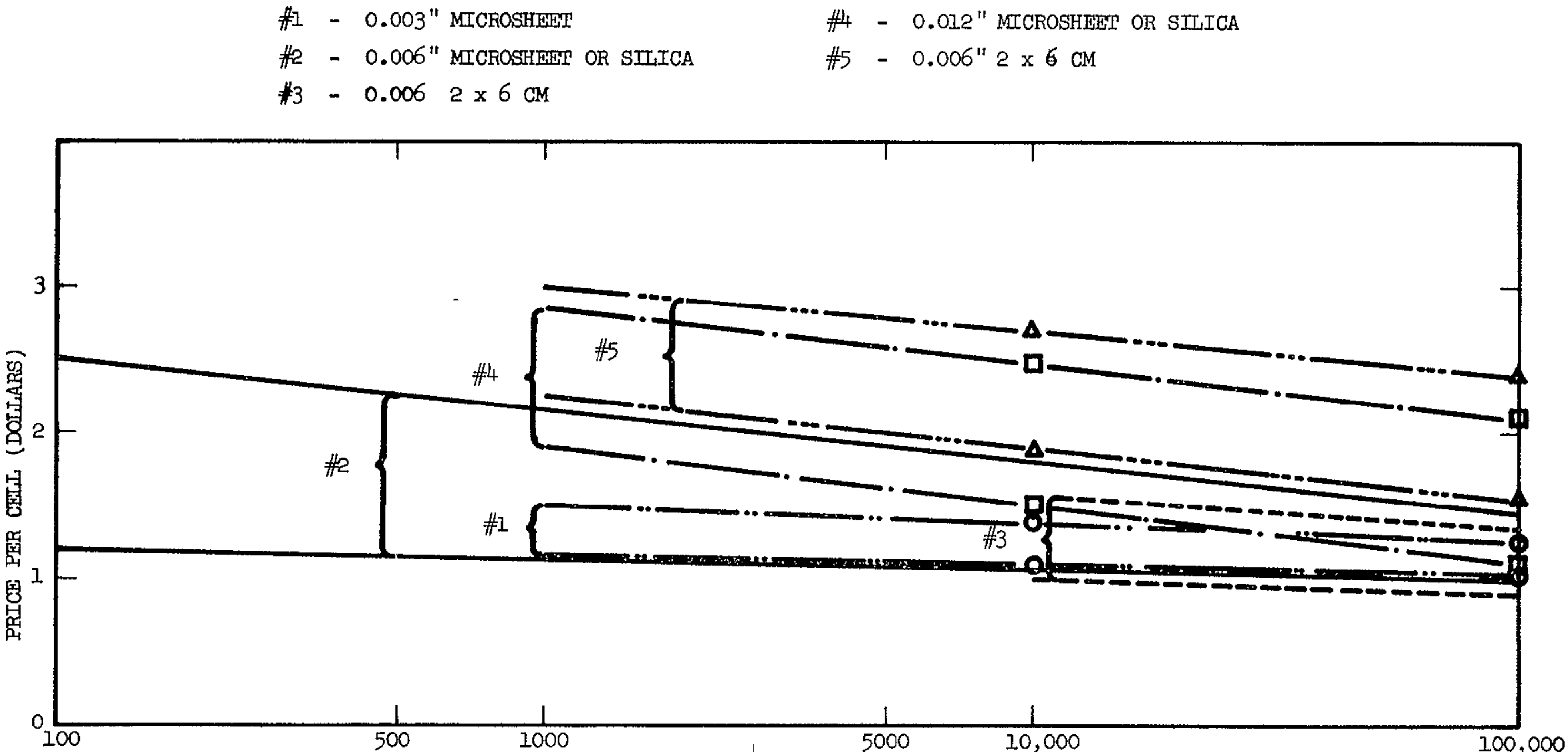

FIGURE 2.2-3 INSTALLATION PRICE* OF VARIOUS TYPES OF SOLAR CELL COVERS VERSUS QUANTITY.

*Spread in price represents variations due to tight and loose fabrication tolerances.

To illustrate the use of the three pricing figures discussed above in performing an engineering trade-off cost analysis, assume that a 0.006 inch thick cover is necessary as a shield due to the radiation environment. Consider a quantity of 50,000 2 x 2 cm cells. Do not include in this trade analysis other design parameters such as power loss due to light transmission losses or temperature effects due to filter type since these characteristics could be defined by another engineering trade-off study. The basic problem can thus be stated What is the cost trade-off for the power levels associated with each filter-coverglass combination? Table 2.2-1 shows a typical price breakdown developed from the three pricing curves by using the following steps.

a. Determine coating cost correction from Figure 2.2-1.

b. Determine upper and lower price for each substrate type from Figure 2.2-2.

c. Determine upper and lower price for tight and relaxed specifications for installation from Figure 2.2-3.

A comparison of the figures in the total cost line provides the means for determining which design parameter will prove to be most economical. Also it shows the impact that cost reduction development efforts will have as a result of decreasing installation costs, eliminating the need for filters, or reducing the cost of the cover material by changing type or mechanical tolerances.

A review of the aforementioned figures gives added impetus to programs directed toward reducing solar cell cover assembly costs. Two of the most promising approaches being considered in this program are the automated ribbon glass process discussed in previous reports submitted under this contract, and the evaporated integral cover. Cost projections indicate that a 0.0013 inch thick cover applied, using the ribbon process should cost about $0.60 to $0.75, and the integral cover may ultimately be reduced to $0.40 or $0.50. Cost savings of this amount will be very significant for large area solar cell arrays containing large numbers of solar cells.

TABLE 2.2-1

PRICE COMPARISON OF COVERED SOLAR CELLS								
COVER MATERIAL	.006" 7940 FUSED SILICA 50,000 PCS.				006" 0211 MICROSHEET 50,000 PCS.			
COVER AND INSTALLATION SPECIFICATIONS	TIGHT		RELAXED		TIGHT		RELAXED	
COATING ON COVER	A.R.ONLY	A.R.& BLUE	A.R.ONLY	A.R. & BLUE	A.R.ONLY	A.R. &BLUE	A.R.ONLY	A.R. &BLUE
COATING COST CHANGE	-.42	0	-.42	0	-.17	0	- 17	0
COVER COST	2 50	2.40	1.73	1 83	1.32	1 25	67	1.85
INSTALLATION COST	1 60	1.60	1.00	1.00	1.60	1.60	1 00	1 00
TOTAL COST	3 68	4.00	2 31	2.83	2.75	2.85	1.50	1 85

2.2.3 Ribbon Glass Coverslide Analysis

The concept of using an ultrathin (0.0013 inch) continuous ribbon of glass for solar cell covers was considered because it offered the advantages of reduced material cost, reduced weight and lower processing labor costs.

Basically the system consists of cleaning the glass and the cell, applying adhesive to the cell, applying the glass to the cell, rolling the glass to achieve a 1 mil adhesive thickness, curing the adhesive and finally trimming the bonded glass to size. This approach was selected because of the handling problems encountered in using the ultrathin glass ribbon.

The analysis was divided into two phases, the first was adhesive selection and application. The second was selection of a suitable glass trimming technique.

Required adhesive properties are

1) Good light transmission
2) Long-term environmental stability
3) Adaptability to automated assembly.

State-of-the-art adhesives that were considered were RTV 602, Sylgard 182, Dow Corning XR6-3489, G.E. SR 585 contact adhesive, and Schjeldahl GT 100 film adhesive, 1 mil thick. The fluid adhesives were applied by spraying both the cell and cover and by applying a metered quantity of adhesive to the cell. The cover was positioned on the cell and then was rolled with a pressure of 500 grams on a one inch wide, one inch diameter roller to achieve the desired thickness of one to two mils and to remove bubbles between the cell and cover. The adhesive was cured at 200°F for 2 minutes prior to trimming. The Sylgard 182 and Dow Corning XR6-3489 proved to be most satisfactory in this study and the metered bead of adhesive method was more satisfactory than spraying.

The second phase of this task was concerned with selection of a glass trimming technique. Three methods of trimming were evaluated during this study. Figure 2.2-4 through 2.2-10 illustrate the type of edges produced by the various methods of trimming. The first method consisted of a Nichrome wire held taut between two spring-loaded insulated posts. Sufficient current is passed through the wire to maintain a temperature of approximately 750°C. The hot wire was passed along the edge of the covered cell edge in a shearing motion to minimize glass buildup on the wire and cell edge. This method of trimming was discarded because of high reject rates due to ragged edges and thermally induced stress cracks in the glass covers.

The second and most successful method consisted of a high velocity jet of abrasive particles 25 microns in diameter at a pressure of 40 pounds per square inch using a gun with a nozzle size of 0.006 x 0.060 inches. In the hands of an experienced operator, this technique had an acceptable reject rate. This method was subsequently selected for use on the demonstration module.

The third method evaluated consisted of scoring the glass at the cell edge with a diamond scribe with a 1/2 to 1 mil radius point and a pressure of 30 grams. Immediately after scribing the glass was bent and broken along the scribed line. This method shows good possibilities but requires a substantial investment in time and tooling to be feasible.

2.2.4 Coverglass Cost Comparison

This section of the final report presents detailed cost analyses for the ribbon glass and integral cover systems. A final summary then compares these values with the costs of the conventional microsheet and fused silica platelet systems discussed in Section 2.2.2.

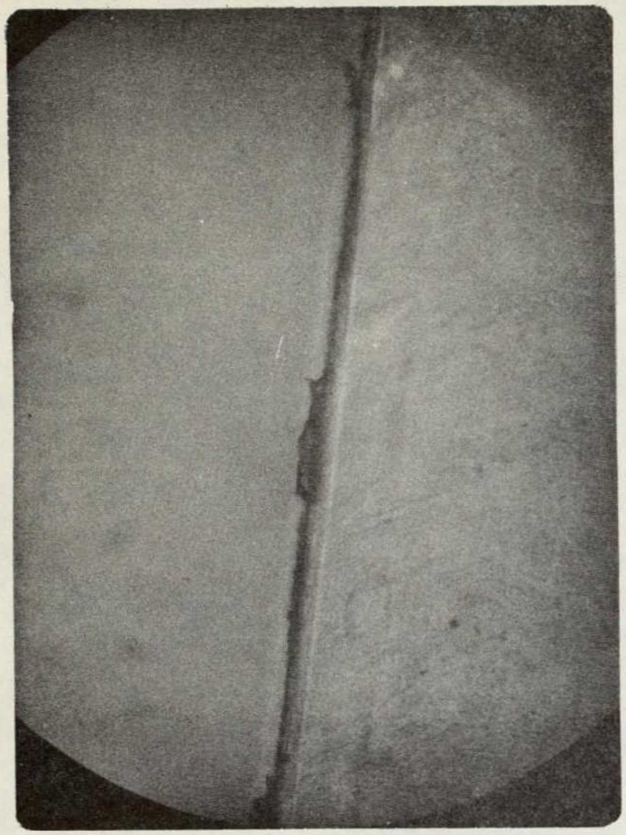

Figure 2.2-4 ACCEPTABLE HOT WIRE TRIMMED (50x) CELL ON RIGHT SIDE

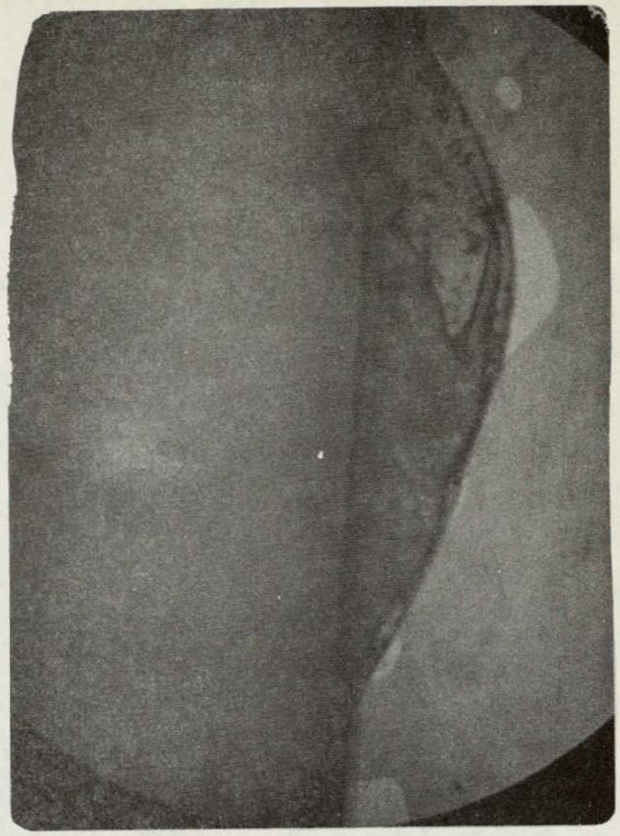

Figure 2.2-5 UNACCEPTABLE HOT WIRE BECAUSE OF GLASS CHIP (50x) CELL ON RIGHT SIDE.

Figure 2.2-6 BUBBLE CAUSED BY OVERHEATING (50x) CELL ON RIGHT SIDE.

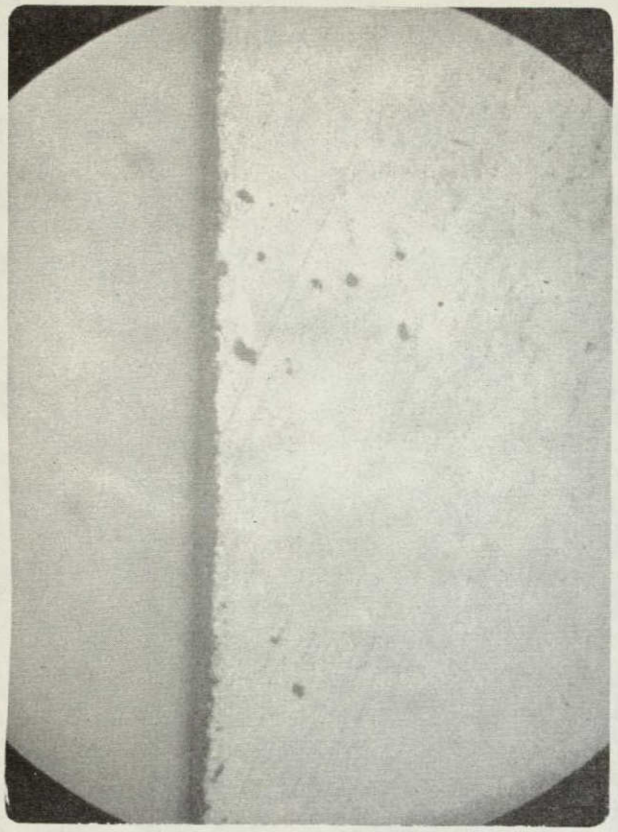

Figure 2.2-7 ACCEPTABLE ABRASIVE CUT (50x) CELL ON RIGHT SIDE.

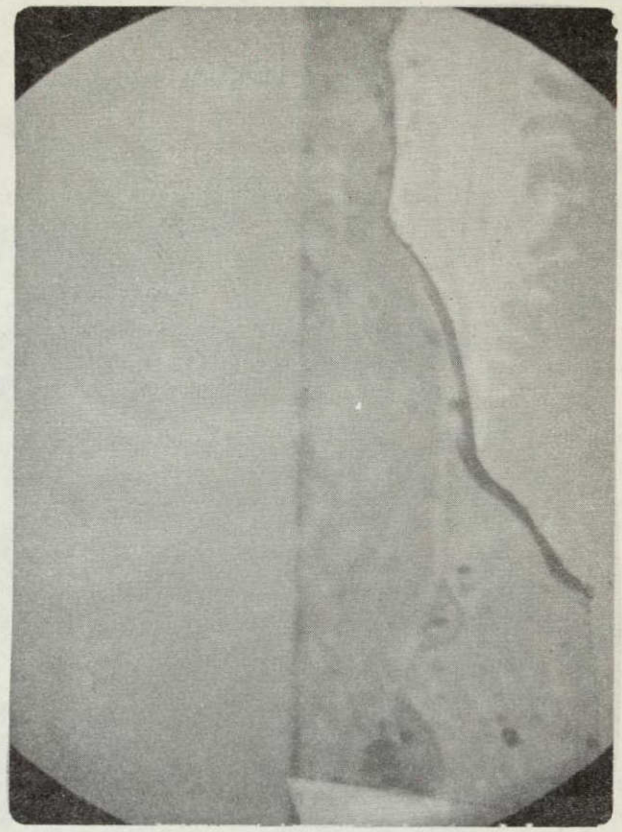

Figure 2.2-8. UNACCEPTABLE ABRASIVE CUT (50x) CELL ON RIGHT SIDE.

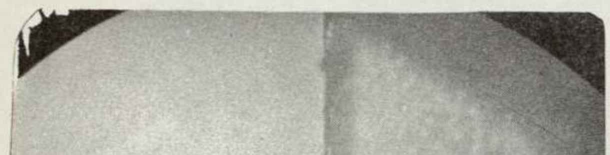

Figure 2.2-9. ACCEPTABLE SCRIBED BREAK (50x) CELL ON RIGHT SIDE

Figure 2.2-10. UNACCEPTABLE SCRIBED BREAK (50x) CELL ON RIGHT SIDE.

2.2.4.1 Ribbon Glass Solar Cell Cover Costs

In this analysis the cost per 2 x 2 cm solar cell 0.014 inch thick has been based on a production quantity of 500,000 solar cells per year. Initial tooling and machining costs of $60,000 were amortized over this production quantity. A cost breakdown is shown in Table 2.2-2 for the coverglass and the installation. This table shows that a price of about $0.62 would be expected for this ribbon glass cover system. No ultraviolet rejection filter is considered, since the glass would be the 0211 type, which has an absorption region in the ultraviolet that protects the adhesive. Also, no antireflection coating is considered for the glass so that this system could be compared directly with the integral coverglass system.

2.2.4.2 Integral Cover System Cost

A significant amount of effort has been devoted to producing a low cost solar cell cover which would be bonded directly to the solar cell without the necessity of using any adhesives. Several methods, including a fused glass slurry, thermal decomposition of silanes, sputtering, and high vacuum electro-beam deposition have been investigated at various laboratories. Heliotek has reported success in the use of high vacuum electron-beam technique. The cost analysis presented in this report is based upon a linear scale-up of existing equipment to produce a quantity of 500,000 cells in one year. Table 2.2-3 gives a cost breakdown for depositing an integral cover of 1 to 2 mils in thickness on 2 x 2 centimeter size solar cells. The glass to be evaporated would be Corning type 1720 glass which has exhibited acceptable resistance to ultraviolet and high energy particle radiation. In general, the 1720 type glass possesses all of the environmental characteristics necessary for an integral solar cell cover.

TABLE 2.2-2. RIBBON GLASS COST ANALYSIS

		Yearly Cost	Cell Cost
Labor	3 Technicians at $3.00 an hour	$18,000	$0.036
O/H at 150%		27,000	0.054
		45,000	0.090
Equipment		60,000	0.120
		105,000	0.210
Material	$1.00 per lineal foot 50% yield	80,000	0.160
			0.370
10% Contingency on above			0.037
			0.407
10% G&A			0.041
			0.448
10% Fee			0.045
			0.493
Price for covering cell with a yield of 80%			$0.617

TABLE 2.2-3

INTEGRAL COVER PROCESS

COST ANALYSIS

			Production Basis 500,000 cells/year Cost per cell	
1.	Direct Labor 12 Technicians	RATE $2.00/hr; HOUR 24,000; EXTENDED $48,000	$0.096	
2.	Overhead 150% D I.	1.5 x $0.096	$0 144	
3	Equipment - 4 chambers at $15,000/unit = $60,000	$\frac{\$60,000}{5 \times 10^5 \text{ cells}}$	$0.120	
4.	Material $6.50/lb	$\frac{25 \text{ lb.}}{\text{run}} \times \frac{5000 \text{ runs}}{5 \times 10^5 \text{ cells}} \times \frac{\$6.50}{\text{lb}}$	$0.017	
			$0.377	SUBTOTAL
5.	Contingency 10% #1 thru 4	0.1 x $0.377	$0.038	
			$0.415	SUBTOTAL
6.	G & A 10%	0 1 x $0.415	$0.042	
			$0.457	SUBTOTAL
7.	Profit 10%	0.1 x $0.457	$0.046	
			$0.503	SUBTOTAL
8.	Yield 90% Estimated	$\frac{\$0\ 503}{9.9}$	$0.56	TOTAL PRICE/CELL

2.2.4.3 Cover Cost Summary

Table 2.2-4 shows a summary comparison of the price of the three alternate types of cover. The prices of the various types have been selected from the previous cost analysis studies such that they are as equivalent in their characteristics as possible, to provide a common base for comparison purposes. The following conditions were used to provide this common base and specify the solar cell cover system.

a. Dimensional Tolerance Tight, zero-gap concept with the cover flush or with a 3 mil overhang on three edges of the cell. No exposed area between the cover and ohmic strip with a maximum of a 5 mil overlap of the cover on the ohmic strip.

b. Surface Treatment or Cover Coating Magnesium fluoride anti-reflective hard coating.

c. Blue Reflecting Filter None.

d. Cover Material

Conventional	Fused silica and 0211 Microsheet
Integral	Evaporated Corning Glass Type 1720
Ribbon	Corning Glass Type 0211

e. Quantity 500,000 pieces to be produced in a one-year period. The conventional cover prices presented in the second quarterly report have been reduced by 3 percent to reflect the change in quantity from 50,000 to 500,000.

As the Table 2.2-4 clearly shows, the integral and ribbon glass concepts offer a significant ($\approx$ 70%) reduction in the cell cover cost. This potential cost advantage in large area arrays clearly indicates that such concepts would provide a dramatic reduction in total array cost.

TABLE 2.2-4 COMPARATIVE COVER COSTS

	Integral	Conventional Fused Silica	Conventional Microsheet	Ribbon
Material	$0.02	$2.04	$0.78	$0.16
AR Coating	$0.30	$0.30	$0.27	$0.03
Installation Labor (Burdened)	$0.54	$1.15	$1.39	$0.46
Total Cost	$0.86	$3.49	$2.44	$0.65

2.3 INTERCONNECTOR STUDY

The examination of the silicon solar cell array interconnector was not intended to principally improve the array power to weight rates or cost factor. Although these weight and cost criteria provided general design guidelines, the major interconnector analysis effort was undertaken so as to improve system reliability for lightweight flexible arrays. This was to be done by a series of analyses and tests providing information which would ensure interconnector integrity through prolonged periods of thermal cycling and vibration without requiring excessive weight or cost increases.

The following outlines the approach undertaken to provide a reliable interconnector system. Although this does not necessarily represent the chronological sequence of events, it does provide a logical and continuous sequence.

1. Definition of interconnector failure modes.
2. Expected peculiarities of rigid and flexible arrays.
3. Flexure fatigue analysis and tests.
4. Thermally induced stresses at the interconnector-silicon bond, analyses and tests.

2.3.1 Common Failure Modes

The most common failure modes encountered during launch and throughout mission life are open circuits due to

1) Interconnectors stressing silicon beyond the ultimate strength
2) Interconnect being stressed beyond ultimate strength
3) Interconnect fracture due to fatigue
4) Solder joint fracture due to fatigue

The remêdy for items 1) and 2) is to design a stress relief in the interconnector so that excessive stress levels in the interconnector and at the interconnector bond joint are removed. Practically speaking, where the stress relieving, such as the conventional Z tab stress relief loop, is employed, failures of exceeding ultimate strengths are eliminated. If stress relieving is not practical, due to spatial limitations for example, then the designer is required to provide interconnector systems which will withstand all direct stress levels. In such a case it is also necessary to consider fatiguing incurred through cyclic stress inducing environments. Again, in the case of stress relieved systems, although items 1) and 2) can safely be eliminated it will be necessary to consider the possibility of system fatiguing due to cyclic motions of the stress-relieving member. The fatigue analyses must also extend to the interconnector bond joint which will experience cyclic stressing induced by the relation of thermal excursion and the various coefficients of thermal expansion for the components of the bond-interconnector, solder, and silicon.

Since excessive direct stresses can and have been successfully eliminated through the use of stress relieved interconnectors, the Heliotek interconnector analysis was specifically oriented towards solving the problem of designing flexure fatigue resistant systems. This does not mean that failure modes 1) and 2) are trivial, but rather, that good fatigue resistant interconnectors should also exhibit freedom from the first two failure modes and that the overstress failures exhibit themselves rather quickly in any qualification testing. The next section briefly examines the effects of rigid and flexible arrays on stress distribution.

2.3.2 Array Effective Spring Rate

Forces applied to a solar cell array are distributed between the substrate and the metal interconnections in proportion to the spring rates K of the interconnector and the substrate. For conventional arrays the substrate is usually a honeycomb structure made with a

skin of aluminum about 0.010 inch thick. The more advanced designs utilize only a 0.001 inch thick polyimide film. For a force distribution analysis the substrate will be assumed to be continuous with cells mounted on it. The metal interconnects that tie the cells together are assumed to have no expansion loops.

The spring rate K is given as $\frac{F}{D} = \frac{btE}{L}$

where

D = deformation in material

F = applied force

t = material thickness

b = material width

L = length of the material

E = modulus of elasticity

A gap of 0.017 inch between cells of 0.788 x 0.788 inch size will be assumed. This corresponds to an L of 0.788 plus 0.017 or 0.805 inch for the substrate. The total interconnector width of 0.100 inch and a thickness of 0.002 inch will be examined. The spring rate for each element of concern is then as follows

$$K_{\substack{\text{polyimide}\\ \text{substrate}}} = \frac{(0.788)\ (0.001)\ (4.3 \times 10^5)}{0.805} = 4.2 \times 10^2$$

$$K_{\substack{\text{aluminum}\\ \text{substrate}}} = \frac{(0.788)\ (0.010)\ (10.5 \times 10^6)}{0.805} = 1.0 \times 10^5$$

$$K_{\substack{\text{aluminum}\\ \text{interconnector}}} = \frac{(0.100)\ (0\ 002)\ (10.5 \times 10^6)}{0.017} = 1.0 \times 10^4$$

Any force applied to the array structure will be distributed in the ratio of the element spring rates. Therefore, in the aluminum substrate case the force distribution will be

$$\frac{K_i \text{ Interconnector}}{K_s \text{ Aluminum substrate}} = \frac{1.0 \times 10^4}{1.0 \times 10^5} \simeq \frac{1}{10}$$

So the substrate essentially carries the load. In the polyimide sugstrate case, the force distribution will be

$$\frac{K_i \text{ Interconnector}}{K_s \text{ Polyimide substrate}} = \frac{1.0 \times 10^4}{4.2 \times 10^2} \cong 24$$

so the substrate stretches and distributes the load to the interconnect significantly increasing stresses in the interconnector. This last case is a highly undesirable situation since the ultimate loads for these thin interconnectors is low, and a more important consideration is that it is an unreliable design that requires the member providing the electrical integrity to also provide the structural integrity. In order to minimize the problem, a stress-relieving loop is utilized in the interconnector so that the K_1 is reduced to a negligible value. The size of the stress loop required will be dependent upon the inter-cell spacing change anticipated. The cell spacing will change as a result of applied forces on the substrate during deployment, from thermal expansion, and from vibrational forces.

The different spring rate ratios indicate that array behavior under applied forces will be quite different for the rigid and flexible cases. Recalling that vibrational motions accelerating the relatively massive solar cell assemblies will be describable in terms of forces, it is important that the vibrational effects be examined thoroughly. In fact, investigation of the effect of vibrationally and thermally induced array motions show that the rigid and flexible arrays behave quite differently. The rigid array is actually more sensitive to thermal motions (see next section) and less sensitive to vibration, whereas the flexible array is more sensitive to vibration and less sensitive to thermal motions. The vibrational sensitivity of the flexible array is directly related to the above spring rate discussion. And its insensitivity to thermal motions follows from its non-rigidity and better matched thermal expansion between the substrate and inter-connector. Again, these thermal analyses are described in the next section. It is sufficient that different behavior of flexible arrays and rigid arrays be recognized as requiring that the previously industry utilized rigid array interconnection techniques may not be directly applicable to the lightweight flexible arrays.

2.3.3 Flexure Fatigue Analysis and Tests

The flexure fatigue of a stress relieved interconnector will depend on the magnitude of interconnector flexing and the number of such occurrences. These motions are in turn dependent upon the array configurations and environmental exposure. The effective array properties which can affect the array motions during vibration and thermal cycling include coefficients of thermal expansion, relative cross section, moduli of elasticity and mass distribution. Analyses of array motions should consider thermal expansion effects and vibrational effects. However, the complexity of vibrational problems, requiring knowledge not only of the applied environment but of the array configuration and mass distribution, limits our analyses to the significantly simpler case of thermal expansion. This is the approach that was initially conducted in determining typical array motions, and, hence, interconnector flexing.

Thermal expansion effects can be described by one of two models shown in Figure 2.3-1. Case I is typical of the polyimide flexible substrate where the cell is essentially rigidly bonded to the substrate and all thermal expansion effects on cell spacing are dependent upon the expansion of the region Y_1. Case II is typical of the aluminum rigid substrate where the cell essentially "floats" with little rigidity between substrate and cell. The substrate expansion occurs with respect to the centroid of adjacent cells while the cell also expands, so the intercell spacing change is the difference between the two. This model produces much greater intercell spacing changes. The calculations of the intercell spacing change ΔY is simply determined from the thermal expansion coefficient α for the appropriate temperature change ΔT. Coefficients for various array materials commonly used are listed in Table 2.3-1.

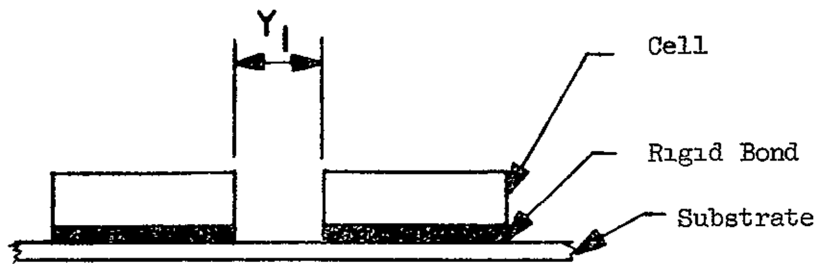

Case I Substrate rigidly bonded to cell

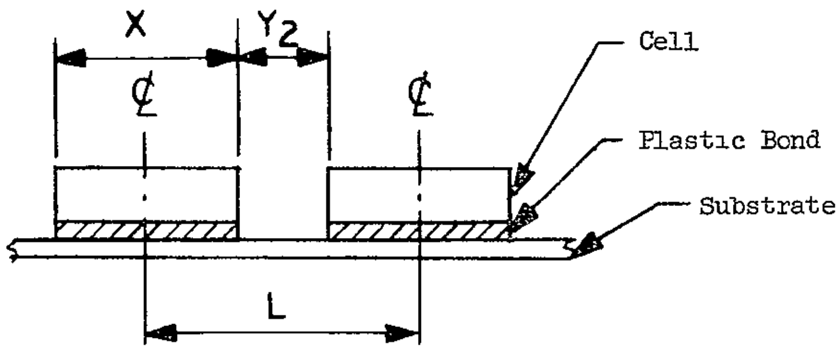

Case II Substrate expands with respect to centroids of adjacent cells.

Figure 2.3-1. Solar Cell Thermal Expansion Model

CASE I.

$$\Delta Y_1 = Y_1 \alpha_k \Delta T$$

where $\alpha_k = 2 \times 10^{-5}$ in/in °C for Kapton polyimide film

CASE II.

$$\Delta Y_2 = \Delta L - \Delta \bar{L}$$

$$= L \alpha_{A\ell} \Delta T - \bar{X} \alpha_{Si} \Delta T$$

where $\alpha_{A\ell} = 2.3 \times 10^{-5}$ in/in °C for aluminum

and $\alpha_{Si} = 3.5 \times 10^{-6}$ in/in °C for silicon

TABLE 2.3-1

Material	Thermal Coefficient of Linear Expansion at 30°C 10^{-6} in/in/°C
Aluminum	23.0
Polyimide	20.0
Silver	19.0
Copper	16.8
Be-Copper	16.0
Nickel	13.1
Molybdenum	5.2
Kovar	5.0
Silicon	3.5
60/40 Solder	22.5 approximate

For a temperature change of 72°C as would be experienced in going from a temperature of 28°C to a temperature of 100°C, Case I would yield a value of 2.5×10^{-5} inch, where $Y_1 = 0.017$ inches. For Case II a value of 9.5×10^{-4} inches is obtained where L = 0.805 inch and X = 0.788 inch

The ΔY values provide intercell spacing variations that would be expected due to thermal changes and provide a minimum value for the length of the interconnector expansion loop. Empirically, thermal cycle tests have shown that this minimum interconnector loop is not satisfactory due to fatigue effects.

The stress relief loop must therefore be further designed to prevent fatigue failure. For a given piece of material the stresses incurred through bending are given by

$$S = \frac{Ex}{R}$$

where E is the modulus of elasticity

x is the distance from the center of bending to the stress point in question

R is the radius of curvature

For a thin uniform interconnector the center of bending will lie in a plane located midway through the thickness of the interconnector. Consequently, the maximum stress will be at the interconnector surface.

$$S_{Max} = \frac{Ed}{R}$$

where d = half the thickness of the interconnector.

It is assumed that the interconnector stress relief loop was bent to its assembly shape and subsequently annealed or the working was done so there was no residual stress. Stress will occur only with further bending. The maximum stress in the interconnector as a result of cell movement can be calculated as follows

$$S_{Max} = Ed\left(\frac{1}{R_i} - \frac{1}{R_f}\right)$$

where R_i and R_f are the initial and final radii of curvature.

The maximum stress level to be used in the analysis is determined from stress fatigue data that has a characteristic similar to that shown in Figure 2.3-2 for each type material[1]. As a practical matter, the stress level that corresponds to 500,000,000 cycles without failure is usually used as the definition of no fatigue. Under some circumstances, such as space missions where the cycle life is expected to be only about 60,000 cycles over a ten year period, it may be possible to use significantly higher stress levels (50% or greater).

A simple interconnect system is schematically shown in Figure 2.3-3 which has essentially no expansion loop, however, there is a radius of curvature change that corresponds to the change in cell motion.

The maximum allowable change in radius that will not make the interconnector exceed the endurance limit can be calculated as

$$R_f = \frac{R_1}{1 - \frac{S_f R_1}{Ed}}$$

where S_f is the no fatigue stress level obtained from the Metals Handbook.

For example, using aluminum (1100-0) interconnector, with $R_1 = 0.010$ inch, $E = 10^7$ psi, thickness $2d = 0.002$ inch, and $S_f = 5000$ psi,

$$R_{f\ Max.} = 0.01005 \text{ inch}$$

Hence, the maximum allowable change in curvature radius is 0.00005 inch. Recalling the previous calculations, cell spacing changes due to thermal expansion (or vibration) are often expected to be on the order of 0.001 inch. Therefore, the stress loop design above would be

1) Metals Handbook, Vol. 1, Eight Edition, American Society for Metals

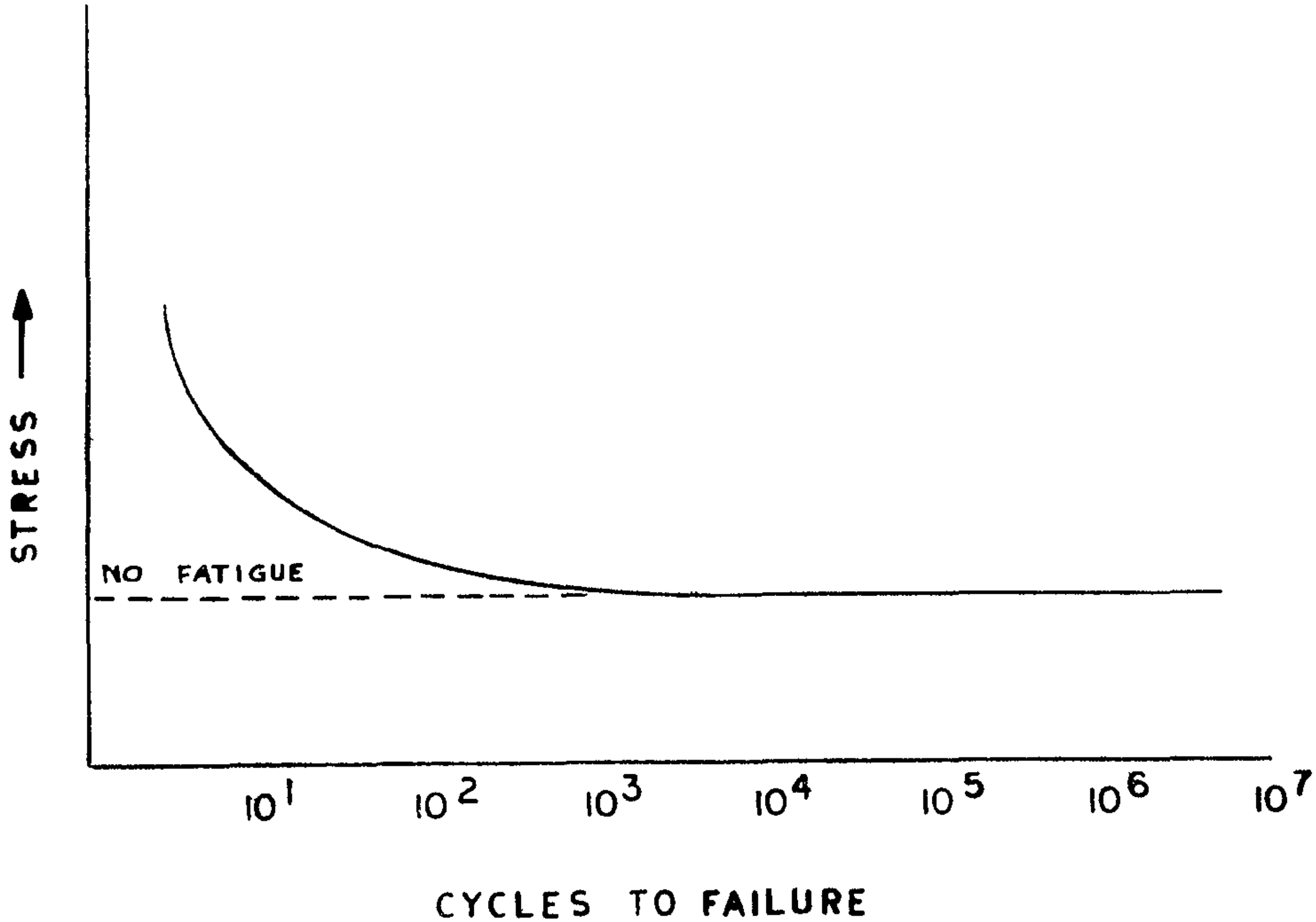

FIGURE 2.3-2 METAL FATIGUE FAILURE CHARACTERISTIC FOR VARIOUS STRESS LEVELS.

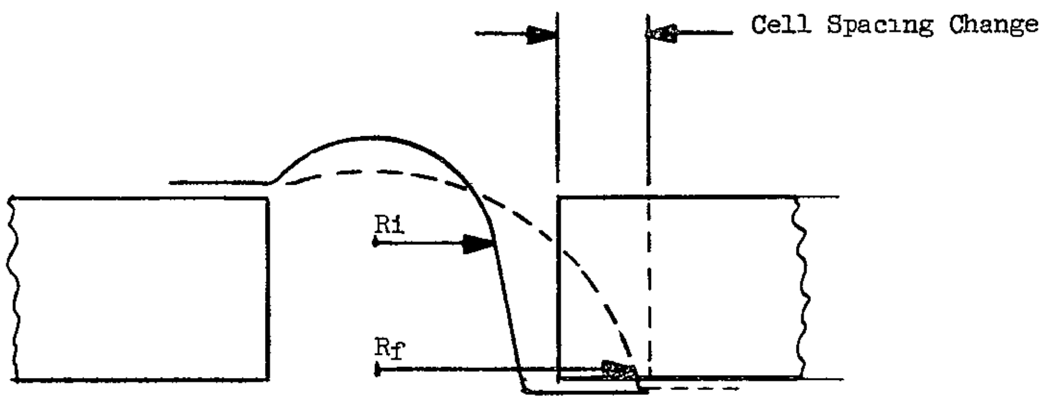

FIGURE 2.3-3. INTERCONNECT DESIGN WITH ESSENTIALLY NO EXPANSION LOOP.

inadequate for the aluminum (1100-0) interconnector if the radius change was equal to the spacing change. Changing to 0.002 inch thick copper with $E = 1.8 \times 10^7$ psi and S_f = 11,000 psi results in

$$R_f \text{ Max} = 0.01006 \text{ inch}$$

which is essentially no improvement over the above example using aluminum. Hence, the copper interconnector offers no significant fatigue advantage over aluminum.

One way in which improved fatigue resistance can be obtained is to place the stress loop higher above the cell surface. In this type design there will be less change in radius with linear cell motion. Figure 2.3-4 schematically approximates the impact of changing the interconnector height. The change in bend radius is significantly smaller than the change in cell spacing. The total loop height h' is defined as h + R where R is the initial bend radius and R_f is the maximum radius allowable without exceeding the endurance limit. Y is one-half the initial cell spacing and ΔY is one-half the cell spacing change due to expansions. From Figure 2.3-4*

$$h = \frac{\Delta Y - \delta}{\sin \varphi} \tag{1}$$

where $\delta = R_f \cos\varphi - Y$, (2)

$$\sin\varphi = \frac{\Delta Y - \delta}{h} = \frac{(\Delta Y + Y) - R_f \cos\varphi}{h} \tag{3}$$

and $2h + \pi R = 2h + (\pi R_f - 2\varphi R_f) \longrightarrow R = \frac{2R_f}{\pi} (\frac{\pi}{2} - \varphi)$ (4)

Using the 0.002 inch thick copper interconnector where R = 0.010 inch, and taking a cell expansion of 0.001 inch (corresponding to a $\Delta T \sim 100°C$) which makes ΔY = 0.0005 inch, then

$$\varphi = 0.009368,\ h = 0.047 \text{ inch and } h' = h + R = 0.057 \text{ inch}$$

hence the no fatigue stress loop must have a total height of 57 mils for this example. Since most interconnector designs are not designed to eliminate fatigue, a shorter and more practical loop height is commonly used.

---

* The equations suggested by R. Matlin of J.P.L.

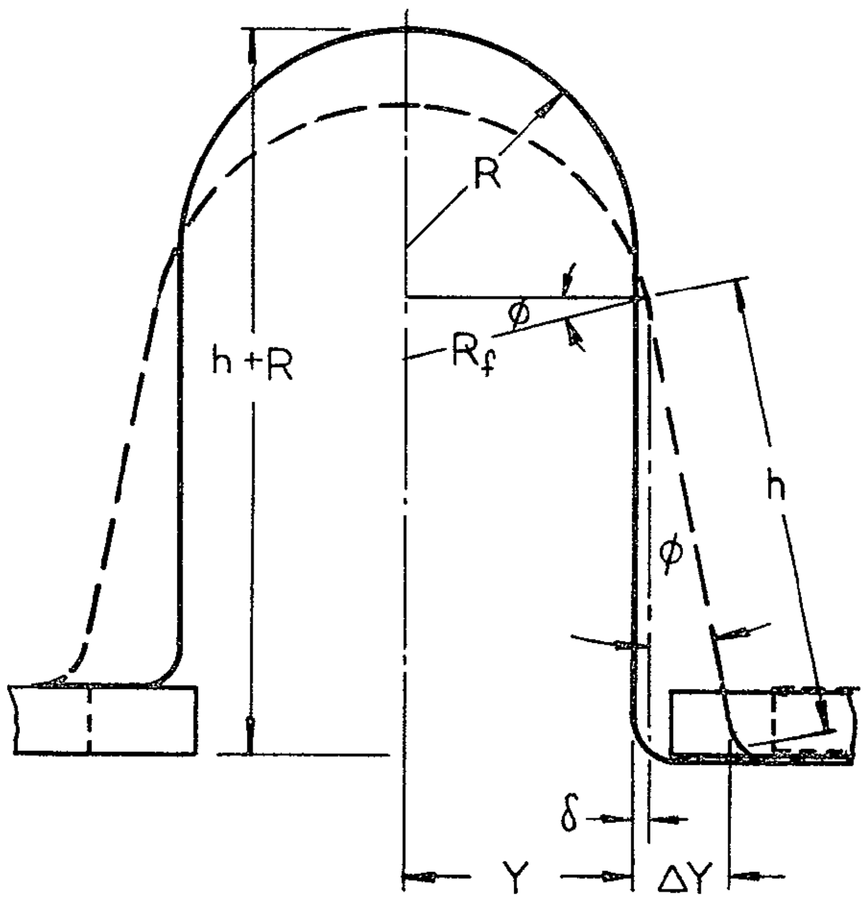

FIGURE 2.3-4 INTERCONNECT DESIGN WITH EXPANSION LOOP EXTENDING ABOVE CELL SURFACE.

For a long life mission where a <u>no</u> fatigue stress loop is desired, the interconnector thickness can be reduced so that the height (h') will be shorter. Also the material or the bend radius can be changed to optimize the design. Similar calculations for 2 mil-thick 5050-0 aluminum alloy yield a value of 0.031 inches for h'. Reducing that thickness to one mil gives h" = 0.017". All the variables in the equations can be summarized as follows

$$h' = h + R$$

and $$h = \frac{\Delta Y - \delta}{\sin \varphi} = \frac{Y + \Delta Y - R_f \cos \varphi}{\sin \varphi} \qquad (5)$$

for small φ, i.e. when

$$\varphi = \frac{\pi}{2}\left(1 - R/R_f\right) \text{ is small, i.e. } R_f - R \text{ is small}$$

$$h \doteq \frac{(Y + \Delta Y) - R_f}{\varphi} = \frac{(Y + \Delta Y) - R_f}{R_f - R}\left[\frac{2 R_f}{\pi}\right] \qquad (6)$$

where $$R_f = \frac{R}{1 - \frac{S_f R}{Ed}}$$

Hence, we have relations for calculating the "no fatigue" loop height for an interconnector design which experiences a cell spacing change due to thermal expansion or applied loads. General guidelines for improving the interconnector design indicate that the thinnest interconnector practical should be utilized (small d), generous bend radii should be employed (large R), and the material should exhibit a high fatigue strength to elastic modulus value. At this point a number of tests were conducted in order to examine the behavior of the interconnector and look for comparisons to the theoretical models. These tests consisted of module wrap tests, interconnect material flexure tests, and flexure/tensile tests.

2.3.3.1 Sample Module Wrap Test

This test was conducted to subject sample modules to cyclic rolling and unrolling. This would reproduce motion which might be expected in a rollout-type array.

The test fixture for this test is shown in Figure 2.3-5. Samples prepared included high and low stress relief S or Z design interconnects and a wraparound interconnector configuration. The wraparound concepts have evolved from considerations as to reducing interconnector stresses during array flexing by placing the interconnector in the plane of the substrate, rather than running it from the top of one cell to the bottom of an adjacent cell. Since the flexible arrays would be expected to experience bending during vibration and deployment, it would minimize interconnector stresses if the interconnector remained in the substrate plane. Ideally, a wraparound contact cell would provide the best cell configuration for such an interconnection, but since this would not be economical, the wraparound interconnector concept evolved as an approximation. By wrapping around the cell before extending to the next cell, all array motions would be absorbed by the segment adjacent to the substrate. The total span and "wraparound" interconnectors represented two approaches to providing the desired interconnector configuration and subsequent configurations, such as the stress-relieved wraparound and laminated wraparound, represented further developments of the "wraparound" configuration, which is presently more practical in terms of array fabrication than the total span concept.

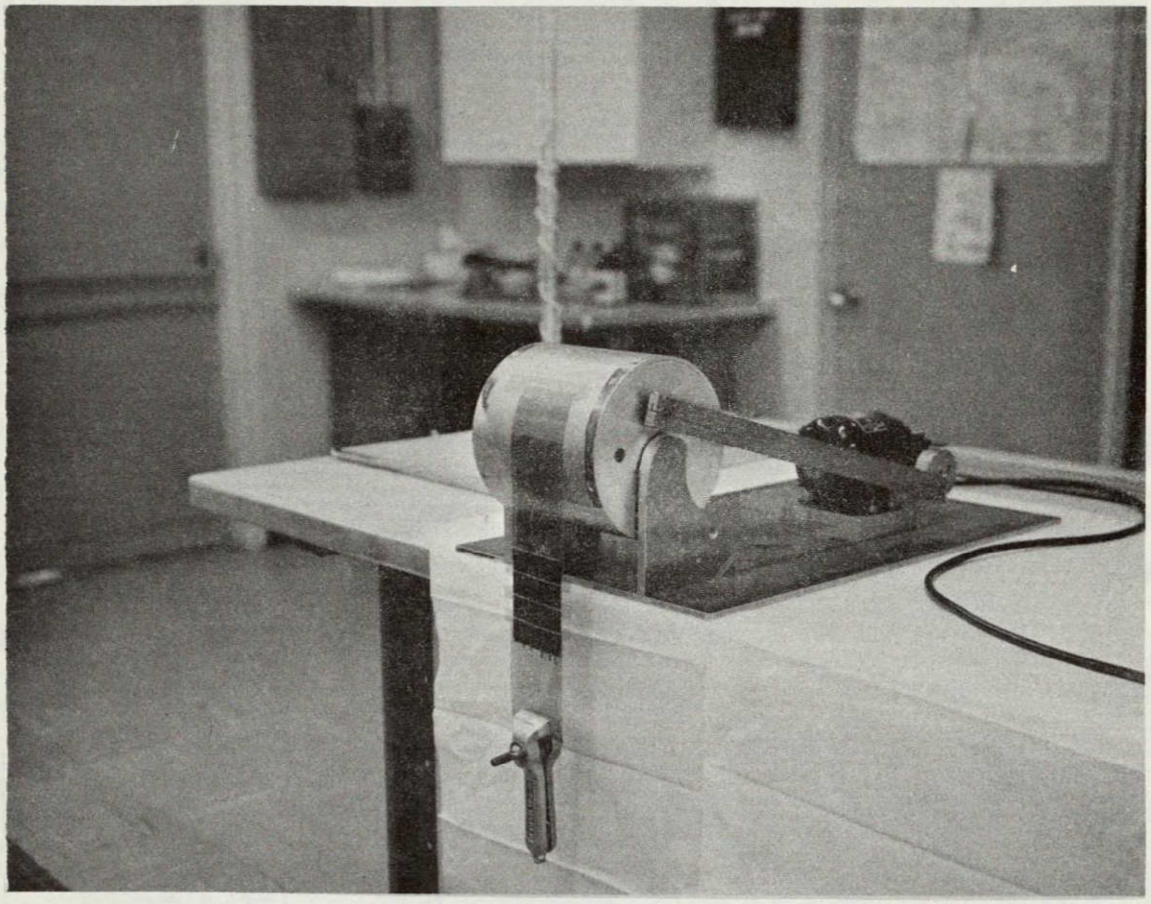

Figure 2.3-5   Module Wrap Test

The high and low stress relief S, or Z, design interconnects and a wraparound interconnector sample were fabricated into 3 x 4 cell modules and bonded to a polyimide ribbon substrate and a weight was attached to one end to provide slight tensioning. All interconnectors were fabricated from 2 mil-thick copper. These and other interconnector configurations subsequently tested are shown in Figures 2.3-6 and 2.3-7. The rolling and unrolling on a 6 inch diameter drum of the conventional S, or Z, design interconnect was terminated at 108,000 cycles when the last tabs of one parallel connected submodule failed completely. This type of failure opened the circuit so that there was no electrical output from the circuit. The complete failure occurred on the module with the high stress relief interconnects while only minor damage was observed on the low stress relief interconnects. These two sample modules were cycled simultaneously on the same fixture under identical conditions.

Examination of the failures showed that the failures were not due to the flexure of the interconnector loop, rather, improper bonding of the substrate to the interconnector lead to a complete separation of the substrate from the interconnector up to the region where adhesion to the cell's bottom surface occurred. This in turn allowed the flexure stresses to be concentrated in the interconnector at the bond line. Hence, the interconnectors were cyclically bent at the bond line along a fairly sharp radius until failure occurred.

Although it is not expected that this roll-up type array motion will occur more than a few times in a typical mission, a similar bending of the interconnects might be experienced as a result of vibrational motions. Therefore, designing for no fatigue in an extensive rollup test appears to have merit. If cells are not bonded completely to the substrate with adhesive, the edges can lift during vibration to produce a similar bending failure.

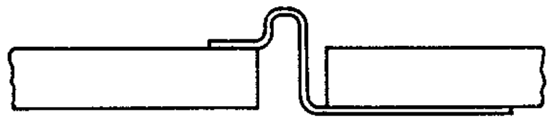

Z TAB CONFIGURATION

(a)

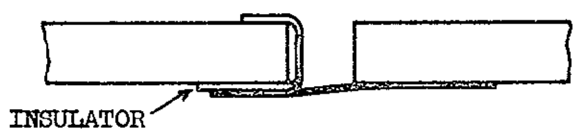

WRAPAROUND

(b)

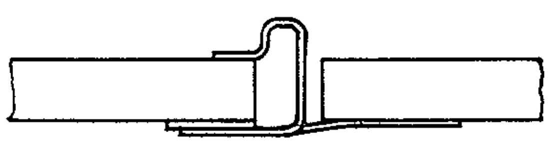

STRESS-RELIEVED WRAPAROUND

(c)

FIGURE 2.3-6 INTERCONNECTOR CONFIGURATIONS A

TOTAL SPAN WRAPAROUND

(a)

TOP VIEW

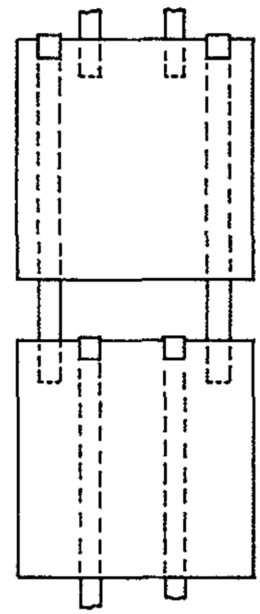

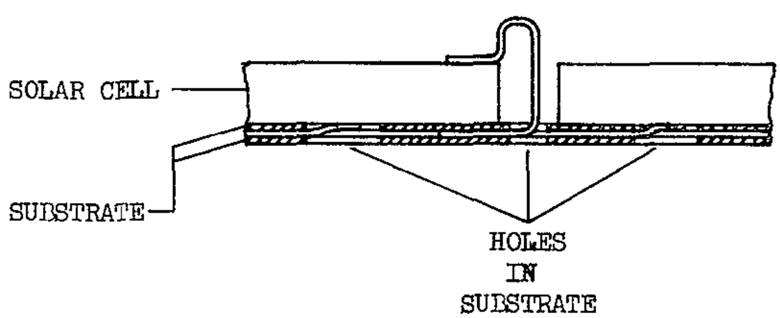

LAMINATED INTERCONNECTOR

(b)

FIGURE 2.3.7 INTERCONNECTOR CONFIGURATIONS B

As a comparison to the Z tab design test above, the wraparound design sample withstood in excess of 250,000 cycles of rolling and unrolling on the 6 inch diameter drum with no visible or electrical degradation.

The test was terminated at this point since it was felt that further cycling would not provide any additional information. The success of the "total span" wraparound concept was due to its ability to prevent sharp bend regions from occurring. This is due to the interconnector design allowing the interconnector to bend with the substrate, and hence follow a gradual curve shape, between the solar cells.

The data at this point indicated that under the low level cyclic bending stresses, induced interconnector failures were caused only when there was poor adhesion between cell and substrate in the conventional S, or Z, tab design which lead to the formation of a sharp bend radius on the interconnector. The wraparound concept showed that its design provided a means for better distribution of interconnector bending loads.

2.3.3.2 Material Flexure Test

In order to evaluate materials for use in bonding applications, a flexure test was designed. In this test a ribbon of the sample material was bent back and forth across two 10-mil radius knife edges of a clamping device. Each 90° bend was considered as one cycle. The results of this test are presented in Table 2.3-2. The sample was cycled until a visible fracture was observed. This test gives an approximate measure of the relative resistance to flexural fatigue of candidate materials being considered for the interconnectors and power distribution system for a flexible lightweight solar array. As was expected, the thinner materials exhibited the greatest fatigue resistance with the laminates exhibiting the greatest fatigue resistance.

Table 2.3-2

BENDING AROUND A 10 MIL RADIUS

Material	Thickness	Ave. No. Bends Til Fracture
Cu/polyimide laminate cemented	0.001"	9.5
Copper	0.001"	5.1
Cu/polyimide (Cu evaporated deposition)	8-10μ	8.4
Cu/polyimide (an evaporated deposition)	3-5μ	7.0
Silver plated copper	0.002"	3.5
Kovar	0.001"	7.5
Ag-plated Kovar	0.0015"	6.9
Aluminum 1100	0.002"	2.7
Aluminum 1100	0.001"	2.6
Aluminum mesh	0.001"	5.3
Molybdenum	0.003"	2.9
Silver	0.002"	1.5
Silver mesh	0.001"	5.1
Beryllium Copper	0.002"	4.4

2.3.3.3 Interconnector Flexure/Tensile Test

The analytic approach to the problem of interconnector flexure fatigue discussed earlier consisted principally in examining the aspect of thermally induced array motions. Vibrational motions were, for the most part, neglected. This neglect was not because such motions were considered to be of no consequence, but rather, because no technique was available for describing the magnitude or frequency of these motions. In the case of thermal motion, it was felt that a model giving the maximum and minimum extent of possible motion could be obtained, and this was done.

The fatigue model thus obtained was used to relate interconnector stresses with the motion of the cells. It was evident that if the vibrational environment could be described in terms of cell motions, the same type of stress relations could be utilized in obtaining interconnector design requirements. Hence, the results of a previous vibrational test conducted by Ryan Aeronautical Company on a roll-out type array were utilized as best available data in order to have some indication of the vibrational problem. Their work had shown that with a one-mil thick polyimide substrate, a typical Saturn launch environment would produce a change in the cell spacing distance of approximately 4 mils. The resonance frequency for this was 4-6 cps. Realizing that the problem of vibrational motion is dependent not only on the input vibration spectrum, but also upon the stowed array configuration, Heliotek felt that the Ryan data could nevertheless be useful in providing a point for designing an experiment which would examine the properties of various interconnect concepts.

With this in mind the apparatus shown in Figure 2.3-8 was constructed. In operation, an eccentric cam on the motor produces a cyclic vertical motion of the 6" diameter drum. This drum, in turn, is thrust up against the fixed module/substrate sample to induce the required loading.

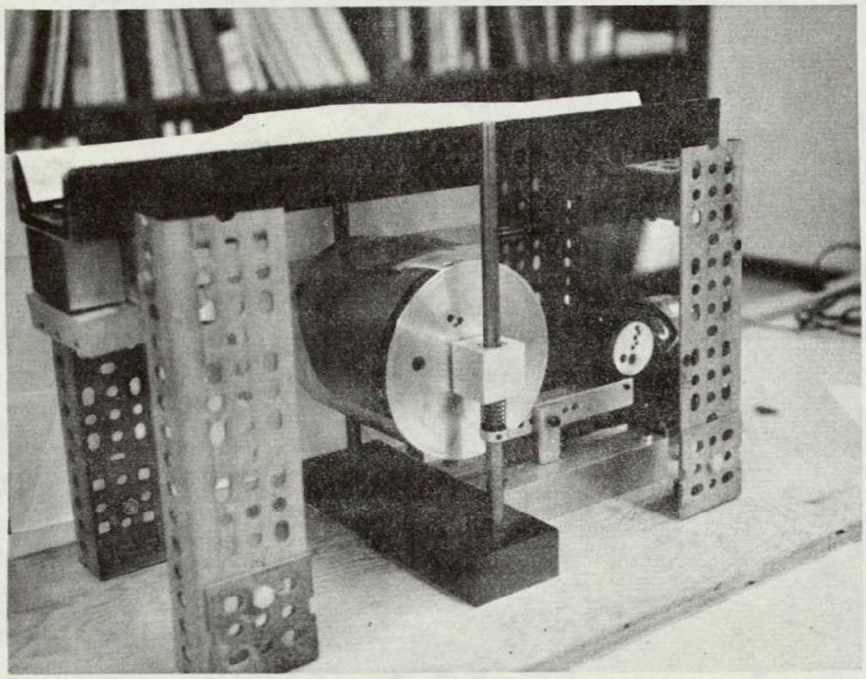

FIGURE 2.3.8 FLEXURE/TENSILE TEST APPARATUS

Calculations were made based on the Ryan data which indicated that the 1-mil thick polyimide substrate need be subjected to a force on the order of 12 pounds per lineal inch in order to provide the 4 mil change in cell spacing. In the test setup, the actual loading is measured by examining the deflection of springs which fix one end of the polyimide substrate to the test fixture. The spring calibration indicated that a total spring deflection of 0.050" will be produced by a total force of 36 pounds. Across the 3 inch wide substrate used in these tests, this deflection corresponds to the required 12 pounds per lineal inch. Optical measurements of the cell spacing has further indicated an actual cell spacing change of 3 to 5 mils.

The frequency used in the laboratory tests was 43 cpm, slightly slower than the Ryan data indicated.

The samples tested (shown in Figures 2.3-6 and 2.3-7) consisted of five different interconnect concepts. These were:

a. High Z (or S) type tab (50 mils stress loop height).
b. Low Z tab (15 mils stress loop height).
c. Wraparound interconnector (with and without stress relief).
d. Total span wraparound interconnector.
e. Laminated wraparound solar cell matrix.

The laminated wraparound solar cell matrix, configuration e, combines some aspects of the composite solar cell matrix (NASA Technical Brief 67-10503) and the wraparound interconnector concept. The composite solar cell matrix was suggested by R. K. Yasui of JPL and incorporated a standard Z, or S, interconnector in a system requiring no adhesives for the series direction array integrity. Rather, the interconnector provides the mechanical strength. The solar cells are placed on one side of the polyimide substrate and the interconnector is bonded to the solar cell through holes in the polyimide. This "sandwich" provides module integrity without adhesives in the series and parallel direction.

For these particular flexure/tensile tests, all sample modules consisted of nine 2 x 2 cm silicon solar cells interconnected in a 3 parallel by 3 series configuration. The polyimide substrates were all 1 mil thick. A modification in configuration was required for the laminated wraparound solar cell matrix due to its catastrophic tearing during the first few cycles. Originally, slits were used where the interconnector passed from the top of one cell to the bottom of the next. Where the bottom surface solder bonds were made circular regions were cut out. The substrate material for the initial design was a single polyimide sheet. With the initial design, tearing commenced at the feedthru slits and rapidly led to complete tearing of the sample, as shown in Figure 2.3-9.

Consequently, this initial concept was modified to provide greater tear resistance. First, all feedthru regions in the substrate were fabricated by punching circular holes. This removed the regions of high stress that were incurred by the slitting techniques. Second, a second 1/2 mil polyimide substrate was bonded to the first, sandwiching the interconnector in between. This configuration, shown in Figure 2.3-7 was used for all further testing.

Another variation had to be made to the original test sequence in the case of the wraparound design. It was discovered that the wraparound concept had to be modified to provide additional stress relieving. The initial test of the wraparound showed a high failure rate, comparable to the low Z tab design. The failure appeared to be caused by a rubbing action of the tab along the cell edge due to motion relative to the cell. Because of the insulation and silicone adhesive underneath the cell at this point, slight motions were possible. Hence, a small stress loop, approximately 5 mils high was incorporated to allow interconnector motion without any rubbing.

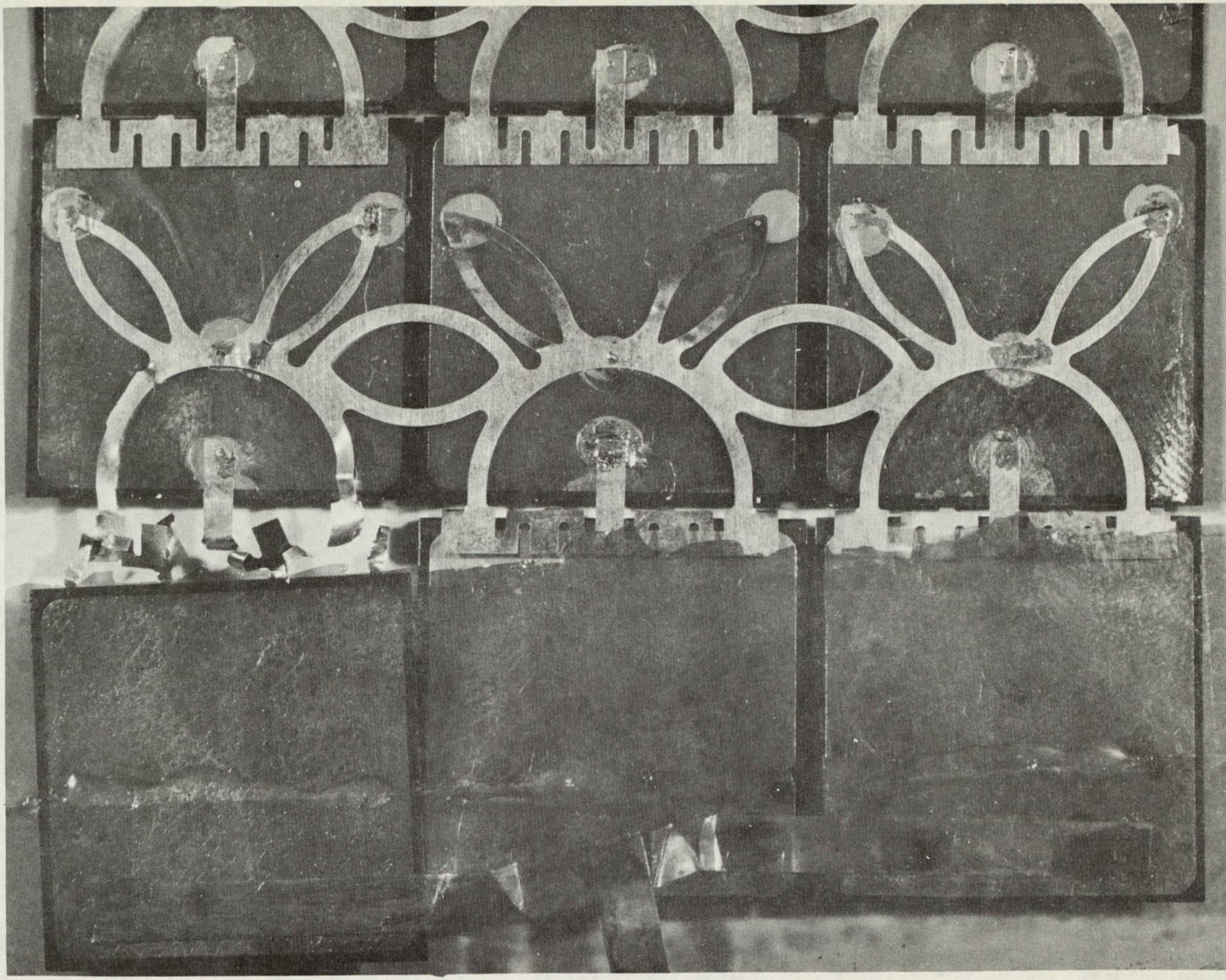

FIGURE 2.3-9. LAMINATED WRAPAROUND SOLAR CELL MATRIX FAILURE

This data for all cycled samples is summarized in Figure 2.3-10. The data is presented as percent of tabs failed versus number of cycles. As a matter of reference and comparison, the Ryan data which was obtained by subjecting a roll-up type array to a typical Saturn launch environment, showed a resonant 4 mil intercell spacing change at approximately 6 cps. The duration of the environment was 5 minutes resulting in a total of 1800 cycles. The number of cycles which the samples experienced in these laboratory tests was well in excess of the 1800 cycles, thus providing information well beyond the design goal.

Furthermore, theoretical calculations of Z tab stress loop height for no failure were made using the model and equations described previously and were based on 500,000,000 cycles, in accordance with the available materials' properties. These calculations showed that for a 4 mil intercell spacing change, a stress loop of approximately 70 mils height would be required. In the experimental tests, the low Z configuration (15 mils stress loop height) and the high Z configuration (50 mils height) were expected to exhibit a wide variance in fatigue resistance. Accordingly, the test data in Figure 2.3-10 conclusively bears out this theoretical data. For the Z type configuration interconnector, failures occurred predominantly at the top of the stress loop (see Figure 2.3-11) in agreement with that expected based on the theoretical model previously mentioned.

Returning to Figure 2.3-10, all the concepts have essentially formed three patterns, characterized by a relatively high fatigue rate, moderate rate, and a low rate. Interestingly the laminated wraparound solar cell matrix, which uses no adhesives to bind the cell to the substrate, although initially exhibiting a greater failure rate than the high Z tab configuration was quite comparable to it after approximately 50,000 cycles. For a mission entailing only a few thousnad cycles, the composite would appear to be somewhat inferior to the high Z configuration, however, the potentially lighter weight and the ease of construction of the laminated wraparound make its use on many missions look promising.

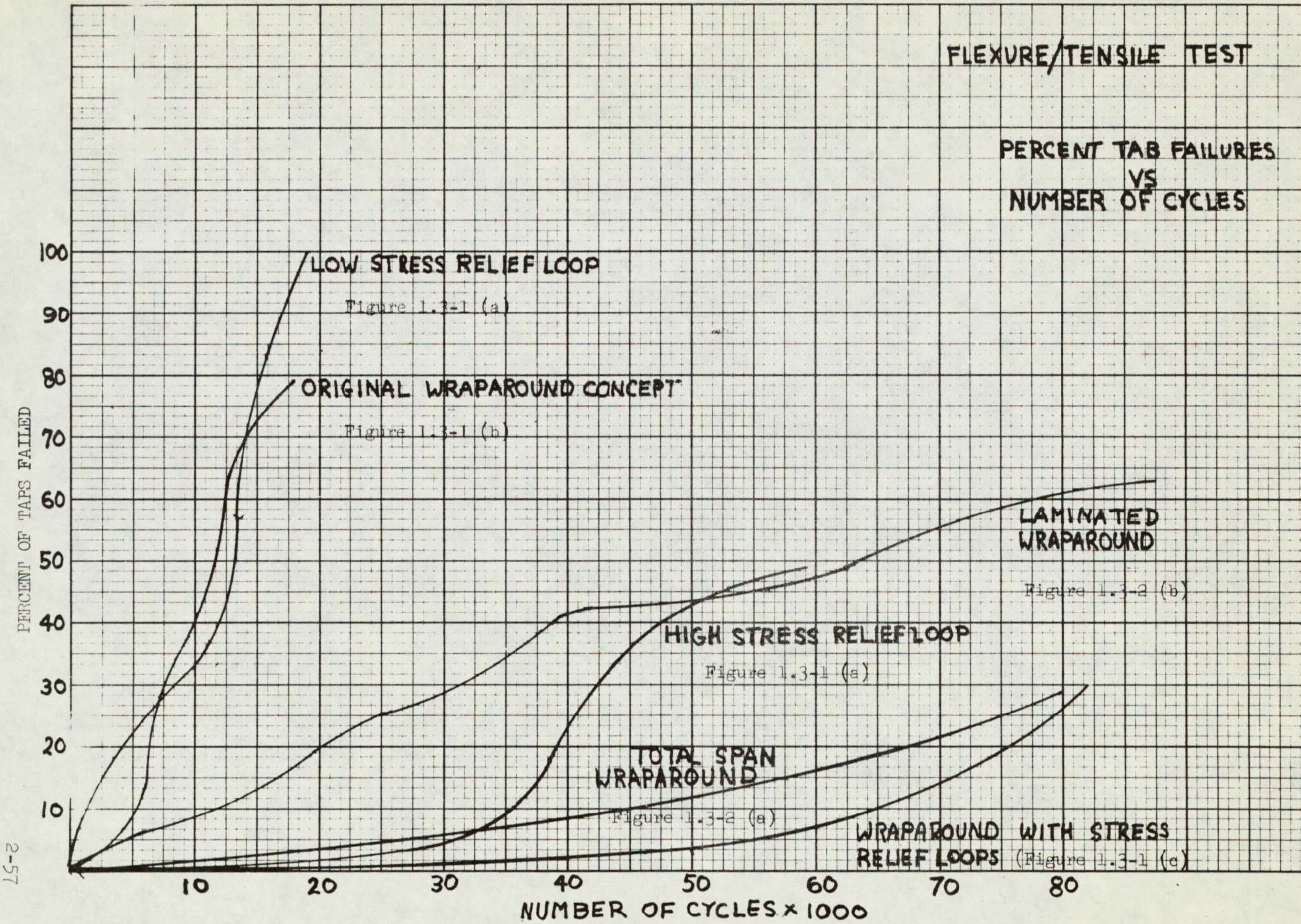
FLEXURE/TENSILE TEST
PERCENT TAB FAILURES VS NUMBER OF CYCLES
LOW STRESS RELIEF LOOP
Figure 1.3-1 (a)
ORIGINAL WRAPAROUND CONCEPT
Figure 1.3-1 (b)
LAMINATED WRAPAROUND
Figure 1.3-2 (b)
HIGH STRESS RELIEF LOOP
Figure 1.3-1 (a)
TOTAL SPAN WRAPAROUND
Figure 1.3-2 (a)
WRAPAROUND WITH STRESS RELIEF LOOPS (Figure 1.3-1 (c)
PERCENT OF TAPS FAILED
100
90
80
70
60
50
40
30
20
10
10
20
30
40
50
60
70
80
NUMBER OF CYCLES × 1000

Figure 2.3-10

Both the total span wraparound concept and the stress relieved wraparound concept were much superior to all other concepts in fatigue resistance tests. When compared to the low stress relief system which approximates many present-day interconnect systems, the improvement in fatigue resistance is quite pronounced. It appears that the total span wraparound and stress relieved wraparound systems shown would provide the best fatigue resistance. The possibility of lower array weight with the laminated wraparound concept, along with its good fatigue resistance should make that concept a candidate for some missions where all-out fatigue resistance was not of prime concern (moderate intercell spacing motions).

The significance of these interconnector design changes can be seen by comparing the number of cycles required to cause a 10% failure rate. The conventional low stress relief loop design only requires 2,000 cycles to fail 10% of the interconnectors. Increasing the height of the stress relief loop increased the number of cycles for 10% failed to 36,000 cycles. The wraparound design with stress relief design could go 65,000 cycles before the 10% failure rate was reached. These improved designs are obviously better candidates for lightweight arrays.

An examination of failure mechanisms showed that in all cases, excepting the laminated wraparound, the failure mechanism consisted of interconnector metal fatiguing. In fact, failures could often be predicted from the appearance of the interconnectors. Prior to failure the tabs in the region of flexing showed evidence of surface pitting and tearing at the edges, along with a generally crystalline appearance.

With the total span wraparound configuration, the fatigue failures occurred underneath the cells and was apparently due to crimping during the cycling.

With the laminated wraparound matrix concept, a large number of failures occurred at the solder bonds and did not appear to be fatigue failures. Rather, it appeared that stress levels had exceeded bond strength.

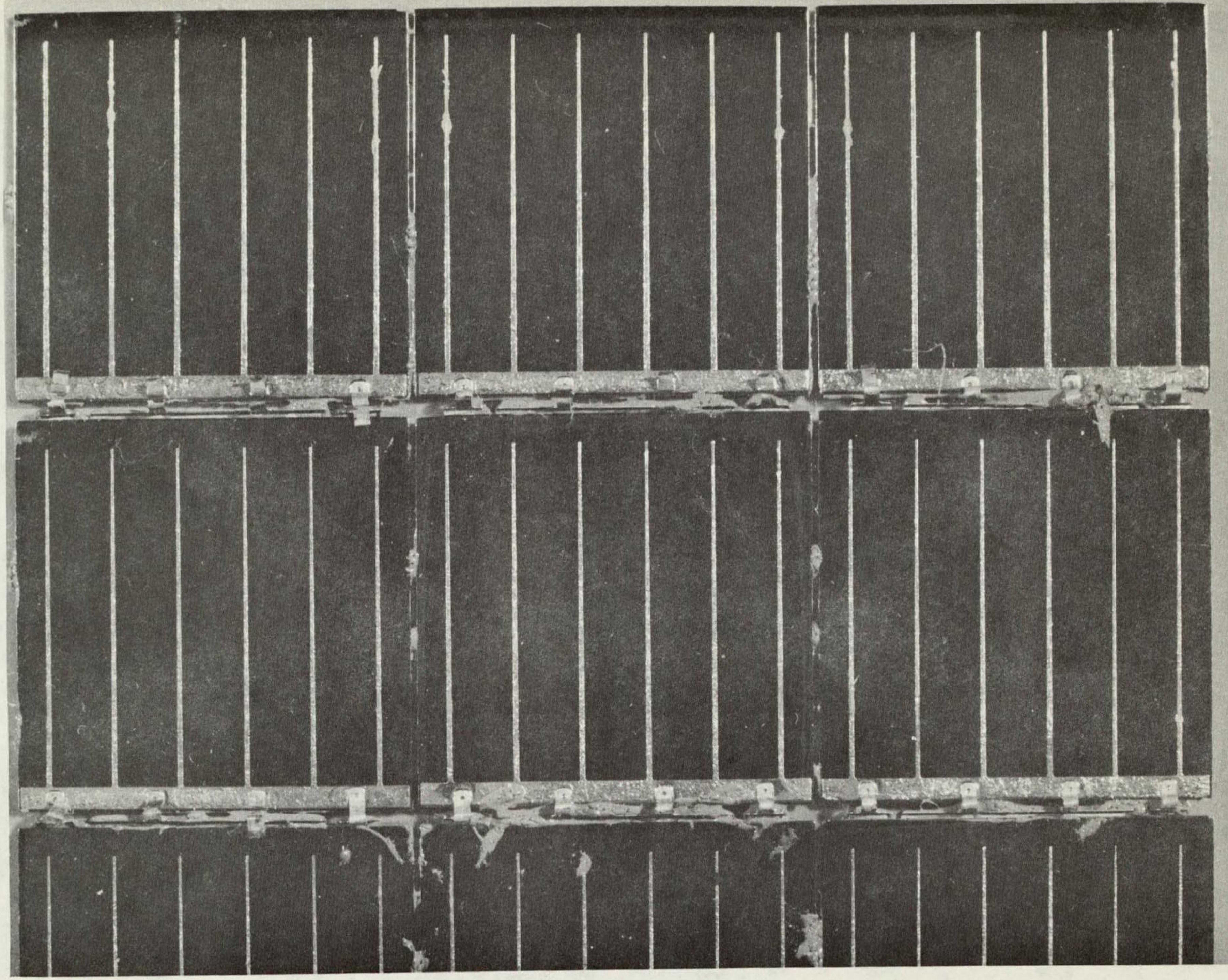

FIGURE 2-3-11. Z TAB FAILURE

With the laminated wraparound matrix concept, the absence of adhesives appeared to minimize the array's ability to absorb stresses over relatively large areas. Instead, they became concentrated at the solder bonds. Possibly, the use of thinner interconnectors would be advantageous in the design so that less twisting torque would be transferred to the bond.

The sequence of testing interconnector flexure fatigue was completed by determining the failure rates for low Z tab interconnectors and stress relieved wraparound interconnectors as tested by the flexure/tensile test apparatus. This was done since the wraparound concept was chosen to be used in the demonstration module. It was felt that this data would be most valuable when the relation to the standard Z tab configurations was included. The failure rate for the standard Z tab interconnector was based on cycling two modules and that for the stress relieved wraparound on three modules. The intercell spacing change of 4 mils was used for all tests. This would correspond to a rather severe launch vibration environment, but will serve to indicate the relative fatigue resistant abilities of the two concepts. The failure rates listed below are based on a 90% confidence level, where failures indicate the complete tearing of interconnector tabs.

Failure Rate - 90% confidence	Configuration
5% $\pm$2%/1000 cycles	Low Z tab
0.8% $\pm$0.4%/1000 cycles	Stress relieved wraparound

2.3.4 Thermal Expansion Stress

In addition to the interconnector stresses caused by cell movement, there are stresses in the interconnector cell interface that can cause failure. These stresses are the result of mismatch in the thermal expansion coefficients of the materials. The type material used, the thickness of the material, the size of the bonded region and the thermal excursion determine the magnitude of the stresses generated. The failure usually is a silicon fracture (divot) or fatigue of the solder joint.

The thermal expansion model for a three component system composed of silicon, solder, and an interconnector tab is shown in Figure 2.3-12. If the members were not mechanically coupled, thermal effects would cause each member to expand or contract to some "free" length ΔL. However, since these members are rigidly bonded together they must all expand to the same length (assuming no bending) and the stresses are distributed within each member. The stress will be determined by the amount of deformation ΔX required to translate each member from the free expansion length to the actual expansion length R. The resultant length change is calculated by considering the weighted expansion as follows

$$R = \frac{\left(L \sum_{i=1}^{i=3} t_i E_i \alpha_i \Delta T \right)}{\left(\sum_{i=1}^{i=3} t_i E_i \right)} = LR'$$

where t_i is the thickness of each member i,

L is the length of the members

E_i is the modulus of elasticity

α_i is the coefficient of thermal expansion

ΔT is the temperature change

and R' is the weighted mean of the length change

The strain induced in the member will then be

$$\frac{\Delta X_i}{L} = \frac{\Delta L_i - R}{L}$$

$$= \alpha_i \Delta T - R'$$

and the stress S_i in each member will be

$$S_i = \frac{E_i \Delta X_i}{L} = E_i(\alpha_i \Delta T - R')$$

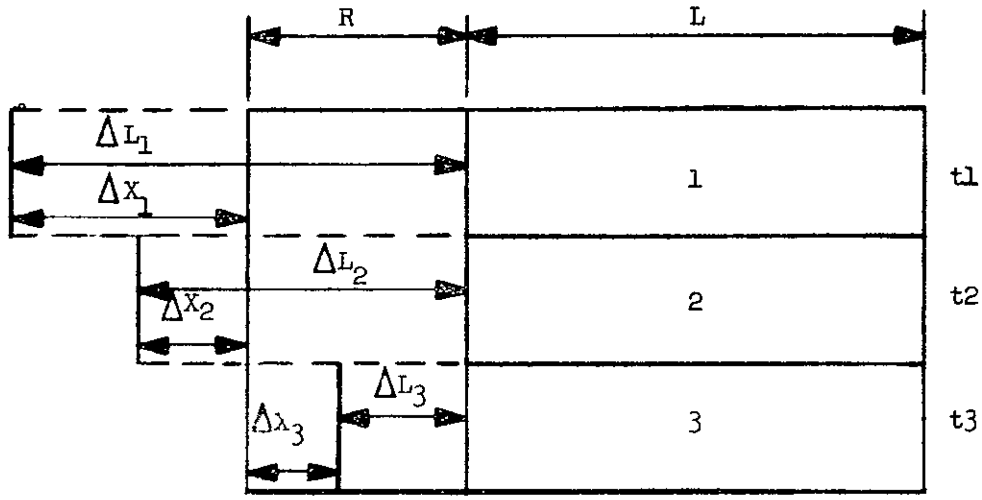

Figure 2.3-12. THERMAL EXPANSION MODEL FOR A THREE-MEMBER RIGIDLY BONDED SYSTEM.

Calculations were made to determine the stresses in the interconnector material, the solder layer, and the silicon cell using the above equation. This analysis showed that the stresses in the solder were quite insensitive to interconnector material type and thickness. Also, it showed that the stress in the solder layer would easily exceed the yield strength of solder at elevated temperatures ($\approx$ 3000 psi at 100°C) which is a common failure mode in thermal cycling tests. Data for various interconnectors is shown in Table 2.3-3.

TABLE 2.3-3

THEORETICAL THERMAL STRESS

Interconnector Material and Thickness	Stresses (p.s.i.) Interconnector	Solder	Solar Cell
0.5 mil Molybdenum	6,500	9,900	1,900
1.0 mil Molybdenum	6,000	9,800	2,000
2.0 mil Molybdenum	4,300	9,600	2,600
0.5 mil Copper	18,400	9,600	2,400
1.0 mil Copper	17,100	9,300	3,400
2.0 mil Copper	15,100	8,700	4,900
4.0 mil Copper	12,100	7,900	7,200
6.0 mil Copper	10,100	7,300	8,700
1.0 mil Silver	18,700	9,600	2,970

At low temperatures (-100°C) the tensile strength of solder increases to about 12,000 psi and the calculated stress in the solder for copper or molybdenum tabs is only about 9,000 to 10,000 psi. Therefore the solder is heavily stressed but provides sufficient strength so that the common mode of failure is fracture of the silicon.

Calculations of the silicon stress values are prone to error from the uniform stress distribution assumption. The reason for this discrepancy is that usually the silicon stresses are not distributed uniformly across the relatively thick silicon as assumed, but instead are concentrated only in a very thin region immediately below the metal tab. Efforts were undertaken to determine an accurate description of the silicon stress distribution, however, due to the complexity of the task and the lack of well-established formulas for the model, this was not accomplished. Therefore, empirical data was used to obtain parameters for determining the silicon failure level.

The test data used* compared the behavior of molybdenum and copper interconnector systems under a thermal cycle of 75°C to -175 °C. The silicon cells in this experiment were 10 mils thick with 3 mil thick interconnectors. The behavior of the molybdenum system showed essentially no failures (characterized by surface cracks) through more than 350 thermal cycles whereas the copper interconnector exhibited a steadily increasing number of surface cracks up to a maximum of 92% cracked solder joints at 350 thermal cycles. These data were interpreted as defining "safe" (molybdenum) and "unsafe" (copper) stress levels.

Application of the Heliotek model to the above experimental data showed a silicon stress value for the copper of 9200 psi, and 7800 psi for the molybdenum system. The 9200 psi value was then taken as the 100% silicon fracture strength value and all other silicon stresses as some percentage of that value. In this manner, although no value for the actual fracture producing stresses in the silicon was obtained (i.e., no stress concentration value was obtained), it was possible to relate all calculated silicon stresses to the relative stress compared to the point of fracture.

---

* W. Luft and E. Maiden, "Temperature Cycling Effects on Solar Panels, Fourth IECE Conference, Sept. 22-6, 1969.

Using this relationship the curve in Figure 2.3-13 was developed. This curve shows the silicon stress for copper and molybdenum interconnectors when the temperature is reduced by an amount ΔT. Copper is a marginal design when a ΔT of 150°C or more in encountered. The advantage of using molybdenum or a metal with a similar thermal expansion coefficient as an interconnector is obvious under all conditions, but it becomes a necessity if reliable bonds are to be made that will survive very low temperature cycling.

2.3.4.1 Interconnector Thermal Cycling Tests

Thermal cycling tests were conducted on interconnector samples with four thicknesses (2, 4, 6, and 8 mils). It was intended that these tests would provide failure rate data to augment the theoretical interconnector failure analyses previously reported. The interconnector samples were formed from 0.050" wide copper strips and then soldered to 14 mil thick silicon solar cells. Two thermal cycle sequences were conducted. The first consisted of 100 cycles between room ambient to -195°C and the second consisted of 100 cycles from room ambient to approximately -100°C. For each sequence, 8 tabs of each thickness were cycled. The thermal cycle rate was approximately a 5 minute excursion with a two minute dwell at each temperature extreme. All samples were examined visually every cycle for bond failure or surface cracks, and at every 10 cycles under a 50 power microscope for evidence of hairline surface fracturing.

Analysis of the test data did not provide a clear correlation between interconnector thickness and failure rate. Rather, for the -195°C to room ambient cycle test, failures were distributed evenly for each thickness. With the less severe -100°C to room ambient cycle test, the intermediate thicknesses of 4 and 6 mils exhibited bond failures of about 50%, whereas the 2 and 8 mil interconnected samples exhibited less than 15% failed bonds. Apparent embrittlement and recrystallization of the solder was noted well before any actual bond failure for all samples.

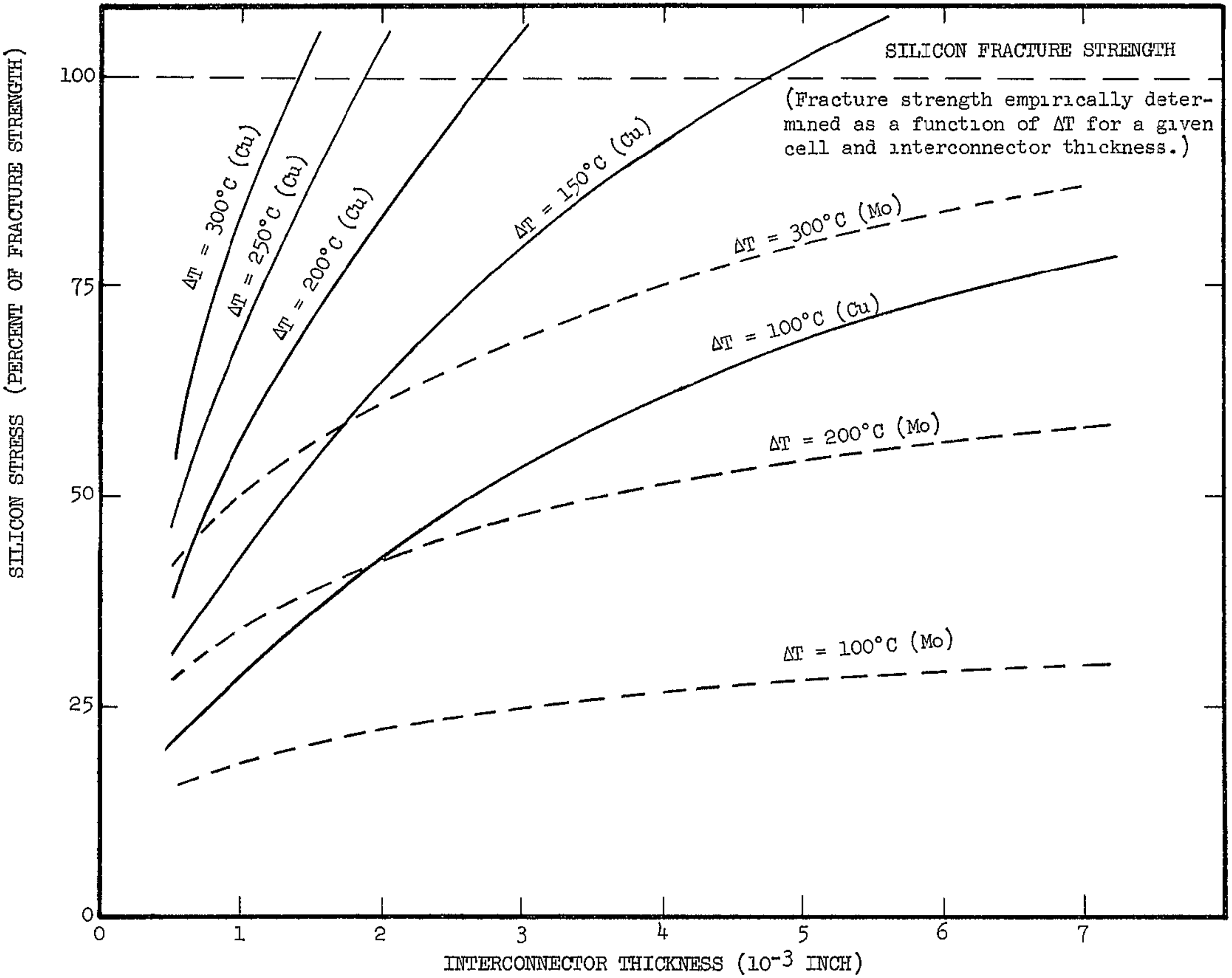

Figure 2 3-13 Thermal stresses in silicon under a metal tab of various thicknesses.

In many cases this significantly weakened the bond strength without, however, producing a visible bond failure. As a result, at the end of each cycle each tab was manually tested in order to provide some indication of weakening due to solder embrittlement. In approximately 1/3 of the bond failures, lightly tapping the part was sufficient to cause bond failure. This data indicates that possibly the failures were influenced by a more important factor than tab thickness.

To recall the earlier theoretical calculations, it should be noted that stress levels in the solder were quite high in reference to the solder tensile strength. Furthermore, incomplete materials' properties data for the solder at low temperature required some extrapolation of strengths. Hence it is likely that the solder strength is marginal under the stresses encountered. For this reason, the effect of interconnector thickness may be of secondary importance to the solder bond fatigue resistance. So, although theory predicts that it is reasonable to expect thinner interconnectors to incur less stress in the solar cell during thermal cycling than thicker interconnectors, the failure of the solder essentially masks the interconnector thickness effects in the experimental work.

As a further investigation of the importance of the possible effect of the solder on the failure mechanism, an additional experiment was conducted. This test consisted of samples with 2 mil copper interconnectors soldered to cells and 2 mil thick aluminum interconnectors ultrasonically welded to the cells. All sample cells had silver titanium contacts. The samples were cycled 60 times from room ambient to -195°C. Additionally, two samples of each system were soaked in LN_2 (-195°C) for approximately 24 hours. The results, plotted as percent of bond failed versus cycles, is shown in Figure 2.3-14.

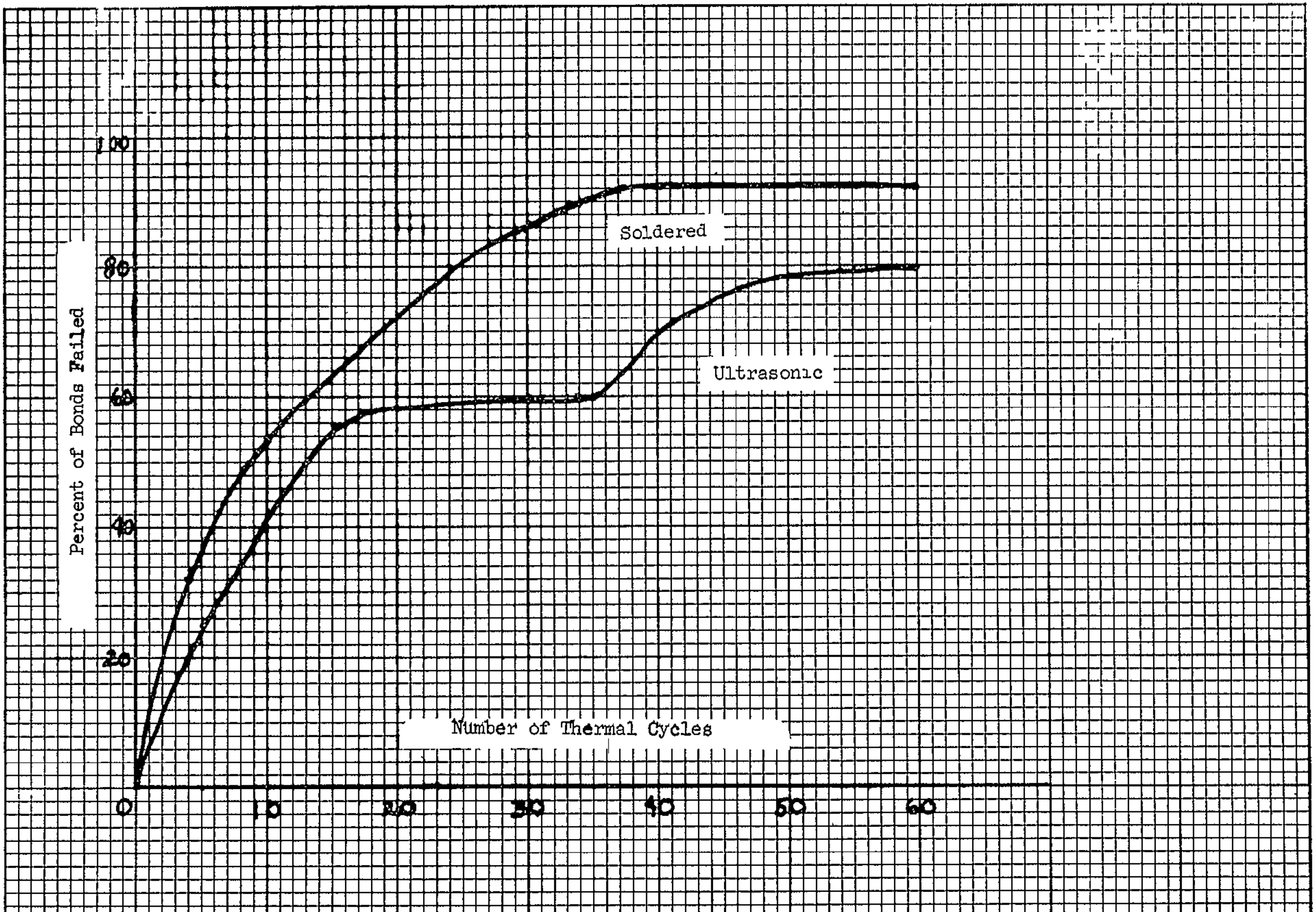

FIGURE 2.3-14 THERMAL CYCLING TEST RESULTS

The difference in failure rates cannot be considered significant since only 28 bonds of each type were used. However, the mechanism of failure was quite different. In the majority of cases, the failed solder bonds removed large divots in the silicon. In sharp contrast, the ultrasonic bonds that failed often left just a slight blemish on the silver-titanium contact or in some cases, a slight deposit of aluminum. Hence the ultrasonic weld failures appeared to be located only in the bond region, whereas the soldered bond failures produced a prouounced disruption or fracture in the silicon solar cell. This same type of occurrence was observed in the samples soaked at -195°C for 24 hours. This would indicate that the actual cycling is not as important a determinent of failure as is the total time spent at low temperatures.

2 4 SUBSTRATE AND SOLAR CELL BONDING SYSTEMS

The substrate for an integrated flexible solar cell array must fulfill a multitude of purposes Of primary concern, the flexible substrate in contrast to the rigid substrate, which achieves a minimum weight of about 0 200 lb/ft^2, must have a weight less than 0 015 lb/ft^2 including cell bonding adhesive to achieve a power to weight ratio of 120 watts per pound for an array The blanket or array in this study includes the cells, covers, interconnects, adhesives, substrates, and the bus connectors, but does not include the deployment mechanism

Additional functions of the array substrate which are important are

1 Maintain solar cell series and parallel spacing
2 Transmit loads from support structure to cell matrix during extension and retraction
3 Insulate the power transmission bus from the cell matrix
4 Resist UV and hard particle radiation
5 Have high temperature and vacuum stability
6 Resist flexural fatigue
7 Have flexibility over a wide temperature range
8 Have the ability to be bonded using conventional adhesives
9 Have a reasonable absorptivity to emissivity ratio to insure adequate temperature control unless an additional surface treatment is used

Although the aforementioned qualities must be considered in designing solar cell arrays in general, this study will direct its attention to the specific properties that are critical to the design of an ultra lightweight flexible array As the first part of this analysis instead of using a continuous substrate sheet, a polyimide film ribbon of some predetermined width was investigated as the support for the solar cell matrix The big advantage of this type substrate design is that it provides support with the least weight and it provides support at the cell edges where it is needed to prevent cell "flapping" during vibrations and roll up It also meets all the other functions required

above The adhesive and primer that were selected for the ribbon experiments were RTV 3145 and Dow Corning 90-198 primer This adhesive and primer were selected based on the results of tests on a lightweight array study performed by Ryan Aeronautical and Spectrolab

An analysis to determine the minimum ribbon width was begun by comparing the spring rates of a lap joint in which a strip of 1 mil thick polyimide film was bonded to a solderless solar cell using a thickness of 1 5 mils of RTV 3145 with the 90-198 primer applied to the cell only

If we consider Figure 2 4-1 and assume that the lap joint was made using two rigid materials, top and bottom, with an adhesive between, then the spring rates of the rigid members would be high and the joint would transmit stresses uniformly across the adhesive region L Failure would occur as a straightforward shear failure as determined by the shear modulus of the adhesive material

In the flexible array case the two members bonded together are not both rigid Instead, the polyimide has a spring rate that is low Therefore, when stressed in shear by tensile loading, they develop a non-uniform stress pattern along the lap as shown in Figure 2 4-2

The stress diagram indicates that the peak stress and the failure front will occur at the leading edge of the adhesive and will gradually shift as the tensile load exceeds the bond strength at the adhesive film interface This failure mechanism will therefore be dependent upon the glue line width W and thickness rather than the overlap length L

To substantiate this model with experimental data, three-cell series modules were bonded together using polyimide film bonded to the cells with RTV 90-024 (a refined version of RTV 3145) and DC 90-198 primer Ribbons of 1 mil polyimide film were bonded to the cell rear surface in cell overlap widths of 0 050, 0 100, 0 150, 0 200 and 0 250 The adhesive thickness was about 0 0015 inches No interconnects were used in these assemblies Ten sample modules of each of the five

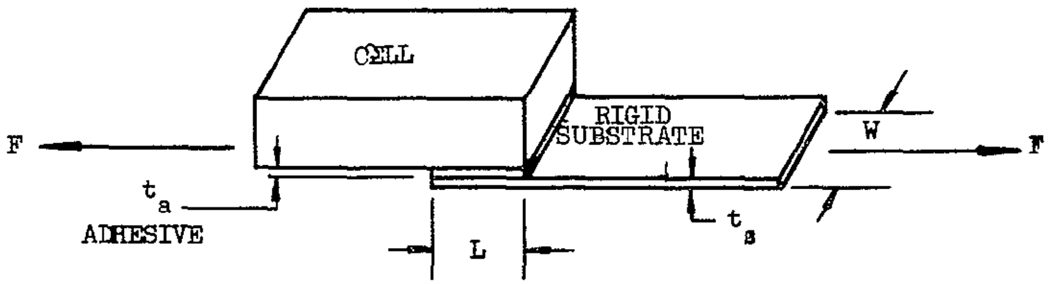

FIGURE 2.4-1

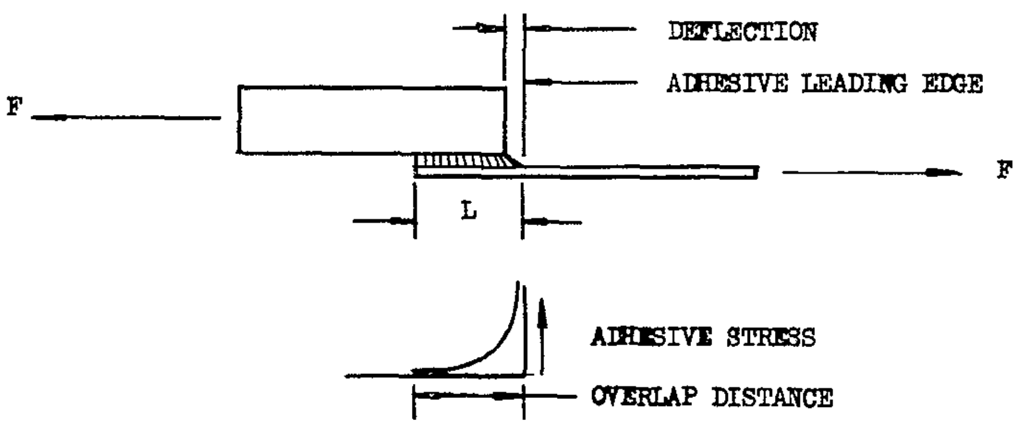

FIGURE 2.4-2

ribbon widths were made and tested. Two mil thick polyimide films were bonded to the ends of the module to provide grips that were stronger than the test joints. The assemblies were subjected to tensile loads until separation occurred. These forces were recorded and the results are presented in Table 2.4-1. These data illustrate the lack of dependence of overlap length L to failure loads although the 0.050 inch ribbon case starts to indicate a limiting effect. The curve also shows that the fracture in some cases was a cement bond failure C and in other cases a polyimide substrate tear K. The failures were distributed about half-and-half between the two failure modes indicating the system was capable of being stressed to a point very near the strength of the substrate material.

Structural loads generated in a large area array during extension and retraction are expected to be on the order of five to ten pounds across a typical array which would be three feet wide or more. The single cell values plotted on Table 2.4-1 would therefore indicate that the ribbon substrate system under consideration will be more than adequate for loads anticipated on this design concept.

2.5 VACUUM DEPOSITED METALLIC LAMINATES--INTEGRATED POWER DISTRIBUTION

The concept of utilizing thin film laminated conductors appears quite attractive, for not only does this suggest the possibility of forming the substrate conduction system in a single fabrication step, but it also allows the use of ultrathin metallic interconnectors which would otherwise be prohibitively fragile. With the laminating of the thin metal to a flexible substrate, an assembly with good flexure fatigue resistance and handling capabilities can be achieved.

There are metal-polyimide laminate systems commercially available that consist of thin metallic layers adhesively bonded to polyimide substrates, however, there are limited sizes available and ultrathin layers to specific designs are not available. Therefore, a technique was developed for incorporating thin layers of copper on polyimide substrates.

RTV 3144 was selected because of high peel strength without the use of primers, and the absence of acetic acid.

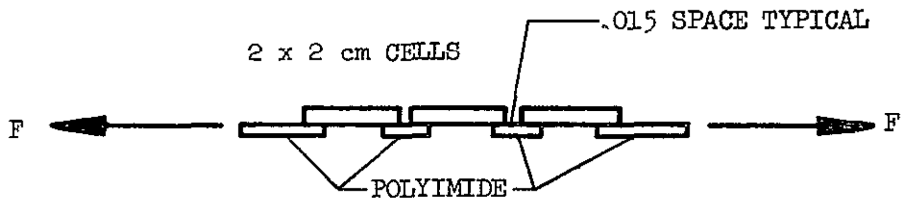

Adhesive	DC 90-024
Thickness	0.0015 inches
Primer	DC 90-198
Substrate	0.001 inch polyimide

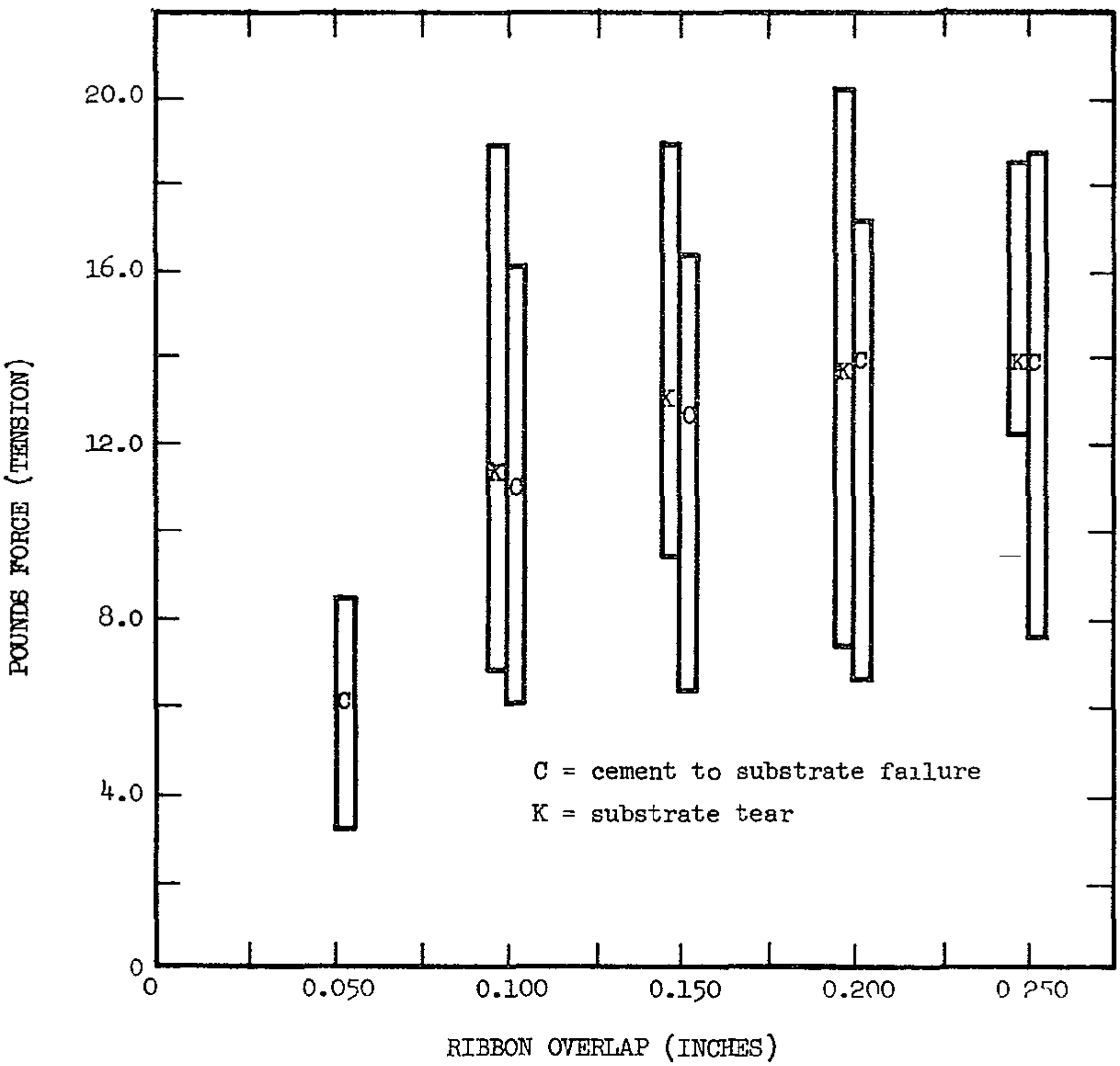

TABLE 2.4-1. TENSILE TEST OF RIBBON SUBSTRATE

The polyimide surface was initially prepared by being chemically etched in concentrated nitric acid for thirty minutes followed by a thorough rinsing in deionized water This step was found to be necessary in order to obtain coatings which would adhere well and pass a tape pull test It is likely that such a preliminary etching could be replaced by subjecting the kapton to a glow discharge just prior to the film evaporation The evaporated copper films formed this way could be subjected to a tape peel test with no visible delaminating or pinholing

Although a good adhering system was thus achieved, it was necessary to check the system's mechanical integrity (i e how the laminate behaved under an applied load) Since the laminate concept appeared to offer strong possibilities for an integrated power distribution system as well as an interconnecting material, it was felt that a test of its behaviour under loading, which is most important to the substrate, should be determined By measuring the deflection of samples under loading it would be possible then to determine the laminate's elastic modulus, elastic limits, and failure (or rupture) point

The copper-polyimide laminate formed as described above was cut into 1/2 inch wide strips and then stretched as shown in Figure 2 5-1. A pointer was attached to the laminate sample to establish a reference point against which the elongation or deflection could be measured Furthermore, wires were soldered to the copper film and connected to an ohmmeter in order to determine the point of electrical continuity failure or the change in conductivity associated with the elongation The laminate strip was clamped in the test fixture at its ends, with insulating material used to isolate the copper film from the vise jaws The elongation data obtained was plotted as a function of applied load in Figure 2 5-2. The hatched area represents the average values for the twenty-five samples tested The variation in data was primarily due to the difference in actual thickness for the deposited copper The ohmmeter readings for each sample remained

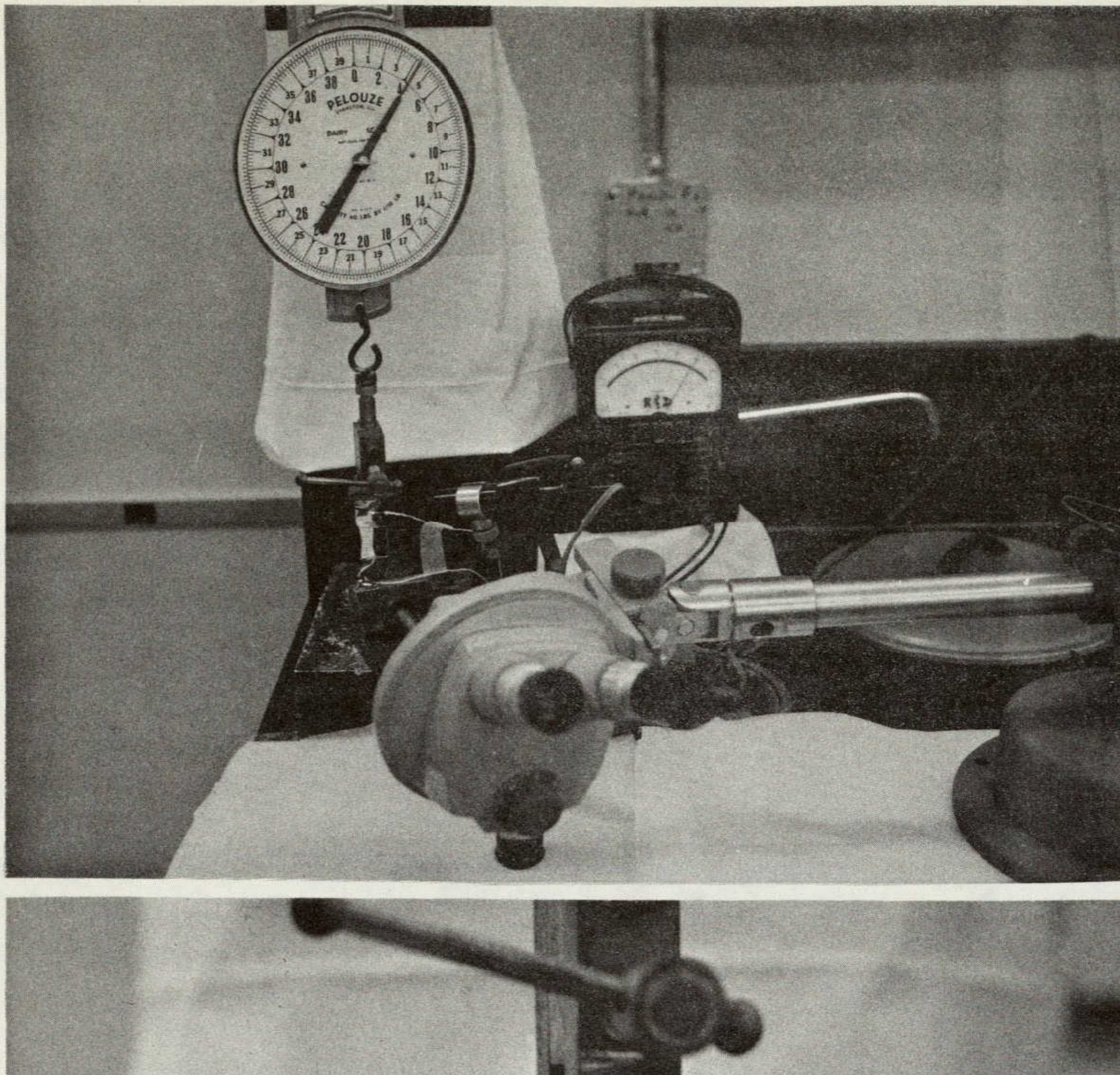

FIGURE 2.5-1. COPPER POLYIMIDE LAMINATE TENSILE TEST

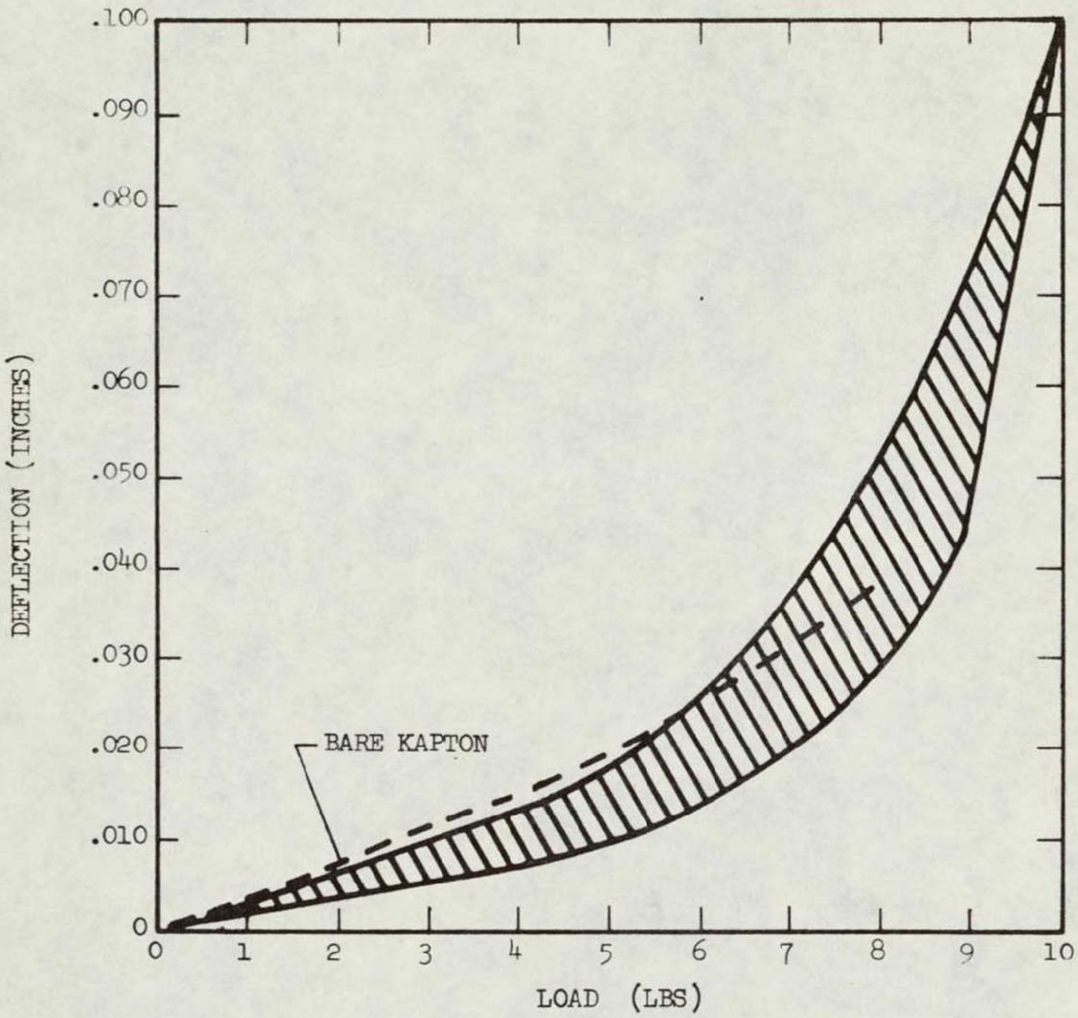

FIGURE 2.5-2 STRESS/STRAIN PLOT
COPPER EVAPORATED ON POLYIMIDE
.001 INCH POLYIMIDE
.0002 INCH COPPER

constant at the unstressed value up to the point where the polyimide substrate failed. Therefore there was no apparent failure in the metal film prior to the substrate failure.

Typically the 25 deflection/load curves, which are directly related to stress/strain, exhibited a linear relationship between the deflection and load up to approximately 4-1/2 pounds. From this point up to the failure point as the load was increased the deflection increased at an increasingly faster rate.

The region from 0 to 4-1/2 pounds is the elastic region where the material acts in an elastic manner such that we can write $F = KY$ where F is the applied force, Y is the material deflection, and K is a constant of the material. An experimental curve for bare polyimide film (same thickness and configuration as the material used in the laminate) is also shown as the dashed line in Figure 2.5-2 for comparison. As expected it exhibits greater deflection for a given load than the laminate.

A comparison of the empirical data for the laminate and theoretical data was conducted by comparing values of the modulus of elasticity obtained in the following manner.

For a given sample the modulus E, is given by

$$E = \frac{Pl}{Ad}$$

where A = cross sectional area

P = force producing the deflection

l = sample unloaded length

d = total elongation

The experiments were conducted on 1/2 inch wide laminate strips, composed of copper 2×10^{-4} inches in thickness deposited on 10×10^{-4} inch thick polyimide.

$A = 1/2\ (10 + 2) \times 10^{-4} = 6 \times 10^{-4}\ in.^2$

$P = 4$ pounds (from Figure 2.4-4)

$\ell = 1$ inch

$d = 10^{-2}$ inch (from Figure 2.4-4)

Therefore, $E = .67 \times 10^6$ psi $\pm .17 \times 10^6$ psi based on the empirical data.

Theoretical considerations indicate a modulus for the composite, based on requiring equal deflections for the copper (Cu) and the polyimide (P) under the applied force, given by:

$$E = \frac{A_{Cu}\ E_{Cu} + Ap\ Ep}{A_{Cu} + Ap}$$

For these materials, published values give

$$E_{Cu} = 1.6 \times 10^6 \text{ psi}$$

$$Ep = .46 \times 10^6 \text{ psi}$$

Further, $A_{Cu} = 1 \times 10^{-4}\ cm^2$

$$Ap = 5 \times 10^{-4}\ cm^2$$

Therefore, the theoretical $E = .62 \times 10^6$, agrees within measurement error, with the average empirical value of $.67 \times 10^6$ psi.

In summary it appears evident that additional study is necessary to make use of the excellent properties of the ribbon substrate. The vacuum deposited copper laminate appears to be a good material for use on both a lightweight current carrying substrate and a fatigue resistant cell interconnector.

2.6 WRAPAROUND INTERCONNECTOR MODULE MANUFACTURING FEASIBILITY AND COST STUDY

A demonstration solar cell module was constructed during the third quarter of JPL Contract 952560 to demonstrate the feasibility of the wraparound interconnector concept. Fabrication of this 380 cell module (19 parallel x 20 series) was performed to obtain information about the various manufacturing tasks employed to assemble the module and provide a comparison of the corresponding manufacturing tasks of the conventional and wraparound interconnects. The manufacturing tasks were reviewed to determine the general overall task efficiency and type of tooling or tooling modification necessary to expedite module assembly. Manufacturing tasks of the conventional and wraparound interconnector were compared to determine the difference in costs of similar tasks. From this demonstration module it was possible to extrapolate the cost of fabricating a wraparound interconnector module.

2.6.1 Solar Cell Module Description

Solar Cells:	2 x 2 cm bar contact solderless
	8 mils nominal thickness
Solar Cell Cover:	0211 microsheet 3 mils thick
Interconnect:	2 mil copper, silver plated
Solder Technique:	Front contacts - impulse
	Rear contacts - resistance
Module Size:	19 cells in parallel by 20 cells in series
Wraparound Insulation:	1 mil glass cloth impregnated with RTV 3145

2.6.2 Interconnector Description

The interconnector configuration shown in Figure 2.6-1 is the type used to fabricate the demonstration test module. The configuration incorporates stress relief features which were designed to alleviate thermal stresses at the interconnector solar cell interface. The major redesign compared to conventional interconnects consisted of relocating and lengthening the ohmic strip tabs to allow the wraparound to be completed. The tabs were stress relieved to allow transverse

movement due to thermal expansion, without exerting large stresses at the cell and tab interface.

The interconnectors were fabricated from 2 mil copper silverplated on all surfaces. The 2 mil copper was selected to parallel the type of material used on the conventional interconnector to insure that established soldering techniques will produce uniform reliable solder bonds.

2.6.3 Module Fabrication

The demonstration module fabrication consisted of the following steps:

A. Cell electrical output matching: Prior to assembly, the solar cells were graded and an average current value of 95.0 mA at 460 mV at 140 mW/cm^2 and 28°C was established for each parallel submodule.

B. Coverglass Installation: Cell covers were bonded with Dow Corning XR63-489 silicone adhesive.

C. Paralleling of Cells: Solar cells were placed in a vacuum hold-down fixture to establish cell spacing. Mylar tape was applied to the face of the cell to maintain spacing during the assembly process. The interconnectors were indexed and soldered in place. A pulse soldering technique and 1 mil x 30 mil solder preforms were used to produce an optimum bond. Figures 2.6-2 and 2.6-3 show taped and soldered submodules.

D. Interconnector Insulation and Bonding: Figures 2.6-4, 2.6-5, and 2.6-6 show the three steps necessary to complete the insulated wraparound contact. Figure 2.6-4 shows the interconnector bent 90 degrees toward its final position. This step is performed to facilitate submodule handling and priming of the surfaces to be bonded.

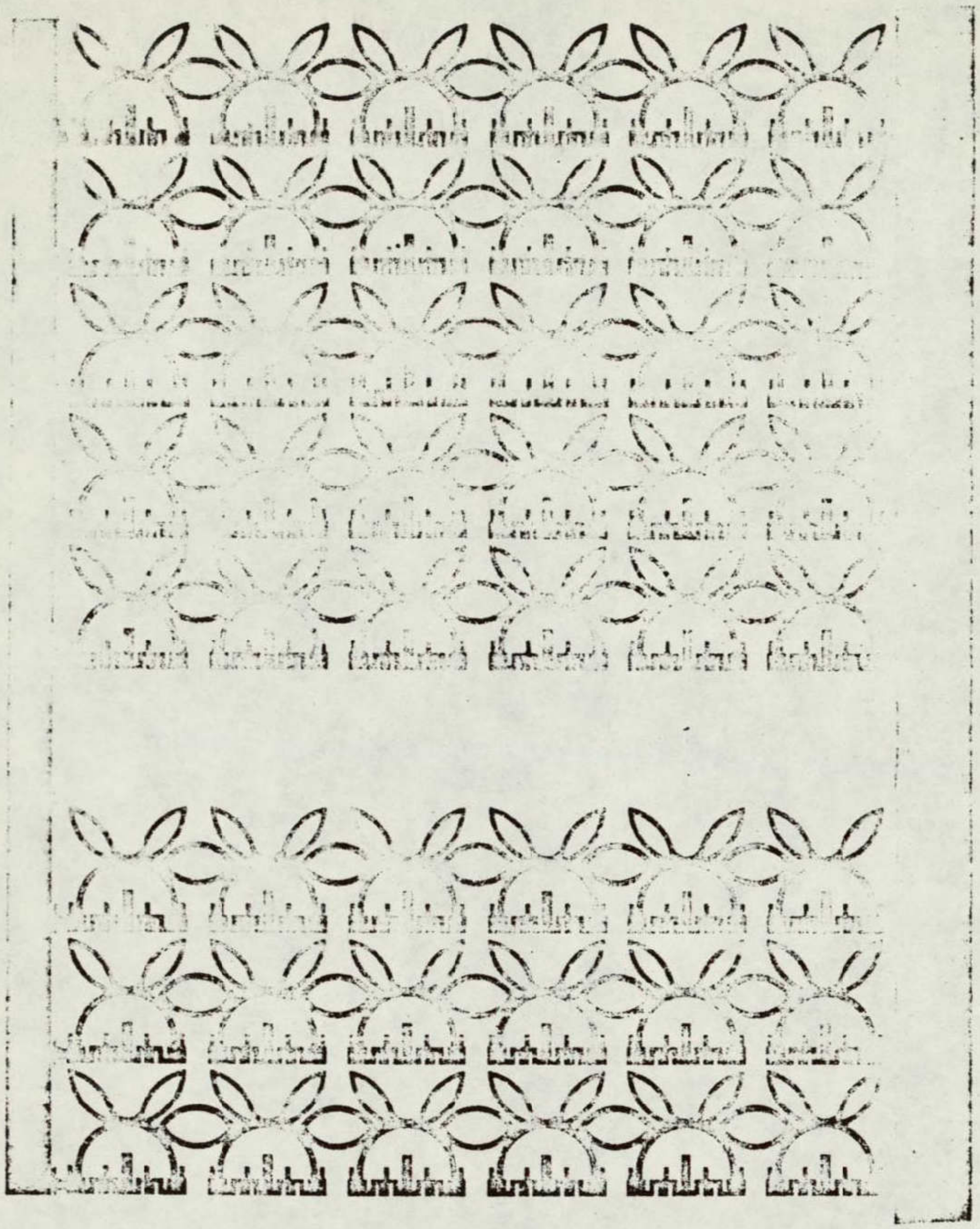

WRAPAROUND INTERCONNECTOR

Figure 2.6-1

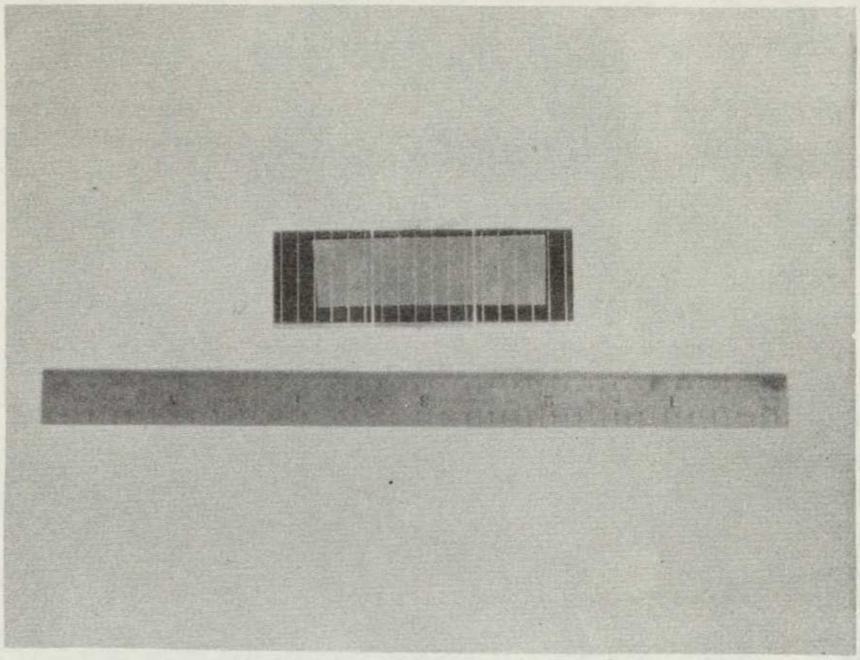

FIGURE 2.6-2. TAPED SUBMODULE

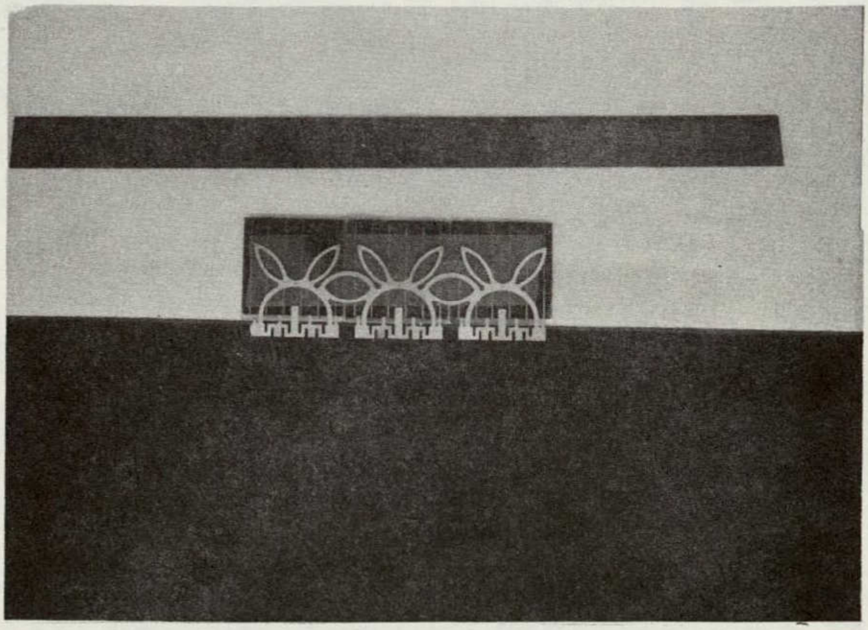

FIGURE 2.6-3. SOLDERED SUBMODULE

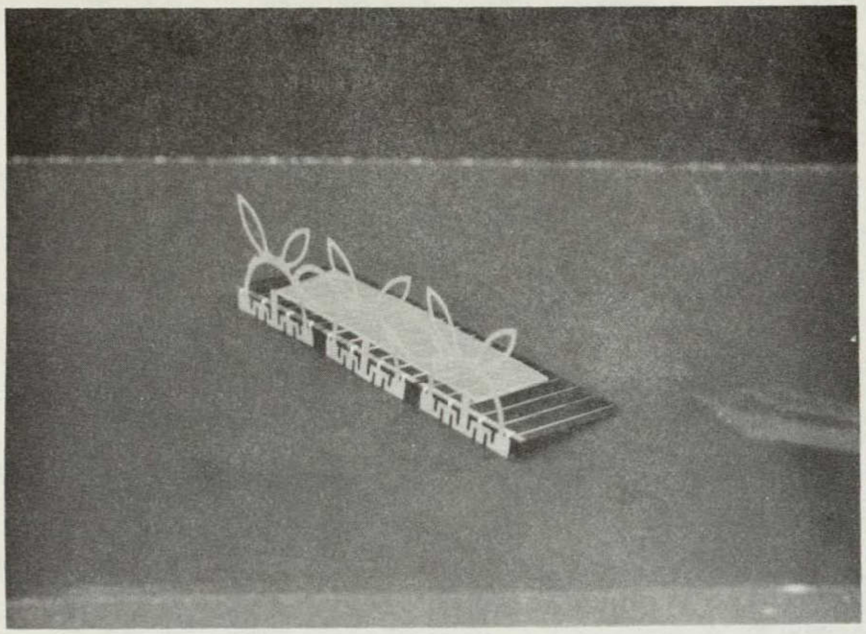

FIGURE 2.6-4. 90° INTERCONNECTOR BEND

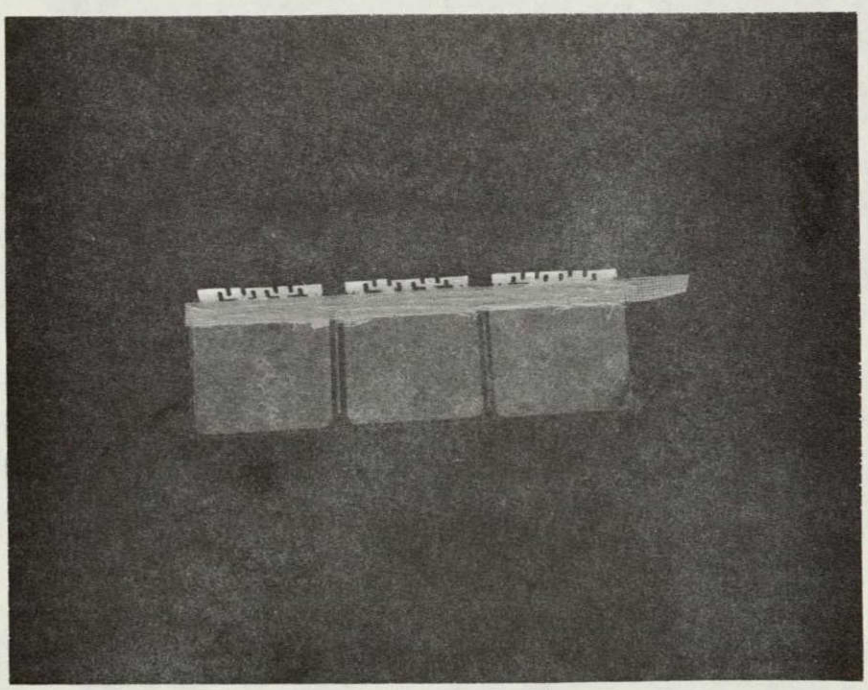

FIGURE 2.6-5. INSULATION ADDITION

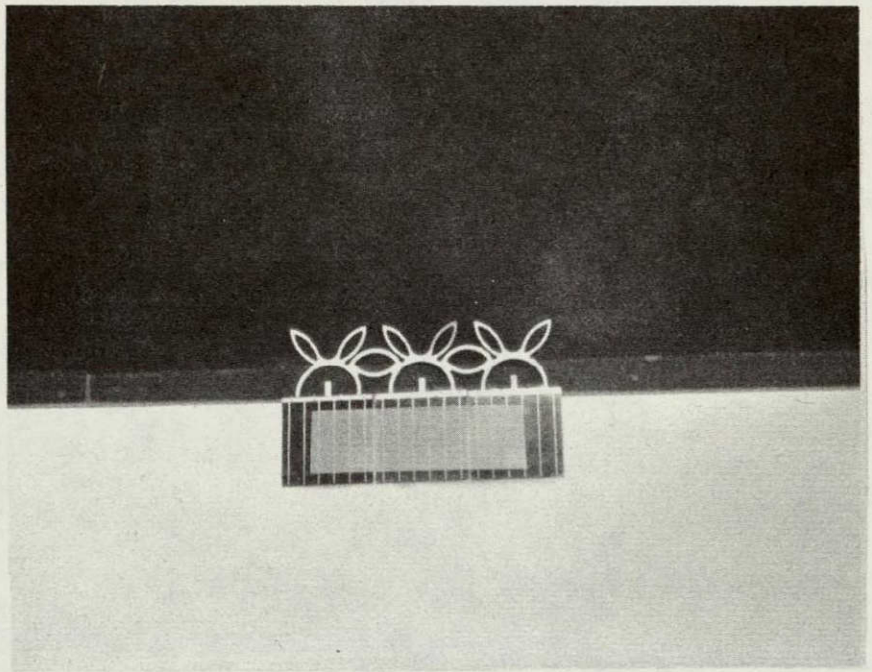

FIGURE 2.6-6. COMPLETED WARAPAROUND SUBMODULE

Figure 2.6-5 shows the cell rear "P" contact with the RTV impregnated glass insulation in place. Initially, a light coating of RTV 3145 is applied to the "P" contact opposite the ohmic strip. The area covered is about 0.15 of an inch wide and running the length of the cell. A strip of 1 mil thick woven glass cloth was placed in the adhesive, additional adhesive was applied to the glass cloth, and the primed interconnector was rolled around the edge of the cell and pressed into the adhesive.

The assembly was placed between two sheets of teflon coated kapton and a pressure of approximately one-half pound per square inch was applied. The assembly was cured for 48 hours at 28°C. The submodules were subsequently inspected, repaired, cleaned, and submitted to final assembly. Figure 2.6-6 shows a completed submodule after the adhesive had been cured.

E. Submodule Series Assembly: Submodules were placed in a vacuum hold-down fixture to maintain cell spacing and the series connections mode. Soldering was accomplished using 1 mil solder preforms 30 mils in diameter and a resistance soldering technique. The module was subsequently inspected and repaired prior to electrical performance evaluation. Each series connected submodule was then parallel connected to the next series string with metal jumper strips. Figures 2.6-7 and 2.6-8 show the front and back of the completed 19 by 20 cell array. Figures 2.6-9 and 2.6-10 show closeup pictures of portions of the front and back connections of the completed array. The module was subsequently inspected and repaired prior to electrical performance evaluation. The I-V curve obtained during the electrical performance is shown in Figure 2.6-11.

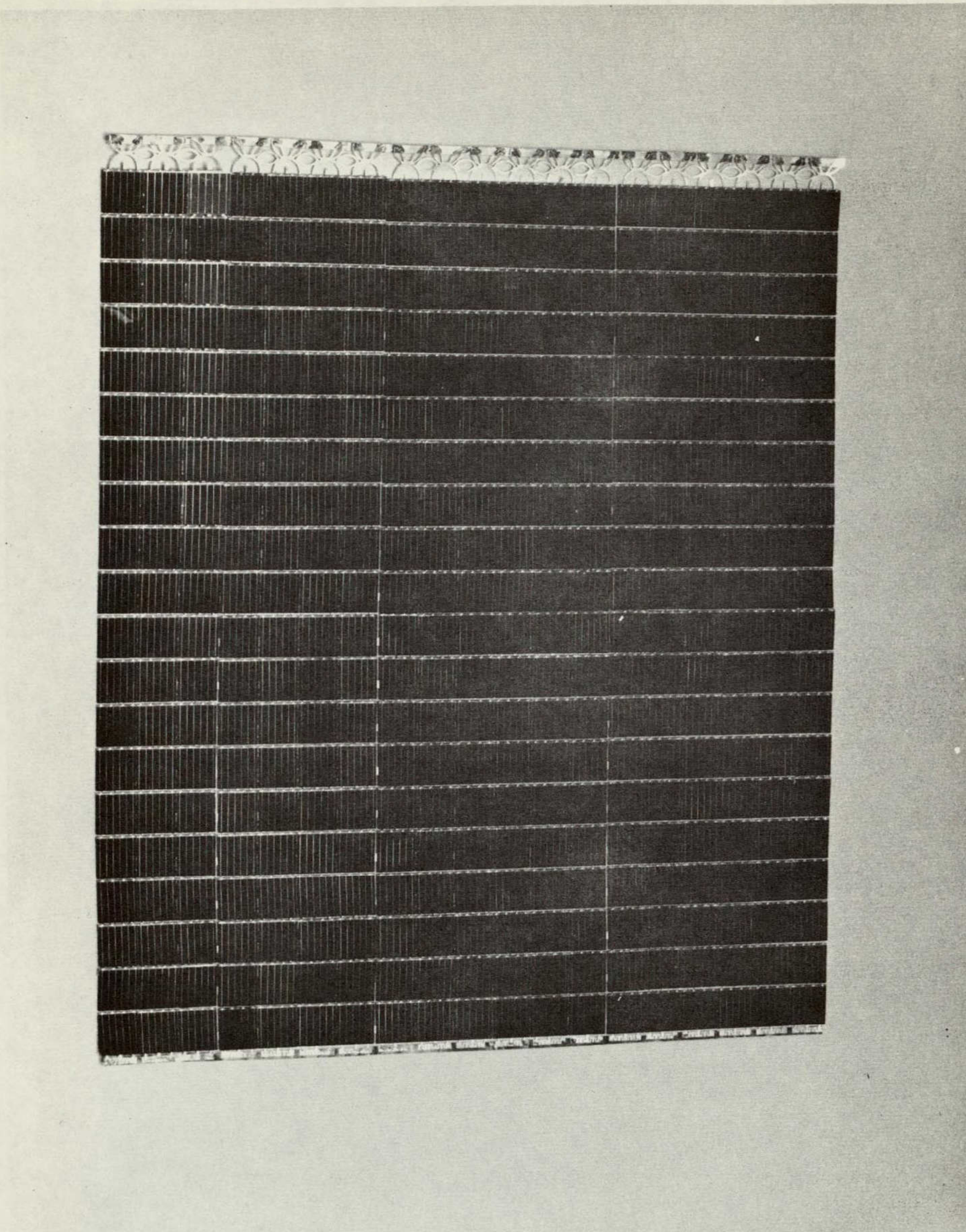

FIGURE 2.6-7. COMPLETE MODULE TOP VIEW

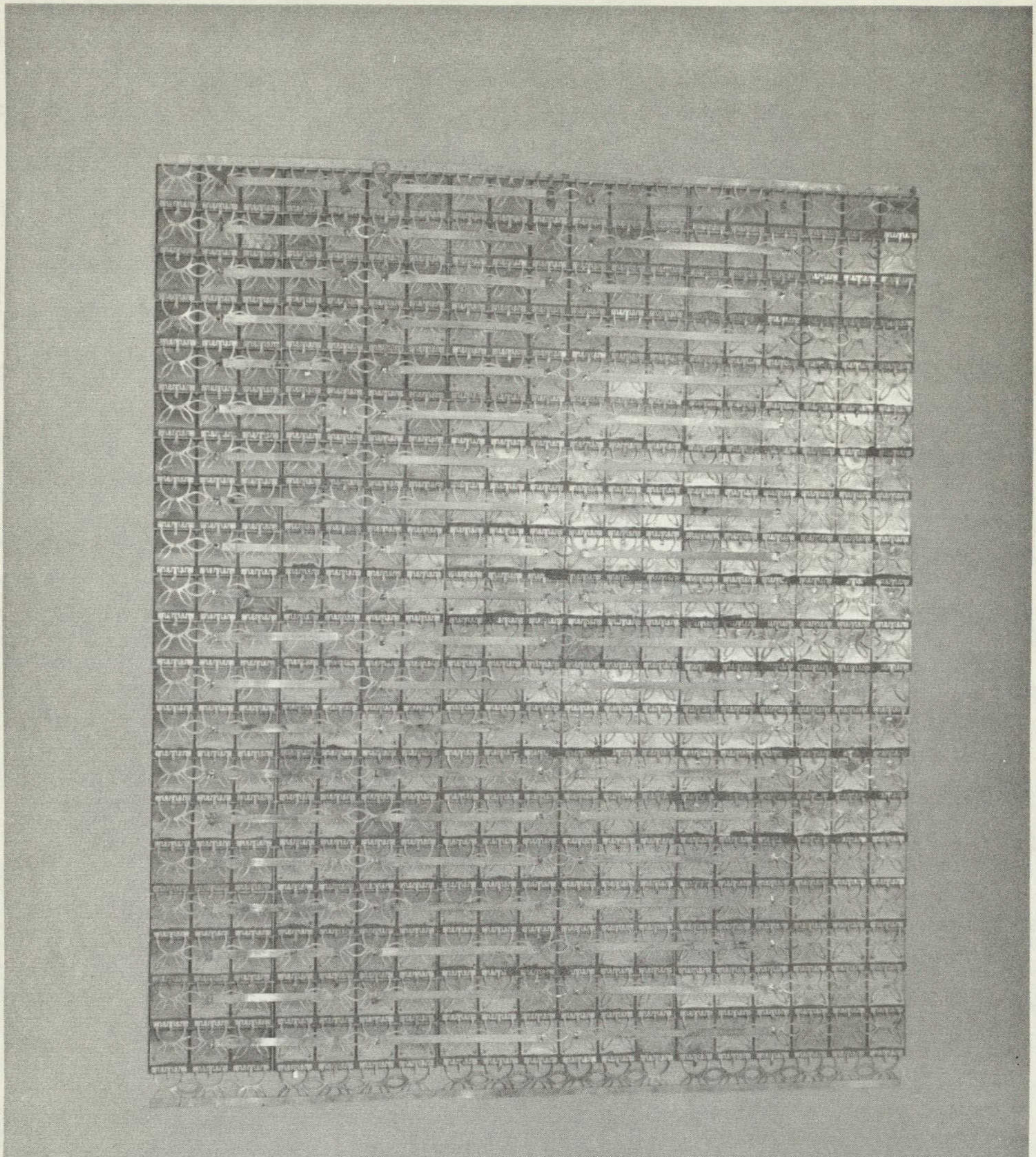

FIGURE 2.6-8. COMPLETE MODULE BOTTOM VIEW

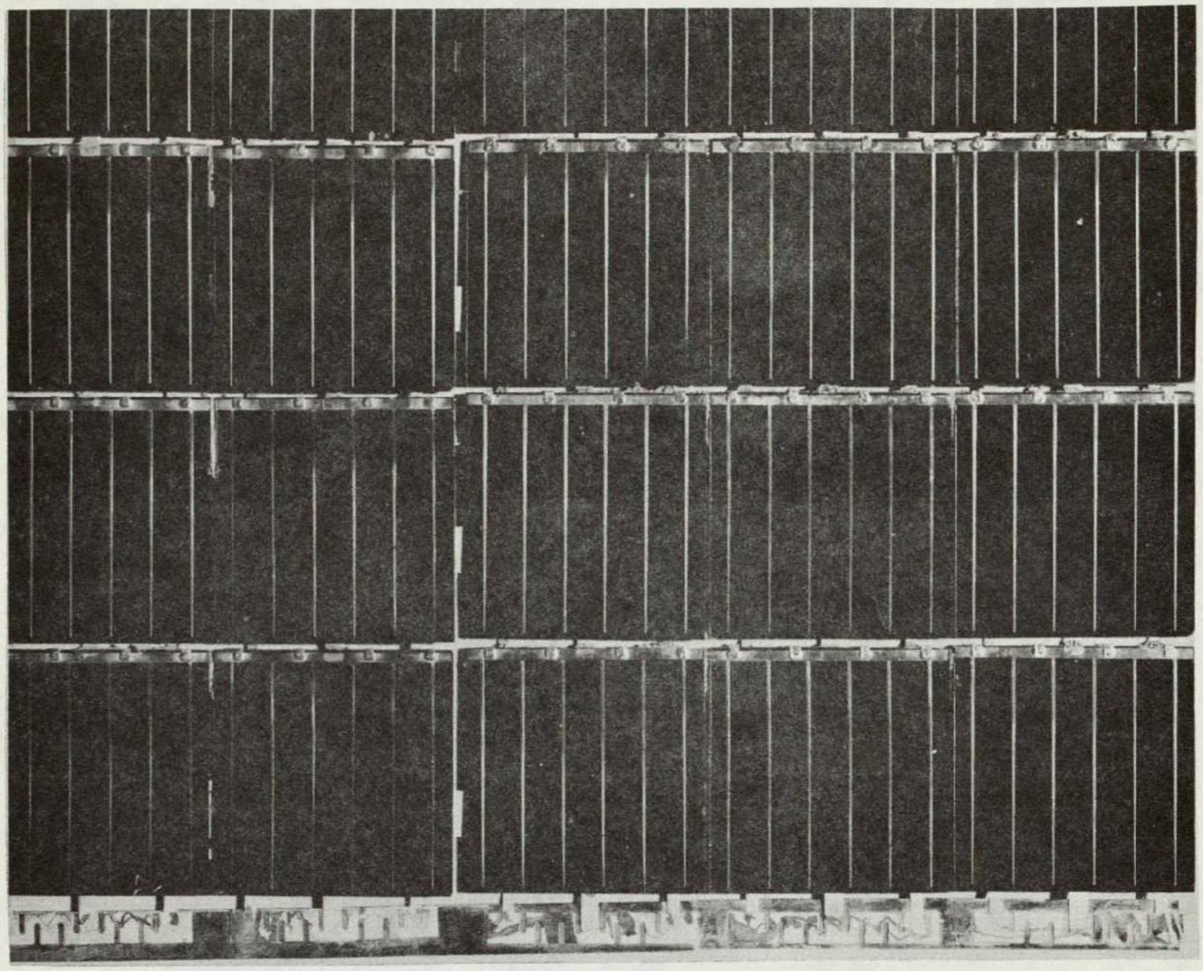

FIGURE 2.6-9. MODULE CLOSEUP TOP VIEW

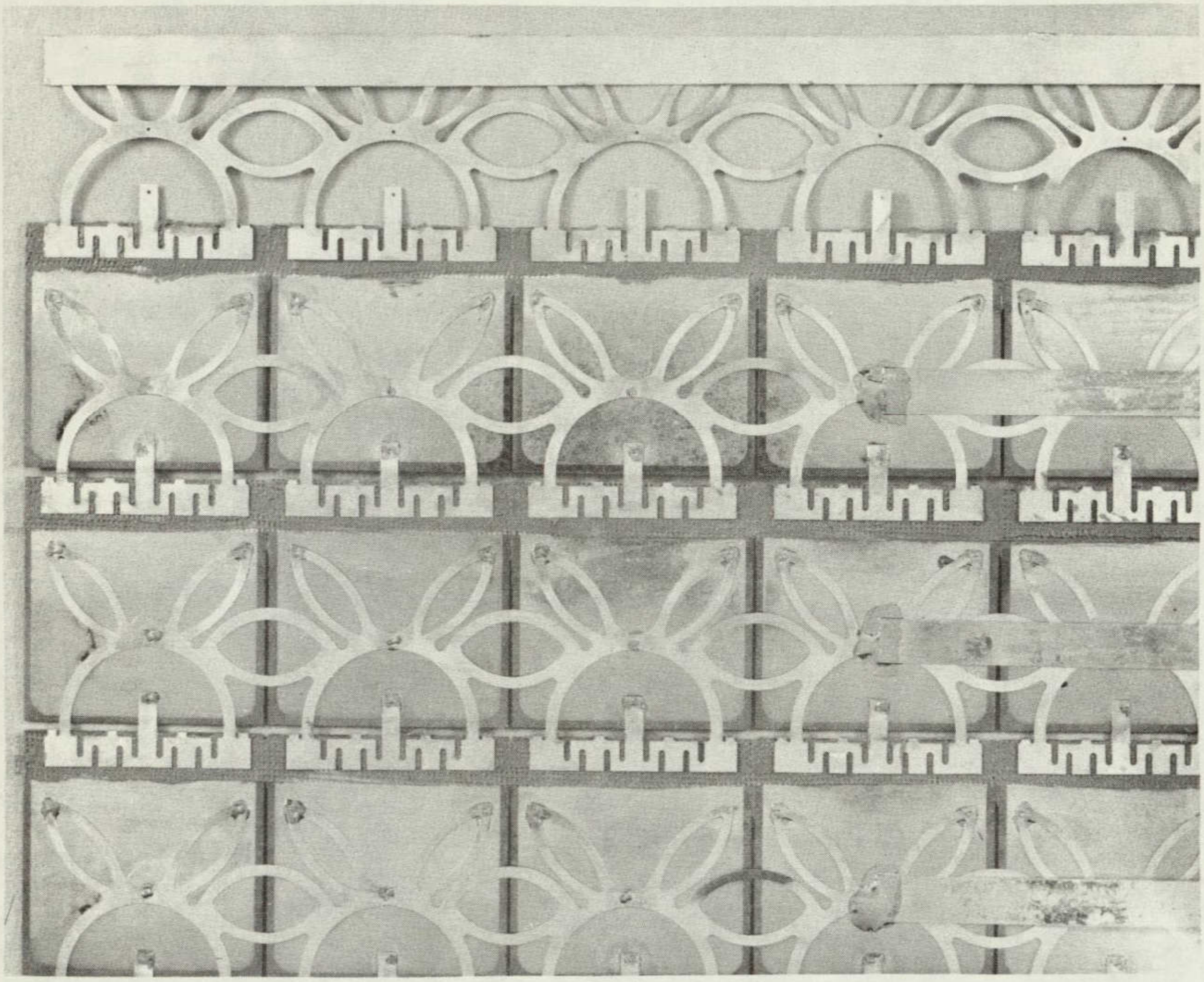

FIGURE 2.6-10 MODULE CLOSEUP BOTTOM VIEW

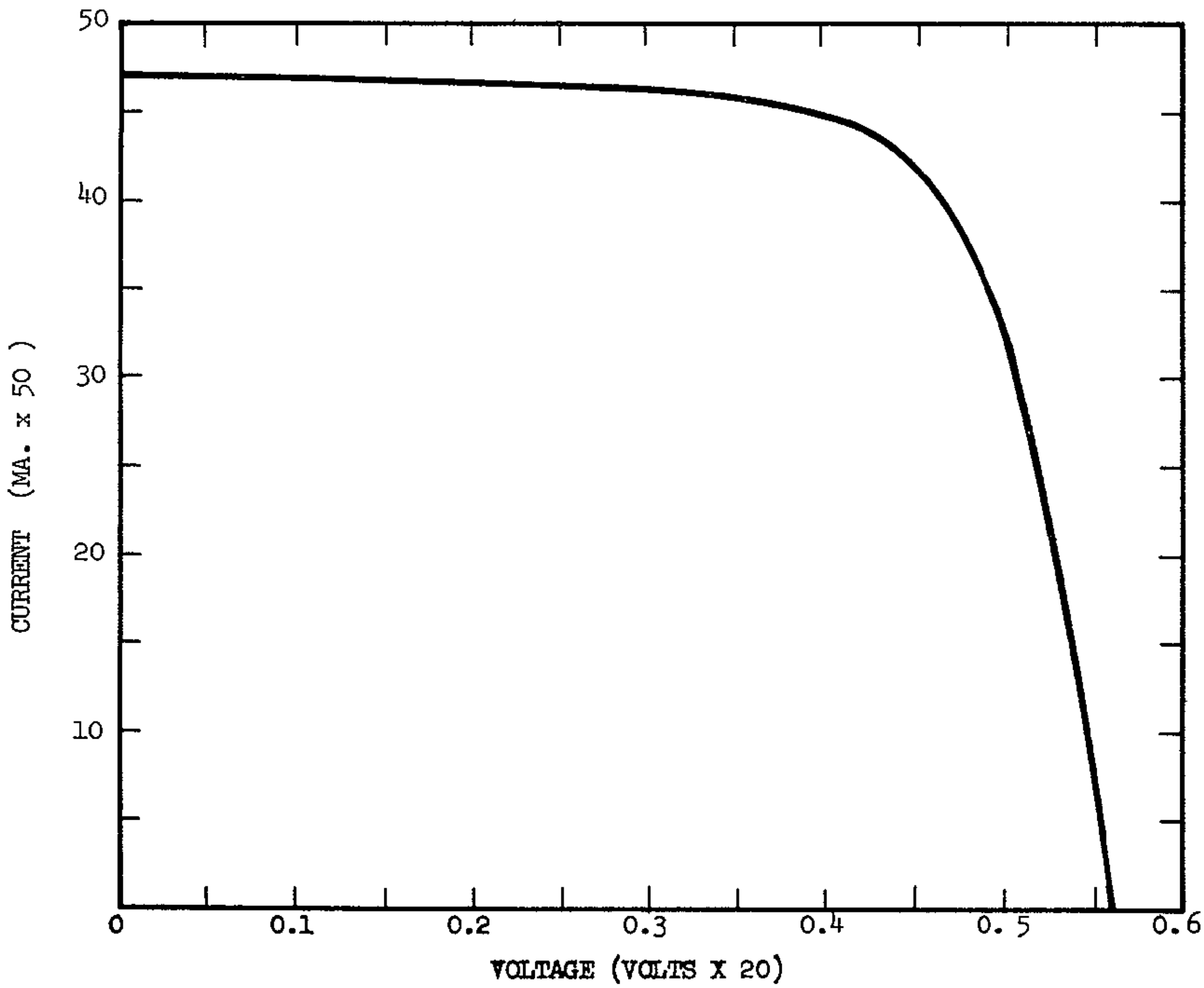

FIGURE 2.6-11. MODULE ELECTRICAL PERFORMANCE

2 6 4 Module Repair

Module repairs consisted of replacement of a broken cover or a broken cell Cover replacement was done using ethanol and a razor blade slipped between the cover and the cell The cell was subsequently cleaned and a new cover was installed Cell replacement was more complex with the wraparound interconnect than the conventional interconnector This complexity in repairs of cells would result in a correspondingly higher per cell repair price, about 12 percent more than the conventional configuration The cost increase is due to the fact that a cell with a wraparound interconnector is replaced as an assembly with the interconnector bonded to the solar cell and requires special handling It is anticipated that this price will be significantly reduced as more advanced and mechanized techniques are developed

2 6 5 Module Manufacturing Feasibility

As a result of the processing performed for the above demonstration array, the wraparound interconnector solar cell module fabrication technique has been demonstrated and has been shown to be feasible for use on an integrated lightweight solar cell array Environmental and performance testing of this module will be performed under the direction of JPL, and these tests will provide information regarding reliability and integration of the design

2 6 6 Wraparound Interconnect and Conventional Interconnect Module Price Comparison

Table 2 6-1 has been compiled to provide a relative price comparison of the wraparound interconnected module compared to the conventional system The conventional configuration uses a stress relieved Z type photo-etched copper interconnector The wraparound uses the technique explained in previous sections The price analysis is broken down into three basic areas

Table 2 6-1 MODULE PRICE COMPARISON

Task	Interconnector Type: Conventional	Interconnector Type: Wraparound
Module Fabrication	\$2 79 per cell	\$3 10 per cell
Module Repair	\$0 80 per cell	\$0 95 per cell
Test	\$0.18 per cell	\$0 18 per cell
*Total Fabrication Price	\$3 77 per cell	\$4.23 per cell

*The total fabrication price does not include the cell cost, cover cost, or cover laydown cost

These areas are module fabrication, which progresses from cell matching to submodule series connection, submodule repair, and final electrical test The price analysis is also based on a 2 x 2 cm cell basis and projects the actual demonstration wrap-around module fabrication labor figures to a large scale production situation.

The projected fabrication price for the wraparound interconnector concept is approximately 12% higher than for the conventional interconnector concept However, the superior fatigue resistance of this concept, as shown in Section 2 3, will, in many instances provide impetus for its utilization rather than the conventionally interconnected system

2 6.7 Second Demonstration Module

At the end of the one year program a second module was built to demonstrate the feasibility of concepts conceived and analyzed during this program The module size was approximately thirty six square inches in area consisting of four 2 x 2 cm cells in parallel by 16 cells in series in a U-type configuration to form a square module with 8 cells on a side

Many of the new concepts developed and tested during this program are incorporated in fabricating the sixty four cell demonstration module New concepts developed during this program that are used are 1 3 mil thick coverglass and a stress relieved wraparound interconnector The coverglass and associated bonding process was developed to reduce the cost and weight of the solar cell blanket. The wraparound interconnect was developed specifically to alleviate the combined flexural and tensile forces generated during the missile launch environment Basically this concept restricts and bending and tensile loads to a plane on the surface of the substrate thereby removing the stresses from the solar cell contact and interconnector interface

In summary the demonstration module consists of the following components

Table 2.6-1

1	Silicon Solar Cell	
	Size	2 x 2 centimeters
	Base Resistivity	2 ohm centimeter
	Thickness	0 007 inches nominal
	Contact Type	conventional bar, solderless
2	Coverslide	
	Thickness	0 0013 inches nominal
	Material	Corning type 8871 glass
	Adhesive	Dow Corning XR63-489
3.	Interconnector	
	Configuration	Stress relieved wraparound
	Material	0 001 inch thick copper silver plated
	Type	Photo etched thermal stress relieved
	Bonding	Pulse soldering using 0 001 inch thick preforms
4	Substrate and Cell Bonding	
	Material	Polyimide
	Thickness	0 0005 inches
	Adhesive	RTV 3144
5	Power Distribution System	
	Material	Copper, vacuum deposited
	Thickness	approximately 0 0005 inches

3 0 CONCLUSIONS

Conclusions for each of the specific tasks investigated during this effort are discussed separately with a final statement regarding the overall effort

3 1 SOLAR CELL AND CONTACTS SURVEY

Examination of solar cell contact configurations indicated that the wraparound bottom contact configuration would provide improved reliability for lightweight arrays by reducing interconnector stresses However, cost trade-offs show such a system to be prohibitive at present because the wraparound contact cell is not developed sufficiently. Consequently efforts in this study were directed toward the use of conventional bar contact configurations in order to keep the scope of work within the contracted effort The cost analyses indicate that trends in cell costs are typically toward decreased costs as a function of time for any specific cell design This trend represents the effects of manufacturing learning curves, small quantity requirements initially, and industry inertia to changes Present-day power/weight/cost trade-offs indicate that the 8 mil thick silicon cell provides an optimum merit factor today and consequently limits the amount of array weight saving and cost per watt decrease which can be presently obtained The cost analysis also indicates that within 5 years (1975) the optimum cell configuration in respect to the power/weight/cost merit factor can drop to 6 mils thickness Since the problem in reducing costs of very thin solar cells appears to be primarily a matter of handling restrictions and tooling any effort toward improving the handling of thin cells will reduce the time required for the cost of the thinner cells to become competitive

3 2 COVERSLIDE ASSEMBLY

Examination of the costs for cover assembly with platelet (microsheet and fused silica), integral, and ribbon glass systems has shown the conventional platelet to cost approximately three times as much as

integral or ribbon systems. Further, the integral and ribbon concepts can be used with material considerably thinner than 3 mils, the marginally practical limit for conventional platelets. This will allow significant weight savings for arrays where low radiation environments will be encountered. The ribbon glass technique has been utilized in the demonstration modules for this program and has been shown to be a practical cover system.

3.3 INTERCONNECTOR STUDY

An effort to improve interconnector reliability, through a program of failure definition, analytical stress analysis and testing provided a number of configurations exhibiting greater fatigue resistance for flexible arrays than the conventional Z tab stress loop interconnector. These improved configurations include the stress relieved wraparound, the total span wraparound, and the laminated wraparound interconnect. Where a Z tab interconnector is to be employed, and small stress loop motions occur, the generalized equation:

$$h' = R + \left[\frac{Y'-R_f}{R_f-R}\left(\frac{2R_f}{\pi}\right)\right], \quad \text{where } R_f = \frac{R}{1 - \frac{S_f R}{Ed}}$$

provides a basis for designing fatigue resistant stress loops. In this relation the quantities are.

- h' = height of stress loop above cell surface
- Y' = half the maximum cell spacing due to array motion (thermal or vibrational)
- E = modulus of elasticity for interconnector
- d = thickness of interconnector
- S_f = fatigue strength of interconnector
- R = initial fabricated radius of curvature of stress loop.

3 4 SUBSTRATE AND CELL BONDING

The ribbon substrate was originally considered in an effort to reduce assembly costs and overall array weight An analytical and empirical study was performed to determine the minimum width of ribbon which would be required and adhesive bond strength between the substrate and solar cell

Tests conducted on sample modules revealed that the ribbon substrate caused uneven stress distribution and premature interconnector fracture Due to the uncertainty of the anticipated loads at this time it was decided to hold the ribbon substrate in abeyance and use a 1/2 mil continuous substrate for the final demonstration module The thin polyimide substrate proved to be satisfactory during the interconnector fatigue tests

3 5 INTEGRATED POWER DISTRIBUTION SYSTEM

An abbreviated examination of the task was conducted due to an increase of program emphasis on interconnector reliability Results of this survey demonstrated that a metallic-polyimide laminate, either using vacuum evaporation of laminate bonding, could withstand severe array stresses without losing electrical or mechanical integrity Hence a laminate can provide not only a mechanical substrate but electrical interconnection and bussing The evaporated metal laminate has a great deal of potential for utilization as the cell interconnector as well as the bus system A significant reduction in array weight and fabrication costs is expected when this laminate system is fully developed

3 6 DEMONSTRATION MODULE FABRICATION AND DOCUMENTATION

The fabrication of actual modules utilizing the concepts and techniques developed in tasks 1-5 exhibited the systems manufacturability Documentation of process techniques and tooling provides information necessary to fabricate further modules

The demonstration module fabrication was conducted in accordance with a modular concept without including however, bussing components between

modules. The laminated substrates discussed above should provide a solution for the requirement. Based on a weight analysis the achieved power to weight ratio for modules fabricated using the demonstration module specifications should be 82 watts per pound. The development of thinner cell handling techniques will be required for accomplishing 120 watts per pound. When this is achieved, a valid power to weight final value can be computed for a system of 120 watts per pound of array weight. However, even with the aforementioned restriction on possible cost savings significant cost reductions were evident, particularly in the cover system.

3.7 OVERALL PROGRAM CONCLUSIONS

The pertinent findings of this study are as follows

- 8 mil thick 2 x 2 cm bar contact cells provide optimum power/weight/cost at present.
- 6 mil thick 2 x 2 cm bar contact cells will provide optimum power/weight/cost by 1974.
- Integral and ribbon glass cover systems can reduce the cover cost for 2 x 2 cm cells from $2.50 minimum for a platelet system to less than $0.86.
- A generalized equation relating interconnector stress loop height and fatigue resistance was derived.
- Deposited metal-polyimide laminates used as interconnectors can provide substrate mechanical strength and electrical integrity.
- Minimum overlap width for no loss in adhesive strength between solar cell and ribbon substrate was determined.
- Silicon stress versus interconnector thickness for various temperature cycling ranges were calculated for copper and molybdenum materials.

4.0 RECOMMENDATIONS

With the high power to weight ratio of the demonstration module, calculated at approximately 82 watts per pound, enough work has been accomplished to indicate that 120 watts per pound could be obtainable through the use of thinner solar cells and laminated interconnect designs. Since the major drawback here has been the lack of time to move all the way to a 4 mil thick cell and the problems associated with this thin cell, it would be worthwhile to extend research and development efforts towards solving these handling difficulties. The use of the low cost cover techniques and laminated interconnect techniques would provide low cost arrays at high power to weight values. The use of wraparound contact solar cells will simplify the interconnector design and also reduce weight and costs of interconnecting the cells.

Interconnector studies in this program showed a number of configurations which can substantially improve the array's reliability. Extending these studies to lighter and thinner wraparound interconnectors or establishing practical handling practices for the wraparound contact cells will provide a further weight-saving without reliability loss.

The integrated power distribution system studies only examined the practicality of a substrate to provide mechanical and electrical integrity under array stresses. Using wraparound contact cells and perfecting methods of bonding, mechanically and electrically, these cells to a laminated metallic polyimide substrate will provide not only a large weight reduction but also a decrease in the array assembly cost through the deletion of the tedious interconnector and bonding techniques now required with top contacted cells.

A direction for further work has been indicated through the present study and shows that techniques and concepts have been defined which can provide a system meeting the present design goals. It is recommended that further efforts as described above be continued so that the potential of the 4 mil solar cell can be demonstrated. The background of the particular survey effort clearly indicates that a developmental effort aimed at economically utilizing thin cells with wraparound contacts, and laminated conductor-substrates has the potential to provide the necessary power to weight values at a low cost so that the original program goals can be met.